APPLIED COMPUTATIONAL ELECTROMAGNETICS SOCIETY JOURNAL

March 2014
Vol. 29 No. 3
ISSN 1054-4887

The ACES Journal is abstracted in INSPEC, in Engineering Index, DTIC, Science Citation Index Expanded, the Research Alert, and to Current Contents/Engineering, Computing & Technology.

The illustrations on the front cover have been obtained from the research groups at the Department of Electrical Engineering, The University of Mississippi.

MARCH 2014 REVIEWERS

Muhammad Ali
Mohamed Bakr
Poongodi C
Alistar Duffy
Mohammed Hadi
Julie Huffman
Zhiping Li
Zah
Rashid Mirzavand
Adam Mock
Truong Khang Nguyen
William Palmer
Christoph Statz
Christopher Trueman
Wei-Chung Weng
Yifan Zhang
Theodoros Zygiridis

THE APPLIED COMPUTATIONAL ELECTROMAGNETICS SOCIETY

JOURNAL

Vol. 29 No. 3 March 2014

TABLE OF CONTENTS

Efficient *Z*-Transform Implementation of the D-B CFS-PML for Truncating Multi-Term Dispersive FDTD Domains

Naixing Feng [1], Yongqing Yue [1], Chunhui Zhu [1], Qing Huo Liu [2], and Liangtian Wan [3]

[1] Institute of Electromagnetics and Acoustics
Xiamen University, Xiamen 361005, P. R. China
fengnaixing@gmail.com, yongqingyue@gmail.com, zhuchhxd@xmu.edu.cn

[2] Department of Electrical and Computer Engineering
Duke University, Durham, NC 27708, USA
qhliu@ee.duke.edu

[3] Department of Information and Communication Engineering
Harbin Engineering University, Harbin 150001, P. R. China

Abstract ─ Efficient *Z*-transform implementation of the Complex Frequency-Shifted Perfectly Matched Layer (CFS-PML) using the D-B formulations are proposed to truncate open region multi-term dispersive Finite-Difference Time-Domain (FDTD) lattices. These formulations are independent of material properties of the FDTD domains and hence can be used for modeling general media because of the D-B constitutive relations. A Three-Dimensional (3-D) simulation of the two-term Lorentz dispersive FDTD domain has been carried out to demonstrate the validity of the proposed formulations. Furthermore, in order to show the validity of the proposed algorithm, the second 3D inhomogeneous problem has also been used for validating the proposed formulations. It is clearly shown that the new formulations with the CFS-PML scheme are efficient in attenuating evanescent waves and reducing late-time reflections.

Index Terms **-** D-B constitutive relations, Finite-Difference Time-Domain (FDTD), multi-term Lorentz, Perfectly Matched Layer (PML) and *Z*-transform.

I. INTRODUCTION

Since 1994, the Perfectly Matched Layer (PML) concept proposed by Berenger [1], has been a highly effective absorbing-material Absorbing Boundary Condition (ABC) to terminate the Finite-Difference Time-Domain (FDTD) domains, the innovation of the PML ABC is that plane waves of arbitrary incidence, polarization and frequency are matched at the boundary between PML and the physical domain. What's more important is that the PML can be used as an absorbing boundary to terminate domains comprised of inhomogeneous, dispersive, anisotropic and even nonlinear media. Among the various implementations of PMLs, the stretched coordinate PML (SC–PML) by Chew and Weedon [2], has the advantage of simple implementation in the corners and edges of PML regions. The SC-PML [2] was proposed through mapping Maxwell's equations into a complex stretched coordinate space. As in the original Berenger's PML; however, the implementation of the SC-PML in [2] needs splitting the field components and modifying Maxwell's equations. Several unsplit-field implementations of the SC-PML formulations have been presented. These algorithms can be classified into three categories: (1) the Convolutional PML (CPML) [3] is based on applying the convolution theorem to the SC-PML formulations, (2) the Auxiliary Differential Equation (ADE) PML [4-6] is based on incorporating the ADE method into the SC-PML formulations and (3) another SC-PML

Submitted On: October 30, 2013
Accepted On: April 20, 2014

implementation presented [7-11] is based on the *Z*-transform methods that have been successfully incorporated into the FDTD algorithm. As in the original Berenger's PML; however, the SC-PML formulations are ineffective at absorbing evanescent waves and various efforts have been attempted to overcome this limitation [12-14]. Among these, the Complex Frequency-Shifted PML (CFS-PML) [14], implemented by simply shifting the frequency dependent pole off the real axis and into the negative-imaginary half of the complex plane has drawn considerable attention, due to the fact that this PML is efficient in attenuating low-frequency evanescent waves and reducing late-time reflections. In [3, 15-17], various modified SC-PMLs based on the convolution theorem, the ADE method and the *Z*-transform methods, respectively, were presented in detail to efficiently implement the CFS-PMLs. Recently, the proposed SC-PML formulations in 2011 [18] based on the ADE method, have been presented for effectively modeling a linear multi-term Lorentz dispersive material in the 2-D simulation. However, as described in the preceding section, the SC-PML formulations are not capable of absorbing evanescent waves in the 2-D simulation and have even worse absorption performance in 3-D numerical tests. Besides, the SC-PML formulations based on the transpose direct form II proposed in [18], are difficult to extend to the case with more than two dispersive terms, because the direct form II structure [19] is extremely sensitive to parameter discretization in general and is not recommended in practical applications.

In this paper, the unsplit-field and efficient D-B CFS-PML algorithm, based on the *Z*-transform method, are proposed to truncate linear multi-term dispersive open-region FDTD domains. In the proposed formulations, an appropriate combination of the *Z*-transform methods with the D-B constitutive relations is used for truncating arbitrary media without any modifications of Maxwell's curl equations. A 3-D numerical test for a linear two-term Lorentz dispersive problem is given to validate the proposed D-B CFS-PML formulations; as the investigation on the performance of the D-B CFS-PML for linear multi-term Lorentz dispersive problem is very rare in the literature. Only the two-term Lorentz dispersive case is described in this paper, but this approach is easy to apply to any number of dispersive terms. For convenience, these PMLs including the proposed CFS and SC-PMLs and the proposed PML in [18], are referred to here as the ZT-CFS-PML, the ZT-SC-PML and the ADE-SC-PML, respectively.

II. FORMULATIONS

In Three-Dimensional (3-D) SC-PML regions, the z component of Ampere's law for the frequency-domain modified Maxwell's equations, can be written as:

$$j\omega\varepsilon_r(\omega)E_z = \frac{c_0}{S_x}\frac{\partial H_y}{\partial x} - \frac{c_0}{S_y}\frac{\partial H_x}{\partial y}, \qquad (1)$$

where c_0 is the speed of the light in free space, S_x and S_y are the complex stretched coordinate metrics and for the conventional PML, they are defined as:

$$S_\eta = \kappa_\eta + \sigma_\eta / j\omega\varepsilon, \quad \eta = x \text{ or } y, \qquad (2)$$

where ε is the permittivity of the FDTD domain, $\sigma_\eta \geq 0$ is the conductivity profile different from zero only in the PML region to provide attenuation for the propagating waves and $\kappa_\eta \geq 1$ is different from 1 only in the PML region to attenuate the evanescent waves.

The conventional PML has been explained for a poor absorption of evanescent waves in [12-13]. With the CFS scheme, proposed by Kuzuoglu and Mittra in [14], S_η is defined as:

$$S_\eta = \kappa_\eta + \sigma_\eta \big/ (\alpha_\eta + j\omega\varepsilon), \qquad (3)$$

where κ_η is positive real and ≥ 1 and α_η is assumed to be positive real and introduced to better absorb the evanescent waves. Several algorithms with this metric have been proposed to successfully validate the capability of the CFS-PML in the absorption of evanescent waves [3, 15-17].

To make the PML completely independent of the material properties of the FDTD computational domains, (1) can be rewritten as:

$$j\omega D_z = \frac{c_0}{S_x}\frac{\partial H_y}{\partial x} - \frac{c_0}{S_y}\frac{\partial H_x}{\partial y}. \qquad (4)$$

In terms of the electric flux density D defined as:

$$D_z = \varepsilon_r(\omega) E_z, \quad (5)$$

where $\varepsilon_r(\omega)$ is the relative permittivity of the FDTD computational domain.

Consider a linear isotropic multi-term Lorentz dispersive media with an electrical permittivity $\varepsilon_r(\omega)$ of:

$$\varepsilon_r(\omega) = \varepsilon_\infty + \sum_{k=1}^{M} \frac{G_k(\varepsilon_s - \varepsilon_\infty)\omega_{pk}^2}{(j\omega)^2 + j\omega\Gamma_k + \omega_{0_k}^2}, \quad (6)$$

where M is the number of dispersive terms, $\varepsilon_s = \varepsilon_r(0)$, $\varepsilon_\infty = \varepsilon_r(\infty)$, G_k is the pole amplitude, $\sum_{k=1}^{M} G_k = 1$, ω_{pk} is the plasma frequency, ω_{0k} is the resonance frequency and Γ_k is the damping factor. Substituting (6) into (5), we obtain:

$$D_z = \left[\varepsilon_\infty + \sum_{k=1}^{M} \frac{G_k(\varepsilon_s - \varepsilon_\infty)\omega_{pk}^2}{(j\omega)^2 + j\omega\Gamma_k + \omega_{0_k}^2} \right] E_z. \quad (7)$$

Transforming (7) from the frequency domain to the Z-domain [19], we obtain:

$$D_z = \varepsilon_\infty E_z + \sum_{k=1}^{M} \frac{\tilde{G}_k \exp(-\gamma_k \Delta t)\sin(\beta_k \Delta t) z^{-1}}{1 - 2\exp(-\gamma_k \Delta t)\cos(\beta_k \Delta t) z^{-1} + \exp(-2\gamma_k \Delta t) z^{-2}} E_z, \quad (8)$$

where $\tilde{G}_k = \Delta t \beta^{-1} G_k(\varepsilon_s - \varepsilon_\infty)\omega_{pk}^2$, $\beta_k = (\omega_{0k}^2 - \Gamma_k^2/4)^{1/2}$ and $\gamma_k = \Gamma_k / 2$. Consequently, this PML can be applied to truncate an arbitrary medium and all that is needed is to modify $D_z = \varepsilon_r(\omega) E_z$ under consideration. The method is available in [8] to obtain E from D.

Transforming (4) from the frequency domain to the Z-domain, we obtain:

$$\frac{1 - z^{-1}}{c_0 \Delta t} D_z = S_x(z) \cdot \frac{\partial H_y}{\partial x} - S_z(z) \cdot \frac{\partial H_x}{\partial y}, \quad (9)$$

where Δt is the time step and $S_\eta(z), (\eta = x, y)$ is the Z-transform of $1/S_\eta$, which can be obtained by first transforming $1/S_\eta$ to the s-domain using the relation $j\omega \to s$ and then applying the bilinear Z-transform method [19] using the relation $s \to (2/\Delta t)(1 - z^{-1})/(1 + z^{-1})$:

$$S_\eta(z) = C_\eta \cdot \left(\frac{1 - a_\eta z^{-1}}{1 - b_\eta z^{-1}} \right) \quad (\eta = x, y), \quad (10)$$

where: $a_\eta = (1 - \Delta t \alpha_\eta / 2\varepsilon_0) / (1 + \Delta t \alpha_\eta / 2\varepsilon_0)$

$b_\eta = (1 - (\Delta t / 2)(\alpha_\eta / \varepsilon_0 + \sigma_\eta / \varepsilon_0 \kappa_\eta)) / (1 + (\Delta t / 2)(\alpha_\eta / \varepsilon_0 + \sigma_\eta / \varepsilon_0 \kappa_\eta))$

$C_\eta = \kappa_\eta^{-1} (1 + \Delta t \alpha_\eta / 2\varepsilon_0) / (1 + (\Delta t / 2)(\alpha_\eta / \varepsilon_0 + \sigma_\eta / \varepsilon_0 \kappa_\eta))$.

Substituting (10) into (9), we obtain:

$$\frac{1 - z^{-1}}{c_0 \Delta t} D_z = C_x \cdot \left(\frac{1 - a_x z^{-1}}{1 - b_x z^{-1}} \right) \cdot \frac{\partial H_y}{\partial x} - C_y \cdot \left(\frac{1 - a_y z^{-1}}{1 - b_y z^{-1}} \right) \cdot \frac{\partial H_x}{\partial y}. \quad (11)$$

Introducing two auxiliary variables P_{zx} and P_{zy}:

$$\begin{aligned} P_{zx} &= C_x \cdot \left(\frac{1}{1 - b_x z^{-1}} \right) \cdot \frac{\partial H_y}{\partial x} \\ &= b_x z^{-1} P_{zx} + C_x \cdot \frac{\partial H_y}{\partial x} \end{aligned}, \quad (12)$$

$$\begin{aligned} P_{zy} &= C_y \cdot \left(\frac{1}{1 - b_y z^{-1}} \right) \cdot \frac{\partial H_x}{\partial y} \\ &= b_y z^{-1} P_{zy} + C_y \cdot \frac{\partial H_x}{\partial y} \end{aligned}. \quad (13)$$

Equation (11) can be written as:

$$\frac{1 - z^{-1}}{c_0 \Delta t} D_z = (1 - a_x z^{-1}) P_{zx} - (1 - a_y z^{-1}) P_{zy}. \quad (14)$$

Considering that the z^{-1} operator corresponds to a single-step delay in the discrete time domain, (12) – (14) can be written in the FDTD form, respectively, as (15) – (17), where:

$$P_{zx}\Big|_{i,j,k+1/2}^{n+1} = b_{x(i)} P_{zx}\Big|_{i,j,k+1/2}^{n} + \frac{C_{x(i)}}{\Delta x} \cdot \left(H_y\Big|_{i,j+1/2,k+1/2}^{n+1/2} - H_y\Big|_{i,j-1/2,k+1/2}^{n+1/2} \right), \quad (15)$$

$$P_{zy}\Big|_{i,j,k+1/2}^{n+1} = b_{y(j)} P_{zy}\Big|_{i,j,k+1/2}^{n} + \frac{C_{y(j)}}{\Delta y} \cdot \left(H_x\Big|_{i,j+1/2,k+1/2}^{n+1/2} - H_x\Big|_{i,j-1/2,k+1/2}^{n+1/2} \right), \quad (16)$$

$$D_z\Big|_{i,j,k+1/2}^{n+1} = D_z\Big|_{i,j,k+1/2}^{n} + c_0\Delta t\cdot[P_{zx}\Big|_{i,j,k+1/2}^{n+1} - a_{x(i)}P_{zx}\Big|_{i,j,k+1/2}^{n} - (P_{zy}\Big|_{i,j,k+1/2}^{n+1} - a_{y(j)}P_{zy}\Big|_{i,j,k+1/2}^{n})] \quad (17)$$

To obtain E_z from D_z, we now introduce two auxiliary variables, Q_k and L_k $(k=1,2,..,M)$, so that we can solve for E_z^{n+1} by:

$$E_z\Big|_{i,j,k+1/2}^{n+1} = \frac{1}{\varepsilon_\infty} D_z\Big|_{i,j,k+1/2}^{n+1} - \frac{1}{\varepsilon_\infty}\sum_{k=1}^{M}(a_k Q_k\Big|_{i,j,k+1/2}^{n} - L_k\Big|_{i,j,k+1/2}^{n} + b_k E_z\Big|_{i,j,k+1/2}^{n}) \quad (18)$$

$$Q_k\Big|_{i,j,k+1/2}^{n+1} = a_k Q_k\Big|_{i,j,k+1/2}^{n} - L_k\Big|_{i,j,k+1/2}^{n} + b_k E_z\Big|_{i,j,k+1/2}^{n}, \quad (19)$$

$$L_k\Big|_{i,j,k+1/2}^{n+1} = \exp(-2\gamma_k\Delta t) Q_k\Big|_{i,j,k+1/2}^{n}, \quad (20)$$

where $a_k = 2\exp(-\gamma_k\Delta t)\cos(\beta_k\Delta t)$, $b_k = \tilde{G}_k\Delta t\exp(-\gamma_k\Delta t)\sin(\beta_k\Delta t)$ and $(k=1,2,..,M)$. We can calculate E_z^{n+1}, the current value of E from the current of D, the previous value of E and the previous values of Q and L. The real advantage comes when we deal with more complicated materials. A similar method can be used for other regions of SC-PML.

III. NUMERICAL RESULT

To show the validity of the proposed D-B CFS-PML formulations, we implement a 3-D FDTD simulation for the linear two-term Lorentz dispersive problem in a cubic FDTD grid. A modulated Gaussian pulse with a vertically polarized point electric dipole source, was excited at the center of a $40\Delta_x\times 40\Delta_y\times 40\Delta_z$ electrically dispersive computational domain, entirely composed of a two-term Lorentz material with the following parameters: M=2, ε_∞=2, ε_s=4, G_1=0.8, $\omega_{p1}=\omega_{01}=2\pi\times 14\times 10^9$ rad/s, $\Gamma_1=0.06\omega_{01}$, G_2=0.2, $\omega_{p2}=\omega_{02}=2\pi\times 20\times 10^9$ rad/s and $\Gamma_2=0.07\omega_{02}$. The excited Gaussian pulse is given by:

$$E_z = \sin(2\pi f_c t)\exp(-(t-t_0)^2/t_w^2), \quad (21)$$

where f_c=25 GHz, t_w=31 ps and t_0=4 t_w. The simulation is done with a $40\times 40\times 40$ grid including 10-cell thick PML layers at each edge, as shown in Fig. 1. The space is discretized with the FDTD lattice with $\Delta x=\Delta y=\Delta z=120\,\mu$m and the time step is Δt=0.324 ps. Within the PML, σ_η and κ_η are scaled using a fourth-order polynomial scaling and α_η is a constant, as in [3]. The relative reflection error (in decibels) versus time is computed at an observation point located at (48, 48, 48), using error $=20\log_{10}(|E_z(t)-E_{\text{zref}}(t)|/|E_{\text{zref\_max}}|)$, where $E_z(t)$ is the field computed using the test domain, $E_{\text{zref}}(t)$ is the reference field based on an extended lattice and $E_{\text{zref\_max}}$ is the maximum value of the reference solution over the full-time simulation. The relative reflection error of the ZT-CFS-PML is computed first over 6000 time iterations for $\kappa_{\max}$=16, α_η=0.07 and $\sigma_{\max}$=93.78 S/m. This same example is repeated with the ZT-SC-PML ($\kappa_{\max}$=16, α_η=0, and $\sigma_{\max}$=106.28 S/m) and the ADE-SC-PML ($\kappa_{\max}$=10, α_η=0, and $\sigma_{\max}$=112.54 S/m). These optimum parameters are chosen empirically to obtain the lowest reflection. The difference of the optimum parameters of ZT-CFS-PML and ADE-SC-PML results from different schemes (i.e., the coefficients of (15)-(17) are different from the counterpart of proposed SC-PML in [18]).

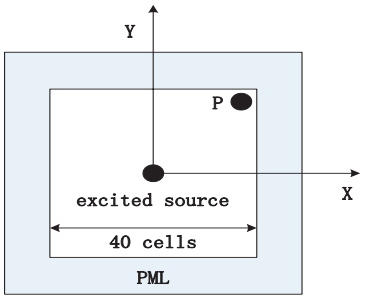

Fig.1. the FDTD grid geometry in this simulation.

These results are illustrated in Fig. 2. It is shown in Fig. 2, that the maximum relative errors of

the ZT-CFS-PML, the ZT-SC-PML and the ADE-SC-PML are -78 dB, -63 dB and -63 dB, respectively. It can be concluded from Fig. 2, that the absorbing performance of the ZT-CFS-PML has 15 dB improvement in terms of the maximum relative error as compared with the ZT-SC-PML and the ADE-SC-PML and much lower reflection error for the late-time region; whereas the ZT-SC-PML and the ADE-SC-PML have comparatively high reflection errors over the entire simulation, due to the oblique incidence of the waves and low-frequency evanescent fields that are interacting with the PML interfaces.

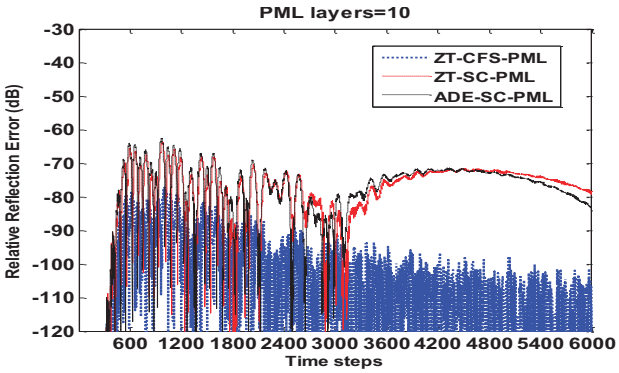

Fig. 2. Relative reflection error versus time: the ZT-CFS-PML, the ZT-SC-PML and the ADE-SC-PML, for a linear two-term Lorentz dispersive FDTD problem.

In the second example, in order to show the validity of the proposed algorithm, the second 3D inhomogeneous problem is used for validating the proposed formulations. We implement the 3D problem of the electromagnetic scattering by a highly elongated object, is studied in [20]. Particllarly, a thin 100 mm × 25 mm plate is immersed in a background media [20] with constitutive parameters ε and σ , shown in Fig. 3.

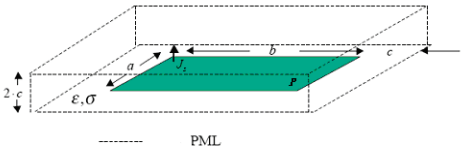

Fig. 3. The FDTD grid geometry in this simulation.

For the purposes of this study, constitutive parameters for soil are assumed, giving σ =0.273 and ε_r =7.73. The plate is illuminated by a vertically polarized electric current source placed just above one corner of the plate. The current source is given a differentiated Gaussian time signature with a 6 GHz bandwidth. The simulation is done with a $126\times51\times26$ grid, including 10-cell-thick PML layers placed only three cells from the scatter on all sides with the space steps $\Delta x=\Delta y=\Delta z=1$ mm. To study the reflection error due to the proposed ZT-CFS-PML, a reference problem is also simulated. To this end, the same mesh is extended 50 cells out in all dimensions, leading to a $226\times151\times126$ cell lattice. The fields within the lattice are then excited by an identical source and the time-dependent fields are recorded within the region representing the original lattice. The relative reflection error (in dB) versus time is computed at an observation point in the corner of the computational domain using equation in [20]. The relative reflection error is first computed over 1800 time iterations. The relative reflection error computed with 10 cells PML is recorded in Fig. 4.

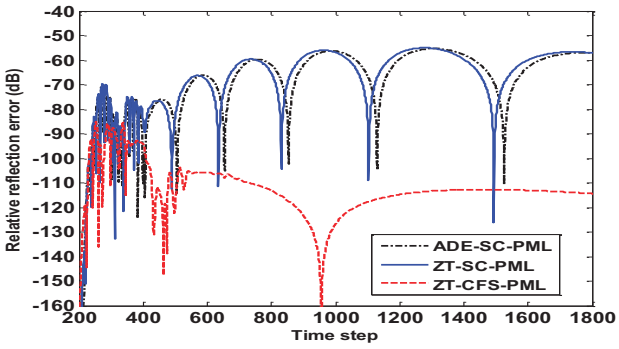

Fig. 4. Relative reflection error versus time: the ZT-CFS-PML, the ZT-SC-PML and the ADE-SC-PML.

These results are illustrated in Fig. 4. It is shown in Fig. 4, that the maximum relative errors of the ZT-CFS-PML, the ZT-SC-PML and the ADE-SC-PML are -85 dB, -54 dB and -54 dB, respectively. It can be concluded from Fig. 4, that the absorbing performance of the ZT-CFS-PML has31 dB improvement in terms of the maximum

relative error, as compared with the ZT-SC-PML and the ADE-SC-PML and much lower reflection error for the late-time region; whereas the ZT-SC-PML and the ADE-SC-PML have comparatively high reflection errors over the entire simulation, due to the oblique incidence of the waves and low-frequency evanescent fields that are interacting with the PML interfaces.

IV. CONCLUSION

The D-B CFS-PML based on the unsplit-field formulations and the *Z*-transform method has been presented for truncating open-region multi-term Lorentz dispersive FDTD domains. These formulations are fully independent of the material properties of the FDTD computational domain and hence arbitrary media, like the Debye and Drude models, can be truncated without any modification and all that is needed is to modify the D-B constitutive relations under consideration. It is clearly shown in the numerical tests that the proposed formulations with the CFS-PML scheme, are efficient in the absorption of evanescent waves and in the reduction of the late-time reflections.

ACKNOWLEDGMENT

These works are supported by the Natural Science Foundation of China (NSFC), under Grants 41240029, ZDYZ2012-1-03, 41390453 and 61301008.

REFERENCES

[1] J. P. Bérenger, "A perfectly matched layer for the absorption of electromagnetic waves," *J. Computat. Phys.*, vol. 114, no. 2, pp. 185-200, October 1994.

[2] W. C. Chew and W. H. Weedon, "A 3-D perfectly matched medium from modified Maxwell's equations with stretched coordinates," *Microw. Opt. Technol. Lett.*, vol. 7, no. 13, pp.599-603, September. 1994.

[3] J. A. Roden and S. D. Gedney, "Convolution PML (CPML): an efficient FDTD implementation of the CFS-PML for arbitrary media," *Microw. Opt. Technol. Lett*., vol. 27, no. 5, pp. 334-339, December 2000.

[4] G. X. Fan and Q. H. Liu, "A well-posed PML absorbing boundary condition for lossy media," *in Proc. IEEE Antennas Propagat. Soc. Int. Symp. Dig*., vol. 3, pp. 2-5, Boston, MA, July 8-13, 2001, Also published in *Antennas Wireless Propag. Lett*., vol. 2, pp. 97-100, 2003.

[5] O. Ramadan, "Auxiliary differential equation formulation: an efficient implementation of the perfectly matched layer," *IEEE Microw. Wireless Compon. Lett.*, vol. 13, no. 2, pp. 69-71, February 2003.

[6] J. Li and J. Dai, "An efficient implementation of the stretched coordinate perfectly matched layer," *IEEE Microw. Wireless Compon. Lett.*, vol. 17, no. 5, pp. 322-324, May 2007.

[7] O. Ramadan and A. Y. Oztoprak, "DSP techniques for implementation of perfectly matched layer for truncating FDTD domains," *Electron. Lett.*, vol. 38, no. 5, pp. 211-212, 2002.

[8] D. M. Sullivan, "Frequency-dependent FDTD methods using z transforms," *IEEE Trans. Antennas Propag.*, vol. 40, no. 10, pp. 1223-1230, 1992.

[9] J. Li and J. Dai, "Efficient implementation of stretched coordinate perfectly matched layer using DSP techniques," *Electron. Lett.*, vol. 42, no. 17, pp. 953-955, 2006.

[10] J. Li and J. Dai, "Efficient implementation of the stretched coordinate perfectly matched layer based on the z-transform method," *IET Microw. Antennas Propag.*, vol. 1, no. 3, pp. 645-650, 2007.

[11] O. Ramadan and A. Y. Oztoprak, "Z-transform implementation of the perfectly matched layer for truncating FDTD domains," *IEEE Microw. Wireless Compon. Lett.*, vol. 13, no. 9, pp. 402-404, September 2003.

[12] J. P. Bérenger, "Evanescent waves in PMLs: origin of numerical reflection in wave-structure interaction problems," *IEEE Trans. Antennas Propag.*, vol. 47, pp. 1497-1503, 1999.

[13] J. De Moerloose and M. A. Stuchley, "Behavior of Berenger's ABC for evanescent waves," *IEEE Microwave Guided Wave Lett*., vol. 5, pp. 344-346, October 1995.

[14] M. Kuzuoglu and R. Mittra, "Frequency dependence of the constitutive parameters of causal perfectly matched anisotropic absorbers," *IEEE Microw. Guided Wave Lett.*, vol. 6, no. 12, pp. 447-449, December 1996.

[15] J. Li and J. Dai, "Z-transform implementation of the CFS-PML for arbitrary media," *IEEE Microw. Wireless Compon. Lett.*, vol. 16, no. 8, pp. 437-439, August 2006.

[16] J. Li and C. Miao, "An efficient FDTD implementation of the CFS-PML based on the ADE method and its validation along with the PLRC method in dispersive media," *ICMMT*, pp. 766-769, April 2008.

[17] D. Correia and J. M. Jin, "A simple and efficient implementation of CFS-PML in the FDTD analysis of periodic structures," *IEEE Microw. Wireless*

Compon. Lett., vol. 15, no. 7, pp. 487-489, July 2005.

[18] O. Ramadan, "General ADE formulations of SC-PML for modeling multi-term dispersive FDTD applications," *Electron. Lett.*, vol. 47, no. 20, pp. 1122-1124, 2011.

[19] J. G. Proakis and D. G. Manolakis, "Digital signal processing: principles, algorithms and applications," *Prentice Hall International Editions, 3rd edn*, 1996.

[20] N. Feng, J. Li and X. Zhao, "Efficient FDTD implementation of the higher-order PML using DSP techniques for arbitrary media," *IEEE Trans. Antennas Propag.*, vol. 61, no. 5, pp. 2623-2629, May 2013.

Naixing Feng received his B.S. degree in Electronic Science and Technology and his M.S. degree in Micro-Electronics and Solid-State Electronics from Tianjin Polytechnic University, Tianjin, China in 2010 and 2013, respectively. He is currently working towards his Ph.D. degree in Radio Physics at Xiamen University, Xiamen. His current research interests include computational electromagnetics and acoustics.

Yongqing Yue received her B.S. degree in Specialty of Communication Engineering at the School of Information Science and Engineering at Shandong University, Jinan, China in 2013. She is currently working towards her M.S degree in Radio Physics at Xiamen University, Xiamen. Her current research interests include computational electromagnetics and acoustics.

Qing Huo Liu received his B.S. and M.S. degrees in Physics from Xiamen University in 1983 and 1986 and his Ph.D. degree in Electrical Engineering from the University of Illinois at Urbana-Champaign in 1989.

His research interests include computational electromagnetics and acoustics, inverse problems, geophysical subsurface sensing, biomedical imaging, electronic packaging and the simulation of photonic and nano devices. He has published over 500 papers in refereed journals and conference proceedings. He was with the Electromagnetics Laboratory at the University of Illinois at Urbana-Champaign as a Research Assistant from September 1986 to December 1988 and as a Postdoctoral Research Associate from January 1989 to February 1990. He was a Research Scientist and Program Leader with Schlumberger-Doll Research, Ridgefield, CT from 1990 to 1995. From 1996 to May 1999 he was an Associate Professor with New Mexico State University. Since June 1999, he has been with Duke University, where he is now a Professor of Electrical and Computer Engineering.

Liu is a Fellow of the IEEE, a Fellow of the Acoustical Society of America, a member of Phi Kappa Phi, Tau Beta Pi and a full member of U.S. National Committee of URSI Commissions B and F. Currently he serves as the Deputy Editor in Chief of Progress in Electromagnetics Research, an Associate Editor for IEEE Transactions on Geoscience and Remote Sensing and an Editor for Computational Acoustics. He was a Guest Editor in Chief of Proceedings of the IEEE for a special issue on large-scale computational electromagnetics published in 2013. He received the 1996 Presidential Early Career Award for Scientists and Engineers (PECASE) from the White House, the 1996 Early Career Research Award from the Environmental Protection Agency and the 1997 CAREER Award from the National Science Foundation.

Chunhui Zhu received her Ph.D. degree in Control Science and Engineering from Harbin Institute of Technology in 2012. From October 2009 to October 2011, she was with the Electrical Engineering Department at Duke University, Durham, NC as a visiting student. Since January 2013, she has been with Xiamen University, where she is currently an Assistant Professor of the Department of Electronic Science. Her research interest is fast algorithms for computational electromagnetics and their applications in engineering.

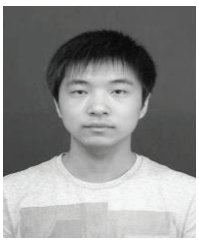

Liangtian Wan was born in Liaoning, China on August 9, 1989. He received his Bachelor degree from Harbin Engineering University. He is studying for his Master and Ph.D. degree at the College of Information and Communication Engineering, at Harbin Engineering University. He is a Reviewer of many international journals. His research interests include array signal processing, compressed sensing and its applications.

Multi-Band Metamaterial Absorber: Design, Experiment and Physical Interpretation

F. Dincer[1], M. Karaaslan [2], E. Unal [2], O. Akgol [2], and C. Sabah [3]

[1] Department of Computer Engineering
Mustafa Kemal University, Iskenderun, Hatay 31200, Turkey

[2] Department of Electrical and Electronics Engineering
Mustafa Kemal University, Iskenderun, Hatay 31200, Turkey

[3] Department of Electrical and Electronics Engineering
Middle East Technical University, Kalkanli, Guzelyurt, TRNC/Mersin 10, Turkey
sabah@metu.edu.tr

Abstract ― This paper presents the design, fabrication, characterization and experimental verification of a perfect Multi-Band Metamaterial (MTM) absorber (MA) based on a simple configuration of a rectangular resonator and strips operating in microwave frequency regime. The proposed multi-band MA provides perfect absorption with TE-incident angle independency. Maximum absorption rate is achieved as 99.43% at 5.19 GHz for simulation and 98.67% at 5.19 GHz for experiment, respectively. The measurement results of the fabricated prototype are in a good agreement with the numerical results. Furthermore, we introduce a numerical analysis in order to show physical interpretation of the MA mechanism in detail. Additionally, a sensor application of the proposed multi-band MA is presented to demonstrate an extra feature of the suggested structure. As a result, the proposed multi-band MA enables myriad potential application areas such as radar, stealth, shielding, communication, imaging and medical applications.

Index Terms – Absorber, metamaterial, microwave and multi-band.

I. INTRODUCTION

Since MTMs present unusual electric and magnetic features which are not commonly found in nature, such as negative refraction, MTM studies have gained a great attention in literature by the science community. In addition, these artificial materials have many potential applications like electromagnetic cloaking, filter, super lens, sensor, absorber and so on [1-7]. Moreover, because of their fabrication flexibility, MTMs can be artificially manufactured in desired frequency regimes of the electromagnetic spectrum from radio frequencies to optics [8-14].

Since MAs have wide potential application areas in these days, for example, radar and medical technologies; various MA studies have been proposed and realized in literature to achieve almost perfect absorption. There are some studies on MAs [15-20] such as bandwidth-enhanced microwave absorber [16], an extremely broad band absorber [18], tunable MA [19], a resonant microwave absorber based on a chiral MTM SRRs [20], etc. Unlike the conventional MA studies, this proposed model has several crucial advantages. One of them is to have properties of TE-incident angle independency for different angles. Another one is to exhibit a wide Fractional Bandwidth as (FBW) ≈ 4.62% at resonance frequency of 5.19 GHz. A third one is to have multi-band perfect absorption feature and the final one is that the suggested structure is very sensitive for sensor applications.

II.THEORETICAL ANALYSIS

Reflection and transmission waves have to be minimized ($\mathrm{R}(\omega)\& T(\omega) \to 0$), in order to achieve a perfect absorption. The reason is that the absorption level of the MAs is calculated by: $\mathrm{A}(\omega) = 1 - \mathrm{R}(\omega) - \mathrm{T}(\omega)$, where $\mathrm{A}(\omega)$ is the absorption, $\mathrm{R}(\omega) = |\mathrm{S}_{11}|^2$ is the reflectance and $\mathrm{T}(\omega) = |\mathrm{S}_{21}|^2$ is the transmittance,

Submitted On: November 15, 2013
Accepted On: April 21, 2014

correspondingly. To achieve perfect absorption with near-zero reflection, the effective permittivity and permeability should have the same value. If both incident electric and magnetic field responses can be properly tuned, it can provide perfect absorption. Moreover, to obtain perfect absorption, the reflection and transmission coefficients should be minimized by impedance matching at a certain resonance frequency range. In the resonance condition, the effective impedance can match to the free space impedance and therefore the reflection is minimized [15-17]. In this case, absorbed energy is constrained in the structure at the resonance frequency and this property of the proposed absorber can also be used on solar cell applications to improve their efficiency [21, 22].

III. SIMULATION AND EXPERIMENT

Proposed MA consists of a rectangular resonator, strips, a metal plate and a dielectric substrate. Top layer resonators and the bottom layer metal plate are separated by an FR4-substrate. While the resonators provide resonance at a certain resonance frequency regime, the metal plate provides zero transmission. Resonators and the metal layer are modeled as a copper sheet. It has electrical conductivity of 5.8×10^7 S/m and thickness of 0.035 mm. The thickness, loss tangent, relative permittivity and permeability values of the FR4 are 1.6, 0.02, 4.2 and 1 mm, respectively. Figure 1 (a) shows the dimensions of the resonators. Dimensions of the proposed model are tuned to increase the resonance and it can be seen that the gaps in the structure are created for this purpose. It is well known that at least one resonance (electric or magnetic) should be provided by the structure for the absorption. The magnetic resonance is generally provided by circulating and anti-parallel currents. The electric resonance is provided by the parallel currents. These resonances are directly related with dielectric thickness sandwiched between front and backside metallic layers. When the distance between the front and back side is increased, the mentioned resonances become weaker. Hence, the thickness of dielectric slab must be selected optimally to provide strong resonances. This issue is also mentioned in the following sections.

In addition, Fig. 1 (b) shows the MA sample fabricated by conventional printed circuit board techniques. The dimension of the sample contains 7x7 unit cells. The overall size of our sample is 70x55 mm^2. Designed MA structure is simulated by using a full-wave electromagnetic solver based on finite integration technique. The sample is then fabricated with PCB technique. To obtain experimental results, the reflection coefficient of the sample is measured by a Vector Network Analyzer (VNA) and two horn antennas, with the experimental setup shown in Fig. 1 (c). Firstly, free space measurement without the MNG structure is carried out and this measurement is used as the calibration data for the VNA. The structure is then inserted into the experimental measurement setup and *S*-parameter measurements are performed. Initially, the distance between the horn antennas and MTM sample is kept sufficiently large to eliminate near-field effects. The discrepancies between the experimental and simulation data as well as the minor noise in the data are imputed to fabrication tolerances related to the etching process and the dielectric dispersion of the substrate used. The misalignment during the experiment may also be considered as another source of error. In addition, the measurement results are normalized values with respect to the peak point to ignore undesired diffraction due to the limited array of the structure. The accuracy of the measurements can be clarified by the good agreement between the simulation and experimental results.

IV. NUMERICAL AND EXPERIMENTAL RESULTS

Simulated and measured reflection-absorption results are presented in Figs. 2 and 3, individually. It can be seen that the maximum absorption rate is 99.43% at 5.19 GHz for simulation and 98.67% at 5.19 GHz for experiment, respectively. In addition, we performed bandwidth calculations to show qualification of the proposed MA model. For this purpose, we carried out a Fractional Bandwidth (FBW) calculation of the negative region. FBW is the ratio between the bandwidth of the MA and the center frequency. It can be calculated as: $\mathrm{FBW} = \Delta f / f_0$, where Δf is the half power bandwidth and f_0 is the center frequency. In this structure, these parameters are obtained as $\Delta f = 0.24$ GHz, $f_0 = 5.19$ GHz and FBW$\approx$4.62%. Moreover, in order to show multi-band property of the suggested MA, we numerically analyzed the model for a high frequency range, as shown in Fig. 4. It can be seen that the designed resonators show perfect absorptions separately in various frequency

points, in which they can be used for the places where multiband operations are needed.

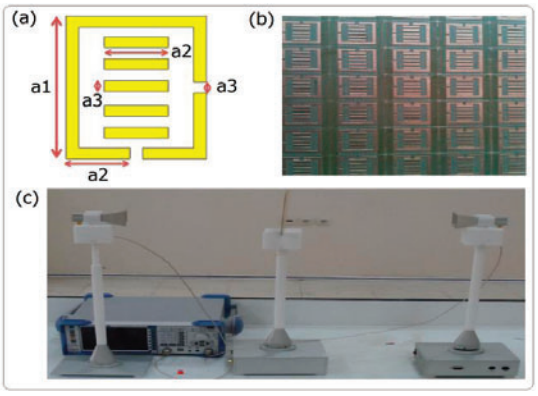

Fig. 1. Multi-band MA; (a) dimensions of the proposed structure with a1 = 13 mm, a2 = 5 mm and a3 = 2 mm, (b) a photograph of the front side of the fabricated sample and (c) a picture from the measurement setup.

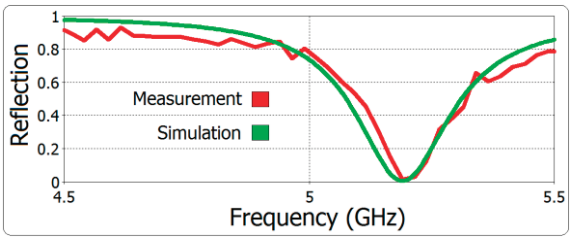

Fig. 2. Simulated and measured reflectivity of the MA as a function of frequency.

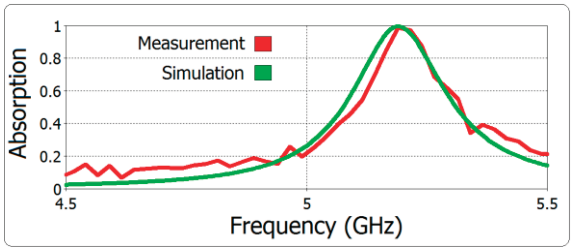

Fig. 3. Simulated and measured absorption of the MA as a function of frequency.

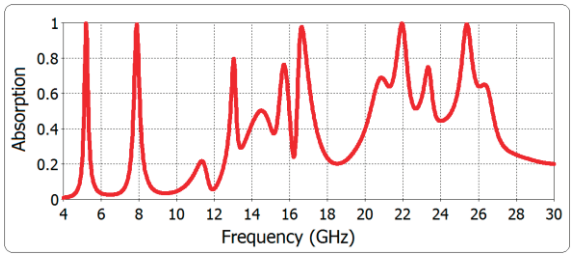

Fig. 4. Simulated absorption of the proposed multi-band MA.

Furthermore, the effects of TE-incident angle on multi-band MA are observed. For this purpose, TE-incident angle was rotated numerically from 0^0 to 90^0 with 15^0 steps, as shown in Fig. 5. The reference plane for the rotated angle is selected as the front face of the periodic structure. When the TE-incident angle is increased from 0^0 to 60^0, the absorption level also increases. Besides, when the value of polarization angle is 90^0, the absorption reaches the lowest level (85.56%). It means that the absorption slightly changes with TE-incident angles. However, all TE-incident angles show resonance at the same frequency level of 5.19 GHz. Note that similar observations are also scrutinized for TM polarization.

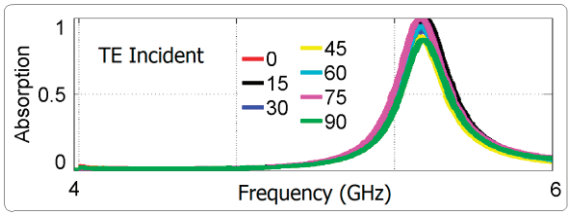

Fig. 5. Angular dependence of the absorption for TE incidence radiation.

We explored the electric field and surface current distributions to show the physical mechanism of the operation principle of the structure at the resonance frequency of 5.19 GHz (Figs. 6 and 7). A high density of the electric field around the rectangular resonator (except the gap area) and a low density around the strips inside are detected, as shown in Fig. 6. The electric field is strongly coupled on the rectangular resonator (except the gap area) and gives an electrical response at the resonance frequency. In addition, magnetic response due to surface charge inductions, leads also to have a magnetic resonance. As seen from the current distribution, parallel currents are responsible for the electric response; whereas the circulating and anti-parallel currents are related with the magnetic response. The configuration is designed as in the proposed form in order to have all mentioned current distributions (parallel, circulating and anti-parallel) for both electric and magnetic resonances together at the resonant frequency. It means that both electric and magnetic resonances occur at the resonance. These responses strongly couple with the electric and magnetic field components of the incident wave and produce strongly localized EM field at

the resonance frequency. Hence, impedance matching condition is provided to confine the incident energy in the absorber that results in minimum reflection and maximum absorption.

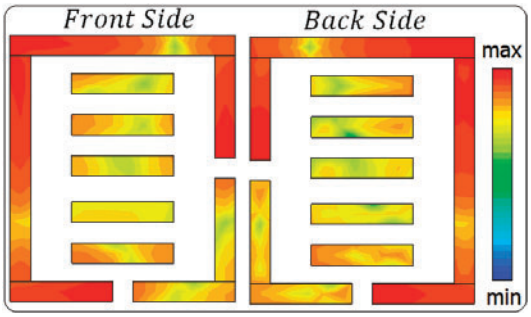

Fig. 6. Electric field distribution at the resonance frequency of 5.19 GHz.

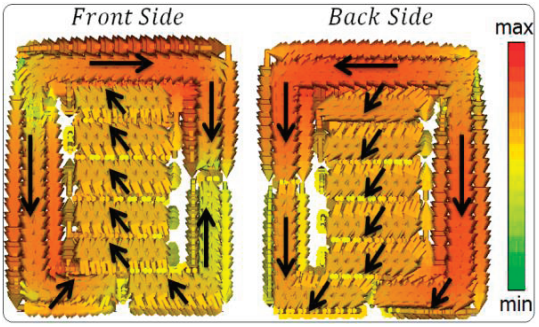

Fig. 7. Surface current distribution at the resonance frequency of 5.19 GHz.

V. SENSOR APPLICATION OF THE PROPOSED MA

The suggested multi-band MA structure can also be used for sensor applications, in the case when the dielectric thickness of the MA is changing. Therefore, in this part, the effect of a variation of the dielectric thickness on the reflection values is investigated for pressure sensor applications. The dielectric thickness is altered from 1.5 mm to 3.5 mm. The reflection data of the simulations for different dielectric thickness are shown in Fig. 8. It can be seen that the reflection values change with the variation of the dielectric thickness (i.e. $S_{11} = 0.02$ for 1.5 mm and $S_{11} = 0.60$ for 3.5 mm at the resonances). The resonance frequency shifts to lower frequencies when the thickness of the FR4-dielectric is increased. The reason of this downward shift can be explained by the variation of the pressure of the overall structure. Hence, the proposed structure can also be used as a pressure sensor in addition to its absorber applications. Besides, a sensor based on the suggested MA would have TE-incident angle independency and easily obtainable frequency range.

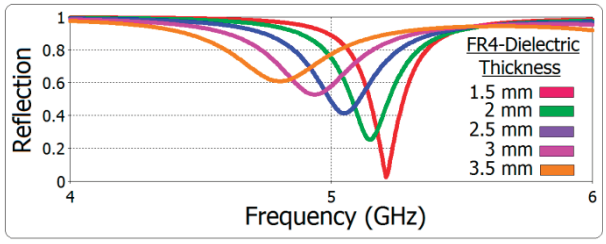

Fig. 8. Sensor application of the suggested multi-band MA.

VI. CONCLUSION

In conclusion, absorption properties of the proposed MA are numerically and experimentally investigated and evaluated. The proposed multi-band MA has simple geometry and shows efficient results for the studied microwave frequency range. Obtained results support our claim that the model can be used as a perfect absorber and is also suitable for absorber applications in a wide frequency range, due to the flexibility of the design. Moreover, the proposed model provides polarization and incident angle independencies and it can be designed for other frequency regimes, such as THz and optics by a simple rescale operation. Additionally, the proposed model can be used in long-distance radio telecommunications, many satellite communications transmissions, some Wi-Fi devices, some cordless telephones, some weather radar systems and so on.

ACKNOWLEDGMENT

Karaaslan acknowledges the support of TUBITAK under the Project Number of 113E290 and partial support of the Turkish Academy of Sciences.

REFERENCES

[1] M. R. I. Faruque, M. T. Islam and N. Misran, "Evaluation of em absorption in human head with metamaterial attachment," *The Applied Computational Electromagnetics Society*, vol. 25, pp. 1097-1107, 2010.

[2] M. Veysi and A. Jafargholi, "Directivity and bandwidth enhancement of proximity-coupled microstrip antenna using metamaterial cover," *The Applied Computational Electromagnetics Society*, vol. 27, pp. 925, 2012.

[3] Y. Huang, G. Wen, T. Li and K. Xie, "Positive-negative-positive metamaterial consisting of ferrimagnetic host and wire array," *The Applied*

Computational Electromagnetics Society, vol. 25, pp. 696-702, 2010.

[4] N. Fang, H. Lee, C. Sun and X. Zhang, "Sub–diffraction-limited optical imaging with a silver superlens," *Science*, vol. 308, pp. 534-537, 2005.

[5] C. Sabah and H. G. Roskos, "Broadside-coupled triangular split-ring-resonators for terahertz sensing," *The European Physical Journal Applied Physics*, vol. 61, 30402, 2013.

[6] J. B. Pendry, D. Schurig and D. R. Smith, "Controlling electromagnetic fields," *Science*, vol. 312, pp. 1780-1782, 2006.

[7] F. Bilotti, L. Nucci and L. Vegni, "An SRR-based microwave absorber," *Microwave and Optical Technology Letter*s, vol. 48, pp. 2171-2175, 2006.

[8] M. C. K. Wiltshire, J. B. Pendry, I. R. Young, D. J. Larkman, D. J. Gilderdale and J. V. Hajnal, "Micro structured magnetic materials for RF flux guides in magnetic resonance imaging," *Science*, vol. 291, pp. 849-851, 2001.

[9] C. Sabah and S. Uckun, "Multilayer system of lorentz/drude type metamaterials with dielectric slabs and its application to electromagnetic filters," *Progress In Electromagnetics Research*, vol. 91, pp. 349-364, 2009.

[10] M. Gokkavas, K. Guven, I. Bulu, K. Aydin, R. S. Penciu, M. Kafesaki, C. M. Soukoulis and E. Ozbay, "Experimental demonstration of a left-handed metamaterial operating at 100 GHz," *Physical Review B*, vol. 73, 193103, 2006.

[11] T. J. Yen, W. J. Padilla, N. Fang, D. C. Vier, D. R. Smith, J. B. Pendry, D. N. Basov and X. Zhang, "Terahertz magnetic response from artificial materials," *Science*, vol. 303, pp. 1494-1496, 2004.

[12] S. Linden, C. Enkrich, M. Wegener, J. Zhou, T. Koschny and C. M. Soukoulis, "Magnetic response of metamaterials at 100 terahertz," *Science*, vol. 306, pp. 1351-1353, 2004.

[13] S. Zhang, W. Fan, N. C. Panoiu, K. J. Malloy, R. M. Osgood and S. R. J. Brueck, "Experimental demonstration of near-infrared negative-index metamaterials," *Physical Review Letters*, vol. 95, 137404, 2005.

[14] G. Dolling, M. Wegener, C. M. Soukoulis and S. Linden, "Negative-index metamaterial at 780 nm wavelength," *Optics Letters*, vol. 32, pp. 53-55, 2007.

[15] Y. J. Huang, G. J. Wen, J. Li, W. R. Zhu, P. Wang and Y. H. Sun, "Wide-angle and polarization-independent metamaterial absorber based on snowflake-shaped configuration," *Journal of Electromagnetic Waves and Applications*, vol. 27, pp. 552-559, 2013.

[16] J. Lee and S. Lim, "Bandwidth-enhanced and polarization-insensitive metamaterial absorber using double resonance," *Electronics Letters*, vol. 47, pp. 8-9, 2011.

[17] N. I. Landy, S. Sajuyigbe, J. J. Mock, D. R. Smith and W. J. Padilla, "Perfect metamaterial absorber," *Physical Review Letters*, vol. 100, 207402, 2008.

[18] J. Sun, L. Liu, G. Dong and J. Zhou, "An extremely broad band metamaterial absorber based on destructive interference," *Optics Express*, vol. 19, pp. 21155-21162, 2011.

[19] B. Zhu, Y. Feng, J. Zhao, C. Huang, Z. Wang and T. Jiang, "Polarization modulation by tunable electromagnetic metamaterial reflector/absorber," *Optics Express*, vol. 18, pp. 23196-23203, 2010.

[20] B. Wang, T. Koschny and C. M. Soukoulis, "Wide-angle and polarization-independent chiral metamaterial absorber," *Physical Review B*, vol. 80, 033108, 2009.

[21] F. Dincer, O. Akgol, M. Karaaslan, E. Unal and C. Sabah, "Polarization angle independent perfect metamaterial absorbers for solar cell applications in the microwave, infrared, and visible regime," *Progress In Electromagnetics Research*, vol. 144, pp. 93-101, 2014.

[22] Y. Liu, Y. Chen, J. Li, T. Hung and J. Li, "Study of energy absorption on solar cell using metamaterials," *Solar Energy*, vol. 86, pp. 1586-1599, 2012.

Furkan Dincer received his B.Sc. and M.Sc. degrees in Electrical and Electronics Engineering from Sutcu Imam and Yuzuncu Yil Universities, Turkey. He is now a Ph.D. student at Mustafa Kemal University, Hatay, Turkey. His research interests are related with the functional microwave structures and metamaterials.

Muharrem Karaaslan received his Ph.D degree in Physics from the University of Cukurova, Adana, Turkey in 2009. He is the coauthor of about 20 scientific contributions published in journals and conference proceedings. His research interests are applications of metamaterials, analysis and synthesis of antennas and waveguides.

Emin Unal received his Ph.D degree in Electrical and Electronics Engineering from the University of Gaziantep, Turkey in 1994. He is the coauthor of about 20 scientific contributions published in journals and conferences His research interest are FSS and metamaterials.

Oguzhan Akgol received his B.Sc., M.Sc. and Ph.D. degrees in Electrical and Electronics Engineering from Inonu University, Turkey; Polytechnic University, Brooklyn, NY, USA and the University of Illinois at Chicago (UIC), Chicago, IL, USA. He is now working at Mustafa Kemal University, Hatay, Turkey. His research interests are EM scattering, antennas and DNG materials.

Cumali Sabah received his B.Sc., M.Sc. and Ph.D. degrees in Electrical and Electronics Engineering from the University of Gaziantep, Turkey. He is currently with Middle East Technical University - Northern Cyprus Campus. His research interests include the microwave and electromagnetic investigation of unconventional materials and structures, wave propagation, scattering, complex media, metamaterials and their applications.

Microstrip-Fed Monopole Antenna with Triple Band Performance for WLAN/WiMAX Applications

N. Ojaroudi [1], M. Mehranpour [1], S. Ojaroudi [2], and Y. Ojaroudi [2]

[1]Young Researchers Club
Ardabil Branch, Islamic Azad University, Ardabil, Iran
n.ojaroudi@yahoo.com, mehranpour.mehdi@gmail.com

[2]Young Researchers Club
Germi Branch, Islamic Azad University, Germi, Iran
s.ojaroudi.p@gmail.com, y.ojaroudi@iaugermi.ac.ir

Abstract ─ In this paper, a printed monopole antenna is presented for wireless local area network (WLAN) and worldwide interoperability for microwave access (WiMAX) applications. The desired resonant frequencies are obtained by cutting four L-shaped slits in both sides of square radiating patch and an H-shaped slot around the slits. Prototypes of the proposed antenna have been constructed and studied. The measured impedance bandwidth for l0 dB return loss is from 2.23 GHz to 2.60 GHz (15.0 %), 3.05 GHz to 4.10 GHz (29.3 %) and 5.02 GHz to 5.86 GHz (15.2 %), covering the 2.4/3.5/5.5 GHz for WLAN/WiMAX applications. Simulated and experimental results obtained for this antenna show that the proposed antenna has a good radiation behavior within the 2.4/3.5/5.5 GHz frequencies.

Index Terms ─Microstrip-fed monopole antenna, L-shaped slit, triple-band, and ultra-wideband (UWB) systems.

I. INTRODUCTION

In the last few years, there have been rapid developments in wireless local area network (WLAN) and worldwide interoperability for microwave access (WiMAX) applications. The 2.4/5.2/5.8 GHz (2.4 GHz-2.84 GHz / 5.15 GHz-5.35 GHz / 5.725 GHz-5.825 GHz) and 2.5/3.5/5.5 GHz (2.500-2690/3400-369/5250-5850 MHz) bands are demanded in practical WLAN and WiMAX applications, respectively. During the last years, there are various antenna designs, which enable antennas with low-profile, light weight, flush mounted and WLAN/WiMAX devices. These antennas include the planar inverted-F antennas [1], the chip antennas [2], and the planar dipole and monopole antennas [3-4].

In this paper, a multiband printed antenna is proposed. The size of the designed antenna is smaller than that of the antennas [1-4] for WLAN/WiMAX application. By cutting four L-shaped slits and an H-shaped slot, we can tune frequency bands. Details of the antenna design are described, and prototypes of the proposed antenna for WLAN/WiMAX operations at the 2.4 GHz, 3.5 GHz, and 5.5 GHz frequencies have been constructed and tested.

II. ANTENNA DESIGN

The proposed monopole antenna fed by a microstrip line is shown in Fig. 1, which is printed on an FR4 substrate of thickness 1.6 mm, and permittivity 4.4. The proposed antenna configuration comprises pairs of L-shaped slits and an H-shaped slot cut on the square radiating patch. The basic monopole antenna structure consists of a square patch, a feed line, and a ground plane. The triple-band performance of the proposed antenna is significantly affected by using the modified radiating patch on top layer of the substrate.

In order to design a multi-band antenna in the first step, two L-shaped slits in the bottom corners of the antenna radiating patch are used to perturb a

Submitted On: July 25, 2012
Accepted On: March 9, 2014

new resonance. By cutting another pair of L-shaped slits in the top corners of the radiating patch the antenna can create the second resonant frequency in individual resonant radiation band.

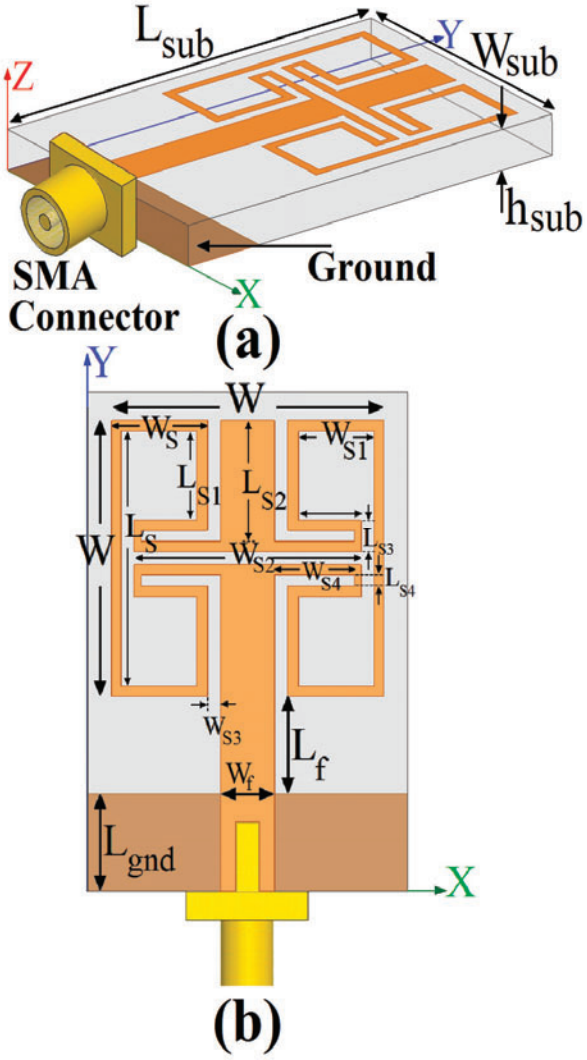

Fig. 1. Geometry of the proposed monopole antenna, (a) side view and (b) top view.

By creating these modified slits additional current paths are provided on the radiating patch. Moreover, these structures change the inductance and capacitance of the input impedance, which in turn leads to change the bandwidth. Therefore, by cutting four L-shaped slits at the square radiating patch and carefully adjusting its parameters, extra frequency resonances are exited and dual-band performance can be achieved. In the proposed configuration the modified H-shaped slot is playing an important role in the multi band characteristics of this antenna, because it can creates another additional surface current path in the antenna therefore additional (third) resonance is excited.

The dimensions of the proposed antenna are as follows: W_{Sub} = 12 *mm*, L_{Sub} = 18 *mm*, h_{Sub} = 1.6 *mm*, W = 10 *mm*, W_f = 2 *mm*, L_f = 3.5 *mm*, W_S = 3.5 *mm*, L_S = 9.5 *mm*, W_{S1} = 3 *mm*, L_{S1} = 3.5 *mm*, W_{S2} = 8.5 *mm*, L_{S2} = 4.5 *mm*, W_{S3} = 0.5 *mm*, L_{S3} = 1 *mm*, W_{S4} = 3 *mm*, L_{S4} = 0.5 *mm*, and L_{gnd} = 3.5 *mm*.

III. RESULTS AND DISCUSSIONS

In this section, the monopole antenna with various design parameters was constructed. The simulated results are obtained using the Ansoft simulation software high-frequency structure simulator (HFSS) [5].

Figure 2 shows the structure of the various antennas used for triple-band performance simulation studies. Return loss characteristics for ordinary square monopole antenna with two L-shaped slits, with four L-shaped slits, and the proposed antenna (simulated and measured results) are compared in Fig. 3.

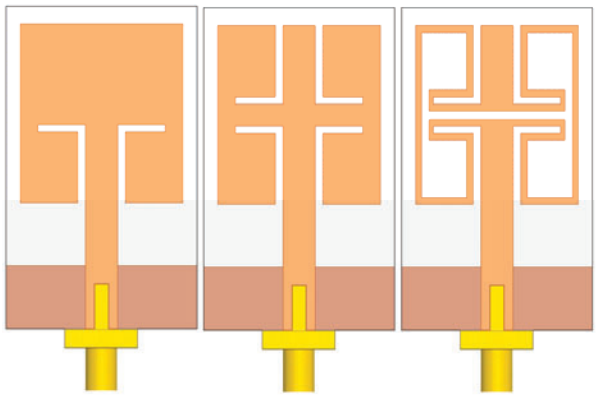

(a) (b) (c)

Fig. 2. (a) Ordinary square antenna with two L-shaped slits, (b) with four L-shaped slits, and (c) the proposed antenna structure.

In Fig. 3, the square antenna with two L-shaped slits resonates single band 3.5 GHz. The square antenna with four L-shaped slits on the radiating patch produces dual-band 3.5 GHz / 5.5 GHz. Finally, by cutting a modified H-shaped slot in the radiating patch a triple-band is achieved that covering all the 2.4/3.5/5.5GHz.

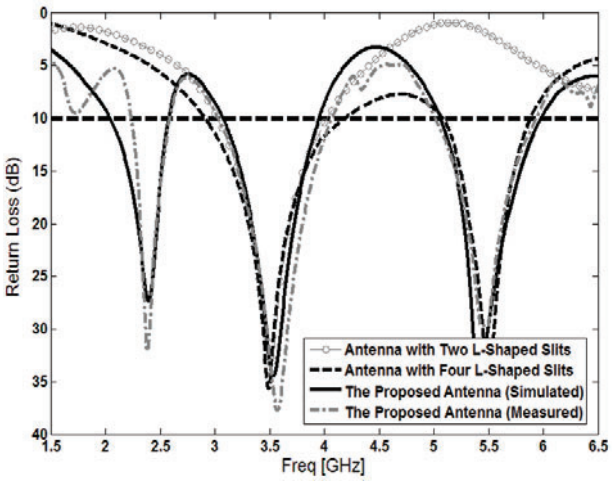

Fig. 3. Return loss curves of three antennas shown in Fig. 2.

In order to understand the phenomenon behind this additional resonance performance, the simulated current distributions on the radiating patch for the ordinary square antenna with two and four L-shaped slits on the radiating patch at 3.5 GHz and 5.5 GHz are presented in Fig. 4 (a) and (b), respectively. It is found that, the current flows are more dominant around of the L-shaped slits at these frequencies [9-11].

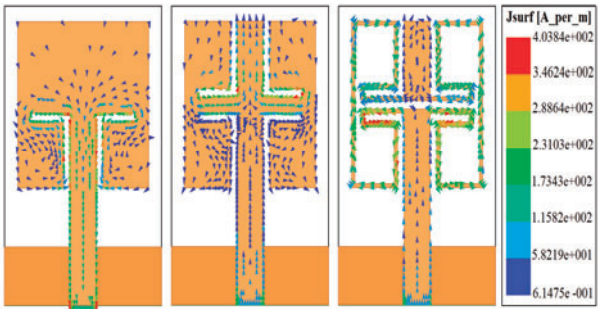

Fig. 4. Simulated surface current distributions for the ordinary square patch antenna with two and four L-shaped slits, and the proposed antenna at (a) 3.5 GHz, (b) 5.5 GHz, and (c) 2.4 GHz.

Another important design parameter of this structure is a modified H-shaped slot on the radiating patch. Figure 4 (c) present the simulated current distributions on the radiating patch of the proposed antenna at the first resonance frequency (2.4 GHz). As shown in Fig. 4 (c), at 2.4 GHz, the current flows are more dominant around of the H-shaped slot.

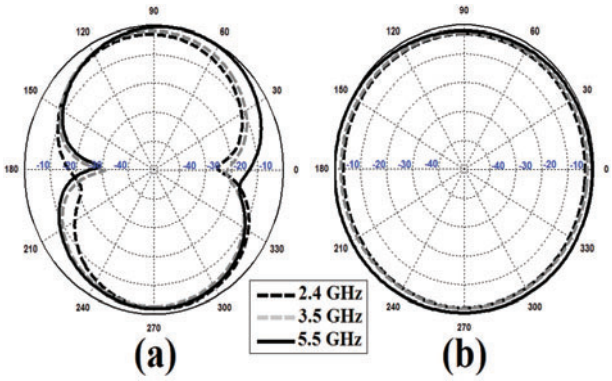

Fig. 5. Measured radiation patterns of the proposed antenna, (a) E-plane and (b) H-plane.

Figure 5 depicts the measured radiation patterns of the proposed antenna including the co-polarization in the H-plane (x-z plane) and E-plane (y-z plane). It can be seen that quasi-omnidirectional radiation pattern can be observed on x-z plane over the whole operation bands. The radiation patterns on the y-z plane display a typical figure-of-eight, similar to that of a conventional dipole antenna. It should be noticed that the radiation patterns in E-plane become imbalanced as frequency increases because of the increasing effects of the cross polarization [12-15].

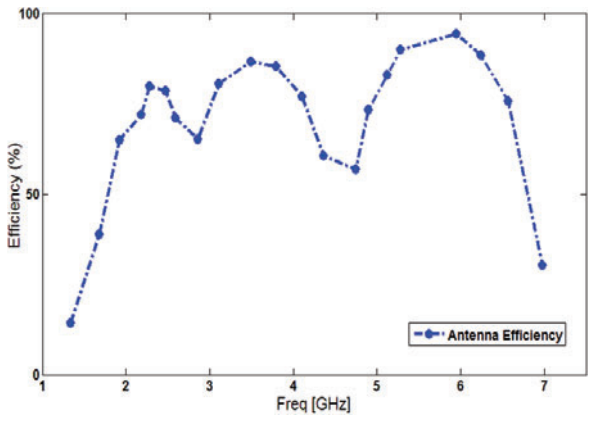

Fig. 6. Simulated radiation efficiency values of the proposed monopole antenna.

The simulated radiation efficiency characteristic of the proposed antenna is shown in Fig. 6. Results of the calculations using the software HFSS indicated that the proposed

antenna features a good efficiency, being greater than 75 % across the entire radiating bands. The measured maximum gains of the proposed antenna are presented in Fig. 7. As seen, the proposed antenna has a gain that is low at 2 GHz and increases with frequency. The proposed antenna has sufficient and acceptable gain level in the operation bands [8].

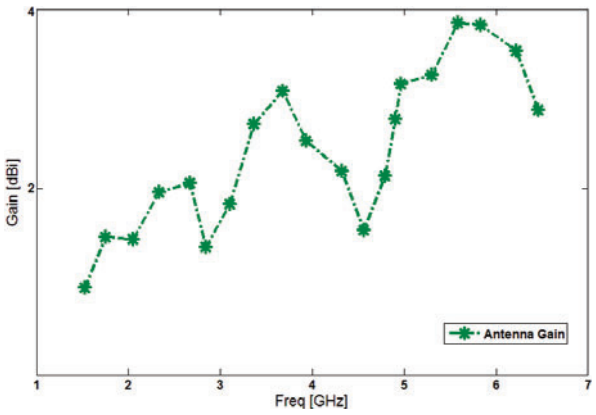

Fig. 7. Measured maximum gain property of the proposed antenna.

Table I summarizes the previous designs and the proposed antenna. As seen, the proposed antenna has a compact size with very wide bandwidth in compared the pervious works. In addition, as the proposed antenna has symmetrical structure, in compared with previous multi-band antennas, the proposed antenna displays a good omnidirectional radiation pattern even at lower and higher frequencies. Also the proposed microstrip-fed monopole antenna has sufficient and acceptable radiation efficiency and antenna gain levels in the operation bands.

Table I: Comparison of previous designs with the proposed antenna.

Ref.	Operation	Size (mm)	Gain (dBi)
[1]	Dual-band	33×33	2.5~3.5
[2]	Single-band	4×12	1~2
[3]	Dual-band	80×20	1~2
[4]	Dual-band	48×60	1.8-4.1
This Work	*Tri-band*	*12×18*	*1.8~3.9*

IV. CONCLUSION

In this letter, a novel multi-band printed monopole antenna for simultaneously satisfying wireless local area network (WLAN) and worldwide interoperability for microwave access (WiMAX) applications is presented. The desired resonant frequencies are obtained by using four L-shaped slits and an H-shaped slot in the radiating patch of the proposed antenna. The size of the designed antenna is smaller than the antennas for WLAN/WiMAX applications that reported recently.

ACKNOWLEDGMENT

The authors are thankful to Microwave Technology (MWT) Company staff for their beneficial and professional help (www.microwave-technology.com).

REFERENCES

[1] M. Ojaroudi, M. Hassanpour, Ch. Ghobadi, and J. Nourinia, "A novel planar inverted-F antenna (PIFA) for WLAN/WiMAX applications," *Microwave and Optical Tech. Letters*, vol. 53, no. 3, August 2011.

[2] W. Choi, S. Kwon, and B. Lee, "Ceramic chip antenna using meander conductor lines," *Electron Lett.*, vol. 37, no. 15, pp. 933-934, 2001.

[3] V. Stoiljkovic, S. Suganthan, and M. Benhaddou, "A novel dual-band center-fed printed dipole antenna," *in Proc. IEEE Antennas Propagation Soc. Int. Symp.*, vol. 2, pp. 938-941, June 2003.

[4] C.-Y. Pan, T.-S. Horng, W.-S. Chen, and C.-H. Huang, "Dual wideband printed monopole antenna for WLAN/WiMAX application," *IEEE Antennas ans Wirless Propagation Letter*, vol. 6, pp. 149-151, 2007.

[5] Ansoft High Frequency Structure Simulation (HFSS), Ver. 13, Ansoft Corporation, 2010.

[6] G. Zhang, J. Hong, B. Wang, and G. Song, "Switched band-notched UWB/ WLAN monopole antenna," *Applied Computational Electromagnetics Society (ACES) Journal*, vol. 27, no. 3, pp. 256-260, March 2012.

[7] Y. Li, W. Li, and W. Yu, "A switchable UWB slot antenna using SIS-HSIR and SIS-SIR for multi-mode wireless communications applications," *Applied Computational Electromagnetics Society (ACES) Journal*, vol. 27, no. 4, pp. 340-351, April 2012.

[8] A. Mallahzadeh, S. Seyyedrezaei, N. Ghahvehchian, S. Mohammad, and S. Mallahzadeh, "Tri-band printed monopole antenna for WLAN and WiMAX MIMO systems,"

Proceedings of the 5th European Conference on Antennas and Propagation (EUCAP), pp. 548-551, 2011.

[9] N. Ojaroudi, "Design of ultra-wideband monopole antenna with enhanced bandwidth," *21th Telecommunications Forum,* TELFOR, Belgrade, Serbia, pp. 1043-1046, 27 – 28 November 2013.

[10] N. Ojaroudi, "A new design of koch fractal slot antenna for ultra-wideband applications," *21th Telecommunications Forum,* TELFOR Belgrade, Serbia, pp. 1051-1054, 27 – 28 November 2013.

[11] N. Ojaroudi, "Compact UWB monopole antenna with enhanced bandwidth using rotated L-shaped slots and parasitic structures," *Microw. Opt. Technol. Lett.*, vol. 56, pp.175-178, 2014.

[12] N. Ojaroudi, S. Amiri, and F. Geran, "A novel design of reconfigurable monopole antenna for UWB applications," *Applied Computational Electromagnetics Society (ACES) Journal*, vol. 28, no. 6, pp. 633-639, July 2013.

[13] N. Ojaroudi, "Application of protruded strip resonators to design an UWB slot antenna with WLAN band-notched characteristic," *Progress in Electromagnetics Research C,* vol. 47, pp. 111-117, 2014.

[14] N. Ojaroudi, "Microstrip monopole antenna with dual band-stop function for UWB applications," *Microw. Opt. Technol. Lett*., vol. 56, pp. 818-822, 2014.

[15] N. Ojaroudi, "Small microstrip-fed slot antenna with frequency band-stop function," *21th Telecommunications Forum*," TELFOR, Belgrade, Serbia, pp. 1047-1050, 27 – 28 November 2013.

A Truncated Waveguide Fed by a Microstrip as a Multi-Band WLAN Antenna

Giovanni Andrea Casula, Giorgio Montisci, Alessandro Fanti, Paolo Maxia, and Giuseppe Mazzarella

Dipartimento di Ingegneria Elettrica ed Elettronica
Università di Cagliari, Piazza D'Armi, Cagliari 09123, Italy
a.casula@diee.unica.it, giorgiom@diee.unica.it, alessandro.fanti@diee.unica.it,
paolo.maxia@diee.unica.it, mazzarella@diee.unica.it

Abstract ─ This paper presents a small truncated waveguide fed by a microstrip line through a transverse coupling slot for multi-band WLAN applications. The analysis of the presented antenna has been performed by replacing the feeding microstrip line with its equivalent Magnetic-Wall Waveguide (MWW) model and using an in-house Method of Moments (MoM) to analyze the structure. The use of entire-domain basis functions both on the slot and on the truncated waveguide apertures allows to obtain a very efficient analysis by exploiting the waveguide modes orthogonality. The proposed radiating element allows to obtain a high radiated power, with a very low cross-polar component in the radiated field, with a -10 dB bandwidth that covers the required frequencies for multi-band WLAN applications (5.2/5.4/5.8 GHz).

Index Terms – Microstrip, waveguide antennas, WLAN antennas.

I. INTRODUCTION

The increasing demands of wireless and short-range and high data rate transmissions, pushed to propose new wireless protocols using different bands of the frequency spectrum in order to support high data rate wireless communications; which led to the request of antennas able to operate at different frequency bands simultaneously (multi-band antennas). In WLAN applications, the most common desirable requirement consists of providing multi-band operations, such as covering 5.2, 5.4 and 5.8 GHz bands for IEEE 802.11a standard.

A number of interesting multi-band antennas for Wireless Local Area Networks (WLAN, IEEE 802.11b/a standard) have been proposed and reported in the literature [1-5]. The most popular solution is the use of microstrip patch antennas, both for their small weight and size, low production cost and ease of fabrication and integration [6]. However, such antennas have a low efficiency, a narrow frequency bandwidth and a relatively high cross-polar component of the radiated field. Moreover, the efficiency of patch antennas is further reduced by the surface waves in the dielectric substrate, which causes power loss and high coupling between the elements in an array environment. All those drawbacks are well known and much literature has been devoted to overcome them. A common choice to improve patch antenna performances is the use of coupling slots in the feeding network in structures with two sandwiched dielectric substrates [7,8]. This solution allows to optimize separately the feeding and the radiating circuit, but increases the production cost and both the design and the realization processes are more difficult.

The narrow frequency band of printed antennas pushed to search for new configurations suitable for broadband applications, which are required for high-speed transfer; such as planar monopoles [9], printed dipoles [10] or slot antennas [11]. The structure proposed in this paper consists of a truncated rectangular waveguide radiator [12], [13], which replaces the patch (and its substrate). This truncated waveguide is fed by the electromagnetic coupling produced by a microstrip transverse slot (Fig. 1). In this way, the

Submitted On: April 18, 2013
Accepted On: April 17, 2014

flexibility (and ease of realization) of the feeding network is retained, but the electromagnetic behaviour of the radiating element is strongly improved. Actually, this configuration allows higher efficiency and a much lower cross-polar component, with respect to a standard patch antenna. Furthermore, the presented structure allows to exploit the advantages of planar technology for the power supply circuit, allowing the realization of matching networks at a low cost and with compact size; especially if compared with the corresponding waveguide network. Another advantage of the described structure is the absence of waveguide-to-microstrip transitions. The performance degradation caused by transitions between planar structures and waveguides can be seen in [14], where a broadband array of circular waveguide radiators is designed with a stripline distribution network fed by a rectangular waveguide. In this structure, the overall efficiency of the array is restricted by unwanted reflections caused by the presence of transitions between the circular waveguide and the stripline and between the stripline and the rectangular waveguide. Finally, the truncated waveguide, as a radiating element, allows to obtain a radiated electromagnetic field with a high polarization purity [13].

The potential drawbacks of the presented structure could be the surface wave, which propagates in the feeding microstrip substrate and the back radiation of the coupling slot. However, the surface wave losses can be minimized by using substrates with suitable dielectric constant and thickness and the back radiation; due to the coupling slot not high since the slot is not resonant (having typical dimensions equal or less than a quarter wavelength) and can be minimized by a suitable choice of the structure parameters.

The radiated power can be modulated by acting on various parameters, such as the length of the coupling slot, its width, the truncated waveguide length and transverse dimensions. Moreover, a thin dielectric slab lying on the slot can be placed inside the radiating element to increase the degrees of freedom in the design process.

The proposed radiating element is designed in this work for multi-band WLAN applications, allowing to obtain a high radiated power, a very low cross-polar component in the radiated field and with a -10 dB bandwidth that covers the required frequency bandwidths (5.2/5.4/5.8 GHz). The analysis of the antenna in Fig. 1 has been performed by replacing the feeding microstrip line with its equivalent Magnetic-Wall Waveguide (MWW) model [15] (as indicated in Fig. 2) and using the well-assessed Method of Moments (MoM) procedure described by the authors in [12], [16-20]. The use of entire-domain basis functions both on the slot and on the truncated waveguide apertures, allows to obtain a very efficient analysis, since their choice has been made in order to exploit the waveguide modes orthogonality.

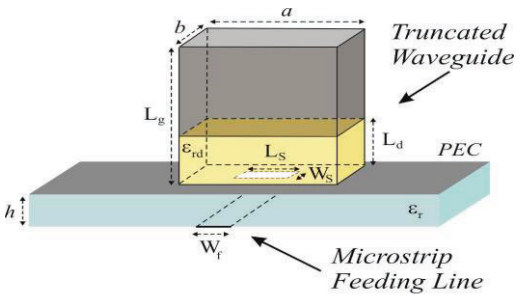

Fig. 1. Radiating element geometry.

II. NUMERICAL ANALYSIS OF THE ANTENNA

The proposed radiating element can fulfill a large range of requirements, thanks to the relatively large number of degrees of freedom. However, the effective use of this flexibility in the design calls for an efficient and accurate analysis procedure. Therefore, our choice has fallen on the Method of Moments (MoM) in the Galerkin formulation using entire domain basis functions (EDBF) [16,21]. As a matter of fact, though it requires some efforts to be devised, compared with differential approaches implemented into general purpose EM solvers, its accuracy and computational effectiveness can hardly be paralleled. Of course, a suitable model of the structure must be devised in order to build-up an in-house software for the analysis of it. The two more critical points are the requirements that the antenna aperture is cut into an infinite PEC plane and the modeling of the feeding microstrip. The former is quite standard [22] and will not be further discussed. On the other hand, an effective modeling of the microstrip line has been achieved by representing the microstrip line with an

equivalent Magnetic-Wall Waveguide (MWW) [23]. This equivalence is a popular tool for analyzing microstrip discontinuities, but it is accurate also for microstrip slots, as long as those slots are well within the MWW [15]. Therefore, the structure that has been actually analyzed is shown in Fig. 2. It consists of a magnetic wall waveguide replacing the microstrip feeding line (Fig. 1), with a transverse coupling slot cut in its ground plane, which feeds a truncated waveguide. The truncated waveguide can be partially filled with a dielectric slab lying on the slot. The slot between the apertures Σ^i and Σ^e radiates into the region bounded by the waveguide and the aperture Σ^r is the antenna element, which radiates into free space.

The MoM full-wave analysis of the structure in Fig. 2 starts by replacing each aperture with an unknown magnetic current. Let $\underline{M}^e$, $\underline{M}^i$ the currents on the two sides of the slot, and $\underline{M}^r$ the current on the external aperture Σ^r. The continuity of the tangential magnetic field is then enforced on each aperture:

$$\begin{cases} \underline{H}_s[\underline{M}^i, \underline{M}^e] - \underline{H}_w[\underline{M}^i] = \underline{H}_{inc} & \text{on } \Sigma^i \\ \underline{H}_s[\underline{M}^i, \underline{M}^e] + \underline{H}_{wt}[\underline{M}^e, \underline{M}^r] = 0 & \text{on } \Sigma^e \\ \underline{H}_{wt}[\underline{M}^e, \underline{M}^r] + \underline{H}_{fs}[\underline{M}^r] = 0 & \text{on } \Sigma^r \end{cases}, \quad (1)$$

where $\underline{H}_{inc}$ is the impressed magnetic field incident under the slot in the feeding microstrip line, $\underline{H}_w$ is the magnetic field in the microstrip region, $\underline{H}_s$ is the magnetic field in the slot region, $\underline{H}_{wt}$ is the magnetic field in the truncated waveguide region and $\underline{H}_{fs}$ is the magnetic field in the free-space region.

Equations (1) are actually a system of integral equations in the unknown currents. In order to solve it, we expanded all unknown in a suitable set of EDBF. The slot can be considered as a waveguide with transverse sections L_S and W_S. Therefore, our EDBF are on all apertures, the lowest-order modes of the relevant waveguides. More precisely, since the slot is narrow we have neglected the longitudinal component of the electric field on it. Therefore, only the magnetic currents directed along x are used as unknowns and are expressed as truncated sinusoidal series with respect to x:

$$\underline{M}^{(i,e)} = \sum_{p=1}^{N} a_p^{(i,e)} \sin\left[\frac{p\pi}{L_S}\left(x + \frac{L_S}{2}\right)\right] \underline{i}_x = \sum_{n=1}^{N} a_p^{(i,e)} \underline{m}^p(x). \quad (2)$$

The magnetic current on the aperture Σ^r is expressed as a linear combination of the truncated waveguide modes. With this choice, in fact, it is possible to exploit the orthogonality of the modal functions (each basis function will excite only one mode of the waveguide), strongly simplifying the calculations of the MoM matrix elements:

$$\begin{aligned} \underline{M}^r &= \sum_{k,j}^{N,M} a_{k,j}^r \sin\left[\frac{k\pi x}{a_T}\right] \cos\left[\frac{j\pi y}{b_T}\right] \underline{i}_x \\ &+ b_{k,j}^r \cos\left[\frac{k\pi x}{a_T}\right] \sin\left[\frac{j\pi y}{b_T}\right] \underline{i}_y \\ &= \sum_{k,j}^{N} a_{k,j}^r \underline{m}_x^{k,j}(x,y) + b_{k,j}^r \underline{m}_y^{k,j}(x,y). \end{aligned} \quad (3)$$

In equations (2) and (3), $a_p^{(i,e)}$, a_{kj}^r and b_{kj}^r are the unknown coefficients of the linear combination.

In the region of the magnetic wall waveguide equivalent to the microstrip feeding line and in the free-space region, the fields are calculated through the Green function of the vector potential $\underline{F}$ in the spectral domain, using a Fourier representation for the currents and potentials [15].

In the two waveguide regions, the fields are simply computed using a model expansion; since every unknown excites a single mode, because of the mode orthogonality.

Expansions (2) and (3) are inserted into (1), which are then projected on the same EDBF used to express the unknown, to get the final linear system of the MoM.

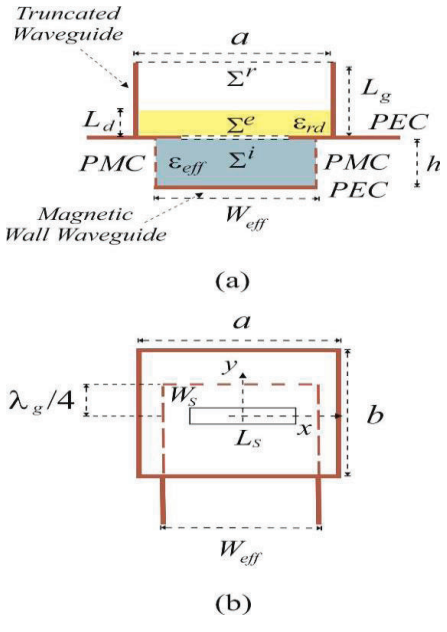

Fig. 2. Radiating element geometry with the MWW replacing the microstrip feeding line: (a) front view and (b) top view.

The reader is referred to section II of [12] for further details of the MoM procedure.

The computational time is mainly due to the matrix filling, while the solution is quite fast. Since the MoM matrix using EDBF is small and relatively well conditioned, a further increase in the computational efficiency can be gained if the matrix is computed only in few points and then interpolated to build-up the full antenna response [16, 24].

Note that the use of the equivalence between a microstrip line and a magnetic-wall waveguide (MWW) [15] is a key point. As a matter of fact, the microstrip line needs not to be discretized and therefore we have to solve a MoM system with about a dozen of unknowns, with respect to the hundreds of unknowns required by a standard planar MoM.

III. ANTENNA DESIGN AND RESULTS

In the analysis of the proposed antenna, the designer has to take into account some specific properties of the structure, in order to obtain an efficient and performing WLAN antenna. In particular, the geometrical dimensions of the radiating element must fulfill the following requirements:

1. The microstrip feeding line must be designed providing that, at the operating frequencies only the fundamental quasi-TEM mode propagates.
2. The transverse dimension a of the truncated waveguide must be chosen in order that only the fundamental TE_{10} mode is excited and the higher modes attenuation is large enough to prevent higher-order mode coupling between the slot and the aperture.

The MoM procedure described in this work has been widely assessed in [12], [16] and [17]; while in [13], both the equivalence between the MWW and the microstrip for our application and the MoM code have been validated by comparison with a general purpose FEM commercial software, Ansys HFSS. In Fig. 3 (a) of [13], a comparison has been performed between the structure fed by the microstrip line and the structure fed by its equivalent magnetic wall waveguide; both simulated with a general purpose FEM commercial software, Ansys HFSS. The results of our MoM procedure have been also reported for a matter of completeness. These comparisons validate both the equivalence between the MWW and the microstrip for our application and the MoM code, since the results of the MoM code and HFSS are virtually equivalent. Since the computational time required by HFSS is about two orders of magnitude greater than the one required by our MoM code [12], [13], for the parametric analysis of the proposed radiating element, we have used the MoM procedure.

In the presented simulations, the design frequency is 5.5 GHz, the dielectric substrate is Roger Duroid 5800 with $\varepsilon_r = 2.2$ and h = 2 mm, the dielectric substrate partially filling the truncated waveguide is Rogers TMM4 with $\varepsilon_r = 4.5$ and the width of the coupling slot is $W_S = 1$ mm.

In order to satisfy the previous requirements 1 and 2 at the design frequency of 5.5 GHz, *a* has been fixed to the value of 50 mm and the width of the microstrip feeding line is $W_f = 6$ mm; which corresponds to a characteristic impedance of 50 Ω. The feeding microstrip line ends with a quarter wavelength termination beyond the coupling slot, as indicated in Fig. 2.

The circuital and radiating properties of the proposed antenna depend on the interaction between the aperture of the truncated waveguide and the coupling slot. The results presented in [12], [13], suggest that the radiated power can be modulated within a very wide range by adequately choosing the geometrical parameters of the structure.

In order to characterize the radiating element, we show its radiated power simulated using the MoM procedure described in section II; as a function of the slot length L_S and of the height L_d of the dielectric substrate partially filling the truncated waveguide for a length L_g of the truncated waveguide equal to 20 mm (Fig. 3). Similar curves are obtained by choosing different lengths for the truncated waveguide. The radiated power has been calculated by the scattering matrix of the structure obtained feeding the radiating element in Fig. 2 using two ports as, $1-|S_{11}|^2-|S_{21}|^2$. The results presented in Fig. 3 suggest that the radiated power can be modulated within a very wide range by adequately choosing the geometrical parameters of the structure. On the other hand, so as to match the radiating element in the required frequency bandwidths (namely, 5.2,

5.4 and 5.8 GHz bands following IEEE 802.11a standard for WLAN applications), its frequency response as a function of the geometrical parameters is shown in Fig. 4; where the reflection coefficient simulated using the MoM procedure described in section II, is shown for different slot lengths, L_S with a length of the dielectric substrate partially filling the truncated waveguide equal to L_d = 7.5 mm and with a length L_g of the truncated waveguide equal to 20 mm. Similar curves are obtained by choosing different lengths for L_d and L_g.

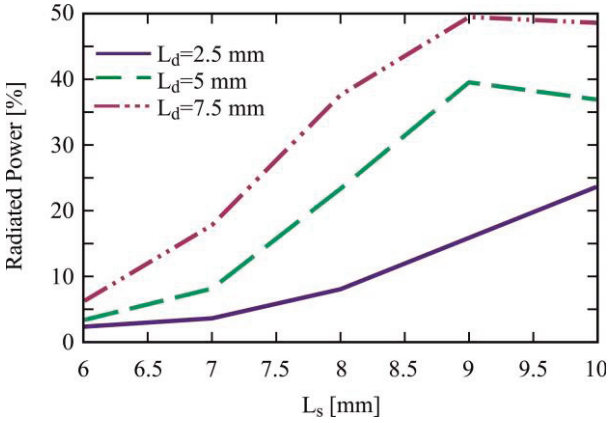

Fig. 3. Simulated (MoM) radiated power (percentage of incident power) for the antenna in Fig. 1, with L_g = 20 mm.

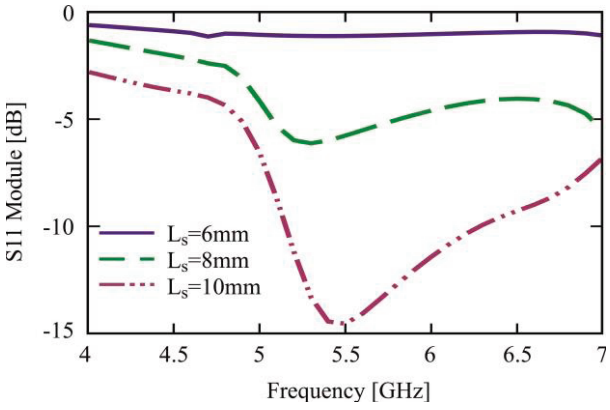

Fig. 4. Simulated (MoM) frequency response for the antenna in Fig. 1, with L_d = 7.5 mm and L_g = 20 mm.

A good compromise between the radiated power, the input matching and the dimensions of the structure is obtained with the following choice of the parameters: L_S = 10 mm, L_d = 7.5 mm and L_g = 20 mm. This choice corresponds to a radiated power around 50% and to a -10 dB bandwidth from 5.1 GHz to 6.4 GHz, as shown in Figs. 4 and 5; where the frequency response of the designed antenna simulated using the MoM procedure described in section II, is reported. In Fig. 5 the reflection coefficient is shown also for different values of the dielectric substrate partially filling the truncated waveguide. It is apparent that the best choice is the use of a dielectric with ε_r = 4.5, namely Rogers TMM4, as we already claimed at the beginning of this section. Figure 6 shows the E-plane and H-plane of the radiated fields for this antenna at the operating frequencies of 5.2, 5.4 and 5.8 GHz, computed using the MoM procedure described in section II. The cross-polar component of the radiated field is very low, with a value below -40 dB, with respect to the co-polar component and the gain of this element is about 6.5 dB in the whole operating bandwidth.

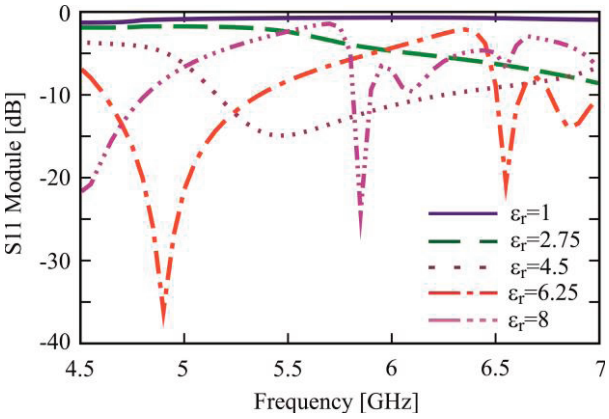

Fig. 5. Simulated (MoM) frequency response for the designed antenna (L_S = 10 mm, L_d = 7.5 mm and L_g = 20 mm).

In order to evaluate the performance improvement of the broadband antenna proposed in this paper, we can compare it with existing solutions for the same WLAN applications. In [25], the proposed multiband E-shaped printed monopole antenna for Multiple-Input–Multiple-Output (MIMO) system, has a good input matching over the operating frequency band; although, the radiated fields are not satisfactory if compared to the radiating element presented in our work showing a high cross-polar component and a significantly lower gain (around 3 dB). The same considerations can be made if we compare the

antenna proposed in this paper with [2], [26] and [27]. These comparisons demonstrate that the presented antenna can be a very competitive candidate as a WLAN antenna.

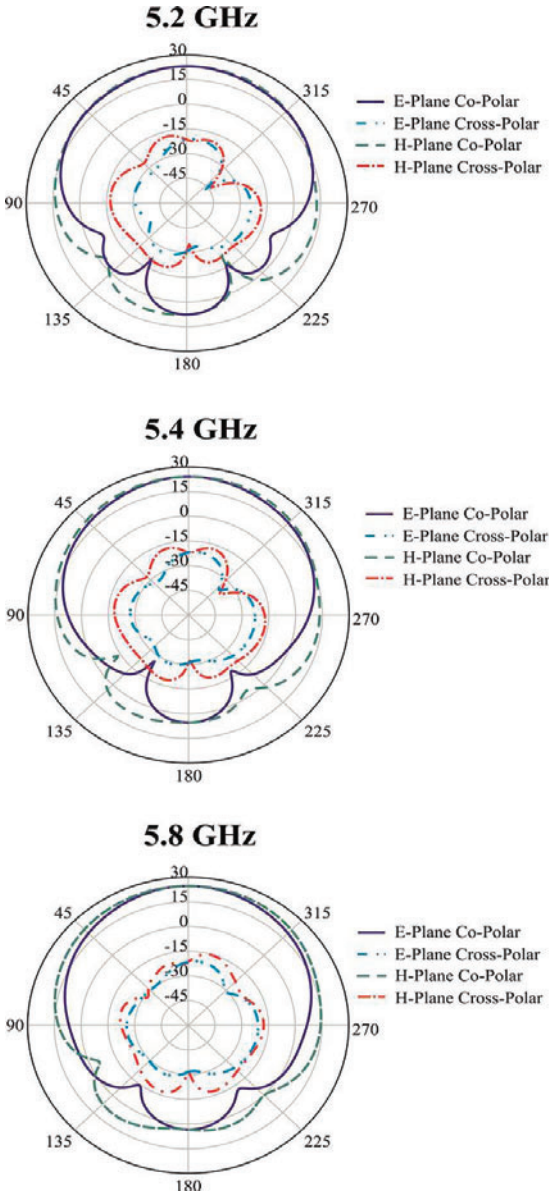

Fig. 6. Far field pattern of the designed antenna, computed using MoM (L_S = 10 mm, L_d = 7.5 mm and L_g = 20 mm).

VI. CONCLUSION

In this work, a small truncated waveguide fed by a microstrip line through a transverse coupling slot for multi-band WLAN applications is presented. An effective and accurate analysis procedure has been devised, using the Method of Moments (MoM), with entire domain basis functions to analyze the structure and replacing the feeding microstrip line with its equivalent Magnetic-Wall Waveguide (MWW) model. This choice allows to fully exploit the flexibility of the proposed radiating element.

A radiating element able to work as a multi-band WLAN antenna, from 5.1GHz to 6.4 GHz, has been obtained. It covers this frequency range with a very good input matching and a negligible cross-polar component in the radiated field and allows a higher radiated power than patch antennas.

ACKNOWLEDGMENT

Maxia gratefully acknowledges Sardinia Regional Government for the financial support of his Ph.D. scholarship (P.O.R. Sardegna F.S.E. Operational Programme of the Autonomous Region of Sardinia, European Social Fund 2007-2013 - Axis IV Human Resources, Objective l.3, Line of Activity l.3.1.).

Alessandro Fanti gratefully acknowledges Sardinia Regional Government for the financial support of his Post-Doc fellowship (P.O.R. Sardegna F.S.E. Operational Programme of the Autonomous Region of Sardinia, European Social Fund 2007-2013 - Axis IV Human Resources, Objective l.3, Line of Activity l.3.1.).

REFERENCES

[1] S. W. Su, "High-gain dual-loop antennas for MIMO access points in the 2.4/5.2/5.8 GHz bands," *IEEE Transactions on Antennas and Propagation*, vol. 58, no.7, pp. 2412-2419, 2010.

[2] J. H. Yoon and Y. C. Lee, "Modified bow-tie slot antenna for the 2.4/5.2/5.8 GHz WLAN bands with a rectangular tuning stub," *Microw. Opt. Technol. Lett.*, vol. 53, RT no. 1, pp. 126-130, 2011.

[3] G. A. Casula, P. Maxia, G. Mazzarella and G. Montisci, "Design of a printed log-periodic dipole array for ultra-wideband applications," *Progress In Electromagnetics Research C*, vol. 38, pp. 15-26, 2013.

[4] P. Wang, G. J. Wen, and Y. Huang, "Compact CPW-fed planar monopole antenna with triple-band operation for WLAN/WiMAX applications," *Applied Computational Electromagnetics Society (ACES) Journal*, vol. 27, no. 8, pp. 691-696, August 2012.

[5] Y. Li, W. Li and W. Yu, "A switchable UWB slot antenna using SIS-HSIR and SIS-SIR for multi-

mode wireless communications applications," *Applied Computational Electromagnetics Society (ACES) Journal*, vol. 27, no. 4, pp. 340-351, April 2012.

[6] M. D. Pozar, "Microstrip antennas: the analysis and design of microstrip antennas and arrays," *IEEE Press*, New York, 1995.

[7] M. Himdi, J. P. Daniel and C. Terret, "Analysis of aperture-coupled microstrip antenna using cavity method," *Electronics Letters,* pp. 391-392, 1983.

[8] G. Di Massa, G. E. Bencivenni, G. Campaniello and G. Mazzarella, "Hole-coupled patch antennas," *IEEE Antennas and Propagation Society, AP-S International Symposium*, vol. 4, pp. 2082-2085, 1995.

[9] G. M. Zhang, J. S. Hong, B. Z. Wang, Q. Y. Qin, B. He and D. M. Wan, "A novel planar monopole antenna with an H-shaped ground plane for dual-band WLAN applications," *Journal of Electromagnetic Waves and Applications*, vol. 21, no. 15, pp. 2229-2239, 2007.

[10] F. J. Wang and J. S. Zhang, "Wideband printed dipole antenna for multiple wireless services," *Journal of Electromagnetic Waves and Applications*, vol. 21, no. 11, pp. 1469-1477, 2007.

[11] Y. L. Chen, C. L. Ruan and L. Peng, "A novel ultra-wideband bow-tie slot antenna in wireless communication systems," *Progress In Electromagnetics Research Letters*, vol. 1, pp. 101-108, 2008.

[12] G. Montisci, G. Mazzarella and G. A. Casula, "Effective analysis of a waveguide longitudinal slot with cavity," *IEEE Trans. Antennas Propagation*, vol. 60, pp. 3104-3110, 2012.

[13] G. A. Casula, G. Mazzarella and G. Montisci, "A truncated waveguide fed by a microstrip as radiating element for high performance automotive anti-collision radars," *International Journal of Antennas and Propagation*, 2012.

[14] J. Navarro, "Wide-band, low-profile millimeter-wave antenna array," *Microwave and Optical Technology Letters*, vol. 34, no. 4, pp. 253-255, 2002.

[15] G. A. Casula, G. Mazzarella and G. Montisci, "Effective analysis of a microstrip slot coupler," *Journal of Electromagnetic Waves and Applications*, vol. 18, no. 9, pp. 1203-1217, 2004.

[16] G. A. Casula, G. Mazzarella and G. Montisci, "Design of shaped beam planar arrays of waveguide longitudinal slots," *International Journal of Antennas and Propagation*, art. no. 767342, 2013.

[17] S. Costanzo, G. A. Casula, A. Borgia, et al., "Synthesis of slot arrays on integrated waveguides," *IEEE Antennas and Wireless Propagation Letters*, vol. 9, pp. 962-965, 2010.

[18] G. A. Casula, G. Mazzarella and G. Montisci, "Design of slot arrays in a waveguide partially filled with a dielectric slab," *Electronics Letters*, vol. 42, pp. 730-731, 2006.

[19] J. Zusheng, G. Montisci, G. A. Casula, H. Yang and J. Lu, "Efficient evaluation of the external mutual coupling in dielectric covered waveguide slot arrays," *International Journal of Antennas and Propagation,* art. no. 491242, 2012.

[20] G. A. Casula, G. Mazzarella and G. Montisci, "Effect of the feeding t-junctions in the performance of planar waveguide slot arrays," *IEEE Antennas and Wireless Propagation Letters*, vol. 11, pp. 953-956, 2012.

[21] S. R. Rengarajan, "Compound radiating slot in a broad wall of a rectangular waveguide," *IEEE Transactions on Antennas and Propagation*, vol. 37, pp. 1116-1124, 1989.

[22] R. E. Collin, "Antennas and radiowave propagation," *McGraw-Hill*, New York, 1986.

[23] I. Wolff, "The waveguide model for the analysis of microstrip discontinuities, numerical technique for microwave and millimeter-wave passive structures," Itoh T. (ed.), *Wiley-Interscience*, NewYork, 1989.

[24] K. L. Virga and Y. Rahmat-Samii, "Efficient wide-band evaluation of mobile communications antennas using [Z] or [Y] matrix interpolation with the method of moments," *IEEE Transactions on Antennas and Propagation*, vol. 47, no. 1, pp. 65-76, 1999.

[25] S. Mohammad, A. Nezhad and H. R. Hassani, "A novel tri-band e-shaped printed monopole antenna for MIMO application," *IEEE Antennas and Wireless Propagation Letters*, vol. 9, pp. 576-579, 2010.

[26] J. Y. Jan and L. C. Tseng, "Small planar monopole antenna with a shorted parasitic inverted-l wire for wireless communications in the 2.4, 5.2, and 5.8 GHz bands," *IEEE Trans. Antenna Propag.*, vol. 52, no. 7, pp. 1903-1905, 2004.

[27] G. A. Casula, G. Mazzarella and N. Sirena, "Evolutionary design of wide-band parasitic dipole arrays," *IEEE Trans. Antenna Propag.*, vol. 59, pp. 4094-4102, 2011.

Giovanni Andrea Casula received his Laurea degree (Summa Cum Laude) in Electronic Engineering and his Ph.D. degree in Electronic Engineering and Computer Science from the University di Cagliari, Cagliari, Italy in 2000 and 2004, respectively. Since March 2006, he is an Assistant Professor of Electromagnetic Field and Microwave Engineering at the Dipartimento di Ingegneria Elettrica ed Elettronica, University of Cagliari; teaching courses in electromagnetics and

microwave engineering. His current research interests are in the field of synthesis, analysis and design of wire, patch and slot antennas. Casula is author (or coauthor) of about 20 papers in international journals, serves as Reviewer for several international journals and is a member of the Italian Electromagnetic Society (SIEm).

Giorgio Montisci received his Laurea degree (Summa Cum Laude) in Electronic Engineering and Ph.D. degree in Electronic Engineering and Computer Science from the University of Cagliari, Cagliari, Italy in 1997 and 2000, respectively. Since November 2000, he has been Assistant Professor of Electromagnetic Eield at the Dipartimento di Ingegneria Elettrica ed Elettronica, University of Cagliari; teaching courses in electromagnetics and microwave engineering. His research activity is mainly focused on analysis and design of waveguide slot arrays, microwave holographic techniques for the diagnostic of large reflector antennas, numerical methods in electromagnetics and printed antennas. He is author (or co-author) of about 30 papers in international journals and Reviewer for EM Journals.

Alessandro Fanti received his Laurea degree in Electronic Engineering and Ph.D. degree in Electronic Engineering and Computer Science from the University of Cagliari, Cagliari, Italy in 2006 and 2012, respectively. He currently holds a Post-Doc scholarship for Design of Microwave Components. His research activity involves the use of numerical techniques for modes computation of guiding structures.

Paolo Maxia received his Laurea degree in Electronic Engineering from the University of Cagliari, Cagliari, Italy in 2008 and since 2011 is a Ph.D. student in Electronic Engineering and Computer Science. His research activity involves the analysis, design and characterization of planar structures, such as printed antennas and passive microwave components.

Giuseppe Mazzarella graduated Summa with Laude in Electronic Engineering from the Università "Federico II" of Naples in 1984 and obtained his Ph.D. in Electronic Engineering and Computer Science in 1989. In 1990, he became Assistant Professor at the Dipartimento di Ingegneria Elettronica at the Università "Federico II" of Naples. Since 1992, he is with the Dipartimento di Ingegneria Elettrica ed Elettronica of the Università di Cagliari, first as Associate Professor and then since 2000, as Full Professor; teaching courses in Electromagnetics, Microwave, Antennas and Remote Sensing. His research activity has focused mainly on: efficient synthesis of large arrays of slots, power synthesis of array factor, microwave holography techniques for the diagnostic of large reflector antennas and use of evolutionary programming for inverse problems solving. He is author (or co-author) of about 50 papers in international journals and is a Reviewer for many EM Journals.

A Novel Design of Reconfigurable Active Integrated Oscillator Feedback Antenna with Electronically Controllable for WiMAX/WLAN Applications

Jalil Mazloum, and Ali Jalali

Faculty of Electrical & Computer Engineering
Shahid Beheshti University, Tehran, Iran
j_mazloum@sbu.ac.ir, a_jalali@sbu.ac.ir

Abstract ─ A novel reconfigurable active oscillator feedback antenna for WiMAX/WLAN applications is presented. By using a rectangular ring with a pair of protruded Γ -shaped strips in the active feedback antenna, two new resonances can be achieved. Also, the proposed rectangular ring with a pair of protruded Γ -shaped strips radiating patch has a major advantage in providing tighter capacitive coupling to the line, in comparison to the known radiating patch. In order to generate DC isolation in the RF path we use a pair of gap distances in the microstrip loop. Also, by using the [S] parameters of the active element a novel design of the microwave oscillator is performed. Simulated and experimental results obtained for this antenna show that the proposed Active Integrated Antenna (AIA) has a good return loss and radiation behavior within the WiMAX/WLAN frequency range.

Index Terms - Oscillator feedback antenna, reconfigurable active integrated antenna, WiMAX/WLAN systems.

I. INTRODUCTION

In multi-band wireless communication systems, one of key issues is the design of a compact active antenna while providing wideband characteristic over the whole operating band. It is a well-known fact that active feedback presents really appealing physical features such as simple structure, small size and low cost. Because of all these interesting characteristics, multi-band feedback oscillator antenna is expected to become a key device for the next generation multi-band and multi-mode wireless radios [1] and growing research activity is being focused on them [2-4]. Various switching based techniques have been proposed to achieve multi-band performance. Some of the topologies use separate oscillators [2] to obtain multi-band response, while others use distinct resonators [3] or matching networks [4] to achieve the same. An alternative switched resonator technique is discussed, wherein, oscillator's negative resistance is controlled by modifying microstrip line resonator's length using a diode based electrical switch. The technique is utilized to realize a dual-band oscillator.

In the last few years there have been rapid developments in Wireless Local Area Network (WLAN) and Worldwide Interoperability for Microwave Access (WiMAX) applications. The 2.4/5.2/5.8 GHz (2.4–2.84/5.15–5.35/5.725–5.825 GHz) and 2.5/3.5/5.5 GHz (2500–2690/3400–3690/5250-5850 MHz) bands are demanded in practical WLAN and WiMAX applications, respectively. During the last year, there have been various antenna designs which enable antennas with low profile, lightweight, flush mounted and WiMAX devices. These antennas include the Planar Inverted-F Antennas (PIFAs) [5], printed monopole antennas [6], the chip antennas [7] and the planar monopole antennas [8]. However, up to now, a printed antenna that has Γ -shaped notch configuration has not been reported.

In this paper we propose a novel frequency reconfigurable active integrated oscillator feedback antenna with the capability to switch between WLAN and WiMAX modes. The antenna

Submitted On: January 3, 2013
Accepted On: March 11, 2014

which uses a switchable slotted structure for reconfigurability has a simple structure and smallest size in comparison to antennas reported in literature [9]-[10]. In the proposed structure based on Electromagnetic Coupling (EC), a rectangular ring with a pair of protruded Γ -shaped strips in the microstrip transmission line is used to perturb two resonance frequencies at 2.4 GHZ (WLAN) and 3.5 GHz (WiMAX). This structure has a major advantage in providing tighter capacitive coupling to the line, in comparison to the known radiating patch [9]. In the proposed configuration a pair of gap distances are playing important roles in the radiating characteristics of this antenna, because it can adjust the electromagnetic coupling effects between the interdigital radiating patch and the microstrip transmission line [10]. Also, the implemented dual-band oscillator exhibited output power level of -16.21 dBm at frequency of 2.399 GHz and -23.09 dBm at frequency of 3.488 GHz, for various diodes bias conditions.

II. SYSTEM DESIGN CONCEPT

According to the feedback oscillator antenna in classification of active antennas, a two or three-terminal negative-resistance device can be connected directly to the terminals of a single antenna element or an array of elements. In this case, DC power is converted to radiate RF power. Oscillator antennas have been discussed for applications such as low-cost sensors, power combining and synchronized scanning antenna arrays [11].

In the microstrip antenna, resonant modes are excited by an inductance–capacitance (L-C) circuit of the resonant antenna. The passive antenna can be expressed by a series inductor-capacitor (LA-CA), as shown in Fig. 1 [3]. Figure 1 also shows the schematic of a Clapp oscillator circuit [4]. Two capacitors, C_{gs} and C_{ds}, are connected in series in the network of a Clapp oscillator circuit of Fig. 1. The resonant frequency of a Clapp oscillator circuit is mainly given by the elements of CA and LA of the conceptual equivalent circuit of the antenna. The passive antenna has two resonant frequencies: 2.4 and 3.5 GHz. Based on the resonant frequencies, the proposed active integrated antenna can be excited at similar resonant frequencies.

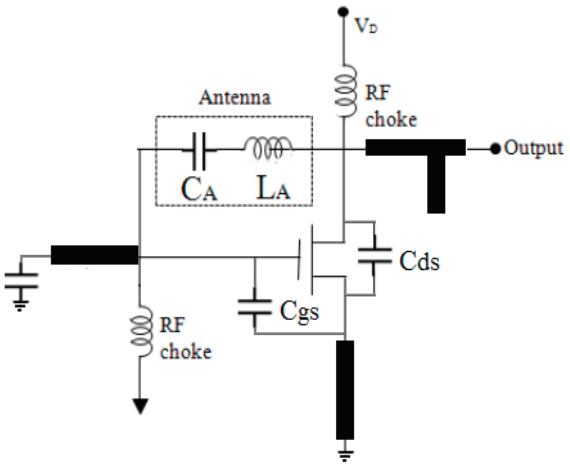

Fig. 1. Schemetice of active integrated antenna having Clapp oscillator circuit.

III. RECONFIGURABLE ANTENNA DESIGN

The proposed passive reconfigurable antenna fed by a 50-Ω feed line is shown in Fig. 2, which is printed on a FR4 substrate of thickness 0.8 mm and permittivity of 4.4. The numerical and experimental results of the input impedance and radiation characteristics are presented and discussed. The parameters of this proposed antenna are studied with parametric study process by changing one or two parameters at a time and fixing the others. The Ansoft simulation software High-Frequency Structure Simulator (HFSS) [12] is used to optimize the design and agreement between the simulation and measurement is obtained.

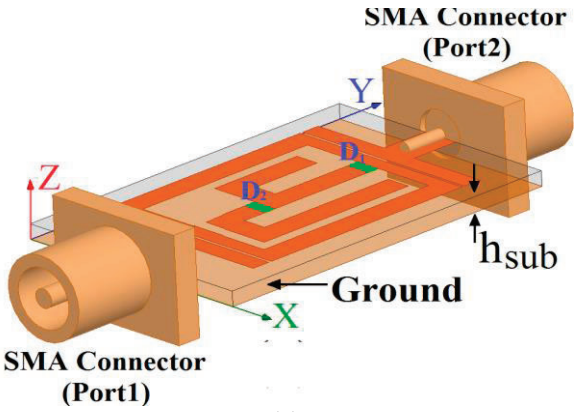

(a)

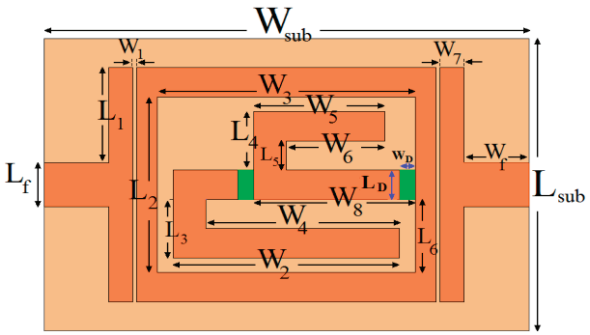

(b)

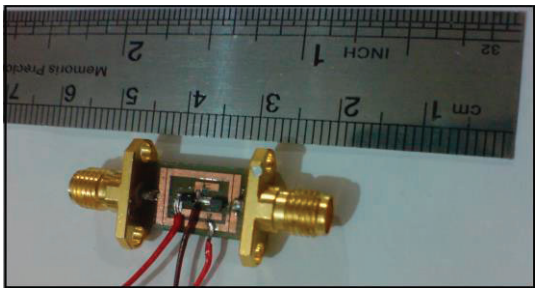

(c)

Fig. 2. Configuration of the switchable antenna: (a) side view, (b) top view and (c) fabricated scheme.

Figure 3 shows the simulated and measured return loss characteristics of the proposed antenna, as shown in Fig. 2. As shown in Fig. 3 in this structure, the rectangular ring with a pair of protruded Γ -shaped strips with two p-i-n diodes is used in order to electronically switch between the WLAN (2.4 GHz) and WiMAX (3.45 GHz) frequency bands.

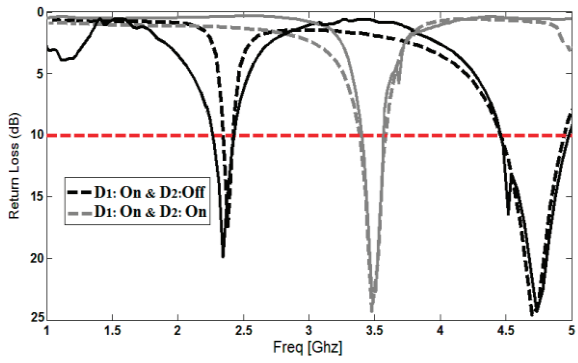

Fig. 3. Reflection coefficient of the antenna for various states of diodes (dashed line: simulated, solid line: measured).

For applying the DC voltage to PIN diodes, metal strips with dimensions of 1.5 mm × 0.6 mm were used inside the main slot. In the introduced design, HPND-4005 beam lead PIN diodes [13] with extremely low capacitance were used. For biasing PIN diodes, a 0.7 volt supply is applied to metal strips. The PIN diodes exhibit an ohmic resistance of 4.6 Ω and capacitance of 0.017 pF in the on and off states, respectively. By turning diodes on, the metal protruded Γ -shaped strips are connected to the rectangular ring radiating patch and become a part of it. The desired frequency band can be selected by varying the states of PIN diodes, which changes the total equivalent length of the strip.

In order to understand the phenomenon behind switching electronically between first and second resonance frequency, the simulated current distributions on the radiating patch of the proposed antenna for on and off statuses of the PIN diode are presented in Figs. 4 (a) and (b), respectively. As shown in Fig. 3 (a), at the first resonance frequency (2.4 GHz), the current mainly concentrates on the bottom edges of the protruded Γ -shaped strips and also it can be seen that the electrical current does change its direction along the bottom of the protruded Γ -shaped strips. Finally, the current mainly concentrates on the upper protruded Γ -shaped strips at the second resonance frequency (3.5 GHz), as shown in Fig. 4 (b).

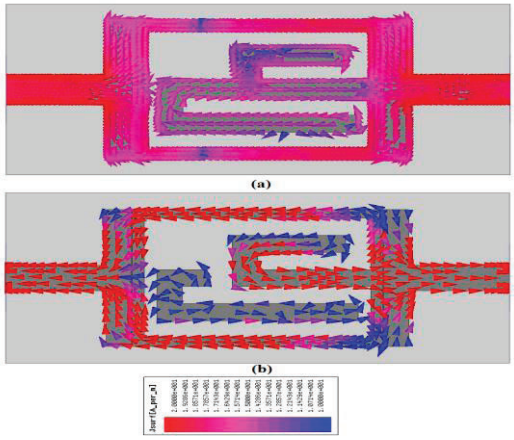

Fig. 4. Simulated surface current distributions on the radiating patch: (a) at the first resonance frequency (2.4 GHz) and (b) the second resonance frequency (3.5 GHz).

IV. MULTI-BAND OSCILLATOR DESIGN

Transistor oscillators can be designed using either bipolar or GaAs MESFET devices [14-15]. Using the [S] parameters of the active element, the design of the microwave oscillator is performed using our full-scale computer simulation program. The stability of the device can be checked by two stability factors K and |Δ|. The mathematical equations for K and |Δ| are [14]:

$$\Delta = S_{11}S_{22} - S_{21}S_{12}, \tag{1}$$

$$K = \frac{1-\left|S_{11}\right|^2-\left|S_{22}\right|^2+\left|\Delta\right|^2}{2\left|S_{21}S_{12}\right|}. \tag{2}$$

The stability of the used transistor at the frequencies of 2.4 GHz and 3.5 GHz is calculated through calculation of the stability factor K and Δ [16]. The transistor is potentially unstable at the operated frequencies 2.4 GHz and 3.5 GHz (i.e. K=0.5718 and K=0.656, respectively). The stability circle at the gate-to-drain port is calculated by (3) and (4). In this design the gate-to-drain port is the terminating port.

$$R_S = \left|\frac{S_{12}S_{21}}{S_{11}^2-\Delta^2}\right|, \tag{3}$$

$$C_S = conj\left(\frac{\left(S_{11}\right)-\Delta.conj\left(S_{22}\right)}{\left|S_{11}\right|^2-\left|\Delta\right|^2}\right). \tag{4}$$

Any Γ_T in the shaded stability circle region produces $\left|\Gamma_{in}\right|>1$ (i.e. a negative resistance at the input port). We select an arbitrary point in mentioned region, at this point $\Gamma_T = 0.9\angle -165^\circ$ and the associated impedance is $Z_T = -j7.5\Omega$. This reactance can be implemented by an open-circuited 50Ω line of length 0.226λ. With Z_T connected, the input reflection coefficient is found to be $\Gamma_{IN} = 12.5\angle -160^\circ$ and the associated impedance is $Z_{IN} = -50 - j3.5\Omega$. The load matching network is designed using (5)-(9), that is $Z_{IN} = 21 - j2.1\Omega$.

$$\Gamma_{in} = S_{11} + \frac{S_{12}S_{21}\Gamma_T}{1-S_{22}\Gamma_T}, \tag{5}$$

$$\Gamma_S = \Gamma_{in}^*, \tag{6}$$

$$Z_{in} = Z_0\frac{1-\left|\Gamma_S\right|^2+2j\left|\Gamma_S\right|\sin\left(\theta_{\Gamma_S}\right)}{1+\left|\Gamma_S\right|^2-2\left|\Gamma_S\right|\cos\left(\theta_{\Gamma_S}\right)}, \tag{7}$$

$$Z_L = \frac{real\left(Z_{in}\right)}{3} - jimag\left(Z_{in}\right), \tag{8}$$

$$Y_{in} = \frac{50}{Z_L}. \tag{9}$$

The terminating circuit is designed to get maximum reflection coefficient at the transistor output. The analytical design of the terminating circuit and the output matching circuit are performed using the developed computer program [4]. As a result of the developed program and the optimization process described elsewhere [5], the lengths and widths of the termination and matching circuits are:

Terminating circuit: Length of open circuit series line (50 Ω)=32.4569 mm and width of open circuit series line =3 mm.

Load matching circuit: Length of series line (50 Ω)=15.318 mm, width of series line =3 mm, length of open single shunt stub =1.51 mm and width of open balanced shunt stub =3 mm.

A series feedback is added to the source of the transistor using microstrip line to maximize the value of S11 of the oscillator operated at 2.4 GHz and 3.5 GHz. As the result of the gradient method optimization process in the ADS, the length and width of the microstrip line connected to the source of the transistor are 28.94 mm and 3 mm, respectively. Figure 5 shows the circuit layout and Fig. 6 shows |S11| in dB versus frequency for the deigned microstrip oscillator.

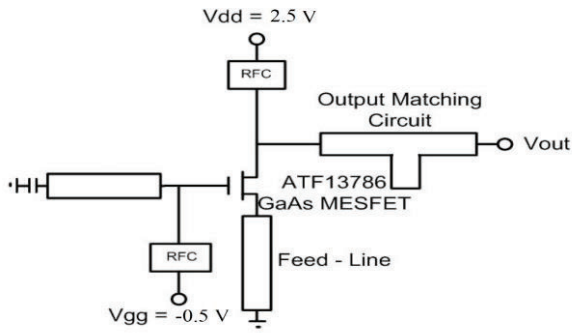

(a)

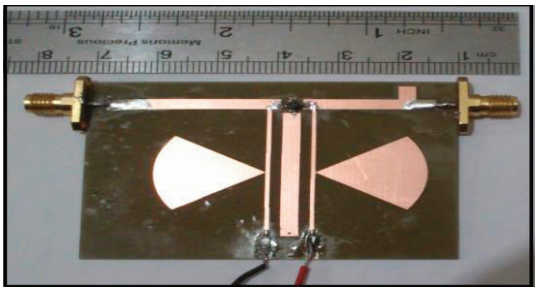

(b)

Fig. 5. Circuit layout of the proposed oscillator: (a) schematic and (b) fabricated oscillator.

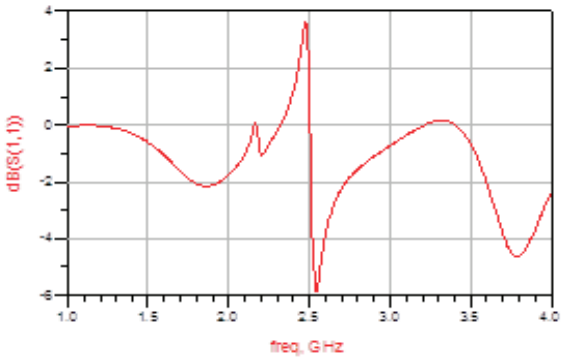

Fig. 6. |S11| (dB) versus the frequency.

V. RECONFIGURABLE FEEDBACK OSCILATOR ANTENNA MEASURMENT

A microwave oscillator presented in this work using a feedback antenna structure with a high-Q factor provides high power; high DC to RF conversion ratio. The feedback antenna dimension barely affects the dimension of the microstrip line located on the top of the substrate when applied to oscillators. In this structure, PIN diodes were used as the frequency selection switch to change effective length of the microstrip line resonator; which forms a part of the overall oscillator circuit. Biasing circuit for the diodes was designed in such a way that it didn't disturb the biasing voltage of the transistor. While forward bias included complete length, reverse bias incorporated length of the resonator just before the diode as a part of the overall oscillator. Nevertheless, negative resistance condition for oscillation was maintained at both the designed frequencies, thereby upholding oscillation at one frequency during forward biasing of D_1 and at another frequency in two diodes biasing case. The switch capacitance was taken into account while deciding resonators' lengths for the two frequencies. Dimensions of the resonators and the matching network were optimized using Agilent's Advanced Design System (ADS) in conjunction with the Electromagnetic (EMDS) Simulation tool to get the required oscillation frequencies for dual-band operation.

The presented active feedback antenna is shown in Fig. 7, which is printed on an FR4 substrate of thickness 0.8 mm, permittivity 4.4 and loss tangent 0.018. The proposed active feedback antenna structure consists of a rectangular ring with a pair of protruded Γ -shaped strips for radiating element, a microstrip loop, an oscillator with DC bias circuit and matching circuit for active part. The width of the 50-Ω microstrip line is fixed at 1.5 mm, as shown in Fig. 7. The matching circuit to the left and right of the device controls the degree of feedback. On the other side of the substrate a conducting ground plane is placed. In addition, to satisfy the oscillation-phase requirement, the microstrip loop is fixed to a suitable electrical length taking the calculated phases of the oscillator and passive antenna into consideration [16]. The proposed antenna is connected to a 50-Ω SMA connector for signal transmission.

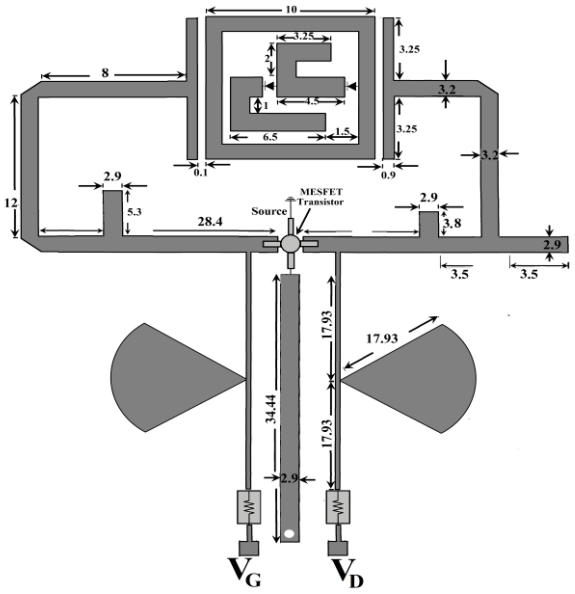

Fig. 7. Configuration of the proposed active integrated antenna with GaAs MESFET.

Conventionally, multi-band oscillators are realized by reconfiguring the frequency selective network [3-5]. Typically, a negative resistance cell is combined with a switch-controlled resonator. Distinct frequency selective circuit units are designed such that the negative resistance cell satisfies the necessary oscillating condition at their corresponding resonant frequencies. As shown in Fig. 7, the proposed multi-band oscillation scheme modifies the frequency selective network by varying only the microstrip length to select the desired frequency response, as depicted in the block diagram of Fig. 1 for dual-band case. At the network's input, two microstrip resonators of different lengths are connected in feedback through an electrical switch to define the required oscillating frequencies. Simultaneously, a dual-band output matching network is designed for optimum output power efficiency to a 50 Ω load at both the designed frequencies. The scheme is extendable to multi-band scenario using additional frequency selective circuits connected through electrical switches with appropriate multi-band matching network at the oscillator's output. A dual-band oscillator prototype was implemented using the proposed reconfigurable antenna scheme with single transistor. The common-source configuration of a GaAs MESFET Transistor (ATF13786) was used to generate appropriate negative resistances for dual-band oscillation at 2.4 GHz and 3.5 GHz [17]. The transistor was DC biased through a radial stub implemented using a high impedance (100 Ω) quarter wavelength (electrical length 90^0) microstrip line, which is further shunted by a low impedance (20 Ω) quarter wavelength open stub. Biasing voltages of *VDS*=2.5 V and *VGS*=-0.5 V were maintained at the drain and the gate terminals of the transistor. It is known that oscillations are achieved at those frequencies where the stability parameter (*K*) value is less than one. In order to meet this instability condition for oscillations at both the desired frequencies, a microstrip line was added to the transistor's source terminal. In effect, the microstrip incorporates an external positive series feedback to the network, thereby ensuring the required network destabilization.

The proposed reconfigurable frequency oscillator feedback antenna is fabricated and tested. Figures 8 (a) and (b) show the radiated output power from the fabricated oscillator feedback antenna for the previously mentioned biasing conditions measured in anechoic chamber. The implemented dual-band oscillator exhibited output power level of -16.21 dBm, at frequency of 2.399 GHz and -23.09 dBm, at frequency of 3.488 GHz for diodes bias conditions. Second harmonics for both the cases were observed to be about 12 dB below the output power at fundamental frequencies. The output power is measured to be about 25.17 dBm, using an Agilent E4440A spectrum analyzer and a double-ridged horn antenna (gain 17 dBi) as a reference antenna placed at a distance of 2 m.

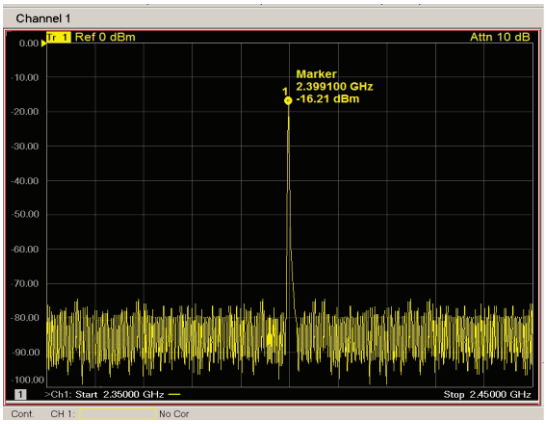

(a)

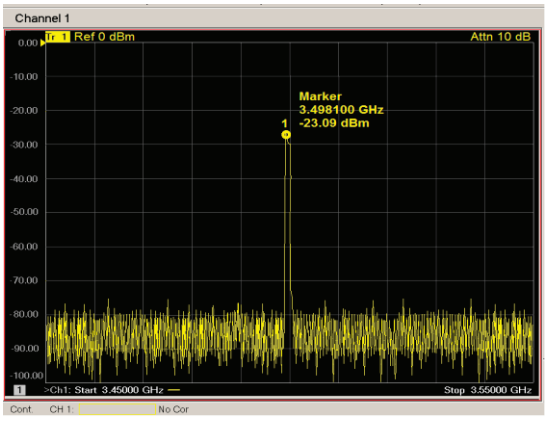

(b)

Fig. 8. Measured output power radiated from active feedback antenna: (a) at 2.39 GHz and (b) at 3.48 GHz.

The measured radiation patterns including the co-polarization and cross-polarization for the E-plane (y-z plane) and H-plane (x-z plane) at the resonance frequencies, are shown in Fig. 9. The

received cross-polarizations in the E-plane and H-plane of the AIA are approximately 19 and 23 dB lower than the maximum co-polarized radiation, respectively. As seen in Fig. 9, the radiation pattern in the H-plane is asymmetrical due to the asymmetrical presence of the distributed oscillator-feedback circuitry.

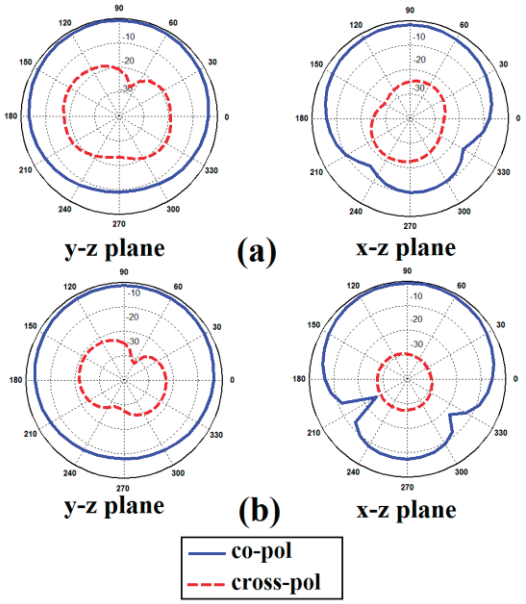

Fig. 9. Measured radiation patterns of the proposed antenna: (a) at 2.4 GHz and (b) at 3.5 GHz.

V. CONCLUSION

As presented above, a novel design of reconfigurable active integrated oscillator feedback antenna with electronically controllable is an interesting subject for for WiMAX/WLAN applications. By using a rectangular ring with a pair of protruded Γ-shaped strips in the active feedback antenna, two new resonances can be achieved. In the proposed structure, based on Electromagnetic Coupling (EC), an interdigital coupling strip in the microstrip transmission line is used to perturb two resonance frequencies at 2.4 GHz (WiMAX) and 3.5 GHz (C-band). The oscillator design based on the AIA concept has been shown to provide an efficient and successful method for designing high efficiency and compact systems. The implemented dual-band oscillator exhibited output power level of -16.21 dBm, at frequency of 2.399 GHz and -23.09 dBm, at frequency of 3.488 GHz for diodes bias conditions. Second harmonics for both the cases were observed to be about 12 dB below the output power at fundamental frequencies.

REFERENCES

[1] A. R. Rofougaran, M. Rofougaran and A. Behzad, "Radios for next-generation wireless networks," *IEEE Microwave Magazine*, 6, pp. 38-43, March 2005.

[2] A. Kral, F. Behbahani and A. A. Abidi, "RF CMOS oscillators with switched tuning," *Proceedings of the IEEE Custom Integrated Circuits Conference*, pp. 555-558, May 1998.

[3] A. P. S. Khanna and R. Soohoo, "Fast switching x and ku band multi frequency dielectric resonator oscillator using a single GaAs FET," *IEEE International Microwave Symposium MTT-S*, 1, pp. 189-191, June 1987.

[4] A. Yamagishi, T. Tsukahara, M. Harada and J. Kodate, "A low-voltage 6-GHz-band CMOS monolithic LCTank VCO using a tuning-range switching technique," *IEEE Microwave Symposium MTT-S*, 2, pp. 735-738, 2000.

[5] B. Catli and M. M. Hella, "A low-power dual-band oscillator based on band-limited negative resistance," *IEEE Radio Frequency Integrated Circuits (RFIC) Symposium*, pp. 251-254, June 2009.

[6] F. R. Hsiao and K. L. Wong, "Compact planar inverted-f patch antenna for triple-frequency operation," *Microwave Opt Technol Lett*, 33, 459–462, 2002.

[7] P. Wang, G. J. Wen and Y. Huang, "Compact CPW-fed planar monopole antenna with triple-band operation for WLAN/WiMAX applications," *Applied Computational Electromagnetics Society (ACES) Journal*, vol. 27, no. 8, pp. 691-696, August 2012.

[8] C. Medeiros, J. Costa, C. Fernandes and B. Kolundzija, "Simulation of frequency agile RF MEMS antennas using WIPL-D," *24th Annual Review of Progress in Applied Computational Electromagnetics (ACES)*, pp. 688-693, Niagara Falls, Canada, March 30 - April 4, 2008.

[9] J. DeSignor and J. Venkataraman, "Reconfigurable dual frequency microstrip patch antenna using RF MEMS switches," *24th Annual Review of Progress in Applied Computational Electromagnetics (ACES)*, pp. 728-732, Niagara Falls, Canada, March 30 - April 4, 2008.

[10] K. Chang, "Active integrated antennas," *Proc. IEEE*, vol. 50, no. 3, March 2002.

[11] P. S. Hall, P. Gardner and G. Ma, "Active integrated antenna," *IEICE Trans. Commun*., E85-B, 9, pp. 1661-1666, 2002.

[12] "Ansoft high frequency structure simulation (HFSS)," ver. 13, *Ansoft Corporation*, 2010.

[13] HPND-4005, "Beam lead PIN diode," *Avago Technologies.*

[14] J. C. Liu, C. S. Cheng, H. C. Chen and P. C. Chen, "Active integration RingAntenna/phase shifter for direct conversions", *IEE Proc. - Microw. Antennas Propag*., vol. 151, no. 4, pp. 357-361, August 2004.

[15] G.Yun, "Compact oscillator-type active antenna for UHF RFID reader," *Electronic Letters*, vol. 43, no. 6, March 2007.

[16] M. Ojaroudi, N. Ojaroudi and Y. Ebazadeh, "Dual band-notch small square monopole antenna with enhanced bandwidth characteristics for UWB applications," *Applied Computational Electromagnetics Society (ACES) Journal*, vol. 27, no. 5, pp. 420-426, May 2012.

[17] J. Mazloum, A. Jalali, M. Ojaroudi and N. Ojaroudi, "Compact oscillator feedback active integrated antenna by using interdigital coupling strip for WiMAX applications," *Applied Computational Electromagnetics Society (ACES) Journal*, vol. 28, no. 9, pp. 844-850, August 2013.

Jalil Mazloum was born on 1974 in Tehran, Iran. He received his B.Sc. degree in Electronic Engineering from Shahid Sattari Aeronautical University of Science and Technology, Tehran, Iran; and M.Sc. degree in Bioelectric Engineering from Amirkabir University of Technology, Tehran, Iran. Since 2010, he is working towards his Ph.D. degree at Shahid Beheshti University. Since 1998, he has been a Research Fellow and a Teaching Assistant with the Department of Electrical Engineering, from Aeronautical University of Science and Technology, Tehran, Iran. His research interests include design and modeling of microwave structures, radar systems and RFID systems.

Ali Jalali received his B.Sc. degree in Electronic Engineering from Sharif University of Technology in 1991. He also received his M.Sc degree and Ph.D degree in Electronic Engineering from Supelec University and Rennes I University, FRANCE, in 1994 and 1998, respectively. Since 1998 till now he is with the Faculty of Electrical and Computer Engineering at Shahid Beheshti University, Tehran, Iran. His research interests include low- power and low-voltage analog and digital integrated circuits, RF microelectronics, Digital Audio Broadcasting (DAB) and VLSI Design.

Compact Wide Band Printed Filter with Improved Out-of-Band Performance

Anjini Kumar Tiwary, and Nisha Gupta

Department of Electronics and Communication Engineering
Birla Institute of Technology, Mesra, Ranchi, Jharkhand 835215, India
aktiwary@bitmesra.ac.in, ngupta@bitmesra.ac.in

Abstract ─ This paper presents a new configuration of a compact wide-band Bandpass Filter (BPF). The filter is realized using embedded stub configuration along with Defected Ground Structure (DGS) and folded stubs. The proposed configuration not only offers a compact structure but also shows a wide passband and improved out-of-band performance. A prototype model is developed and its characteristics are measured. Good agreement is obtained between simulation and measured results. The results show improved wide-band behavior, insertion loss lower than 0.6 dB and 49.16 % of size reduction.

Key-Words - Bandpass filter, compact bandpass filter, defected ground structure and embedded stub.

I. INTRODUCTION

The microwave filters play a very important role in wireless and satellite communication transceiver systems. It is an important passive component in the communication system that rejects unwanted signals in the specified band of interest. Planar microwave wideband BPF's have received greater attention due to several advantages, such as low cost, small size and ease of fabrication. The performance of the filter highly depends on its passband and out-of-band performances. In the past, several techniques have been developed to analyze these filters with improved passband and out-of-band characteristics. In [1] a microstrip wideband BPF with increased fractional bandwidth is reported. Using a ring-resonator a higher filter bandwidth is achieved [2] and Ultra Wideband (UWB) characteristic is realized by combining low pass filter with high pass filter [3]. With the help of Multiple-Mode Resonator (MMR), various wideband and UWB BPF are developed [4-10]. A wideband filter with an extended out-of-band has been constituted by internally installing an Electromagnetic Bandgap (EBG) transmission line into a traditional highpass filter with short-circuited stubs [11]. Wideband microstrip BPF is also reported using Sierpinski fractal stub-based resonator where a greater fractional bandwidth is achieved [12]. Further, a compact wideband BPF using modified non-bianisotropic split-ring resonators is developed [13] and a dual-wideband filter design is implemented with the stepped-impedance resonators using different concepts, such as frequency mapping approach and defected stepped impedance resonator [14-15]. With the application of coupling mechanism, miniaturized wideband BPF's are also reported [16-17]. Using the aperture-coupled technique, a three-layer UWB BPF is studied in [18], which involves a complicated design procedure. In [19], a technique deploying an EBG structure is proposed and wide-stopband behavior is reported with increased circuit size. Several other triple-mode UWB filters have been reported based on varied MMR's, such as stub-loaded MMR [20], one open stub and one short stub loaded MMR [21]. In fact, with the help of MMR in fiber grating, other kinds of filters in optical-electrical fields have been used to realize optical switching because of its high nonlinearity and low insertion loss [22-25]. A novel miniaturized parallel coupled-line BPF with suppression of second, third and fourth harmonic frequencies are realized in [26]. A microstrip BPF based on Folded Tri-Section Stepped Impedance Resonator (FTSIR) and DGS is reported in [27]. A compact microstrip BPF with bandwidth control is developed by employing DGS resonators [28]. In [29], a novel compact LPF and BPF based on DGS using two Complementary Split Ring Resonators (CSRR) are presented. A compact UWB bandpass filter with two controllable highly selective notched

Submitted On: January 10, 2013
Accepted On: April 5, 2014

bands are reported in [30]. An embedded stub is proposed to implement microwave bandstop filter with narrow bandwidth and sharp rejection rate [31].

In this paper a new compact wideband filter is proposed using DGS along with embedded stubs and folded stub configuration to improve the out-of-band performance of the filter.

II. BAND PASS FILTER IMPLEMENTATION AND SIMULATION RESULTS

Conventional BPF configuration employs cascaded short circuited stubs of electrical length θC at some specified frequency fC, separated by connecting lines (unit elements) of electrical length 2θC [11] as shown in Fig. 1. The electrical length θC can be determined from:

$$\left(\frac{\pi}{\theta_C}-1\right)f_C = f_H . \quad (1)$$

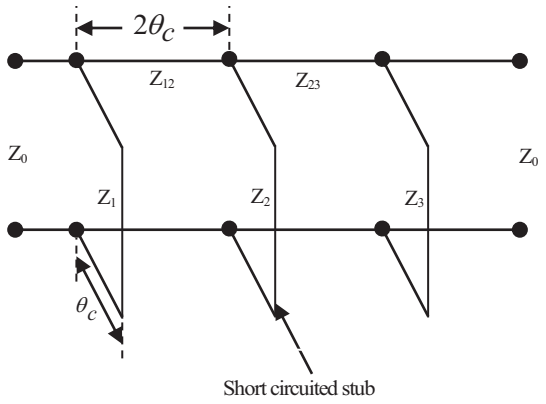

Fig. 1. General circuit model for the conventional wideband BPF.

For fC = 1.4 GHz and fH = 5.4 GHz, the electrical length, θC = 0.647 radians or 370. Next, the filter parameters are obtained for n = 3 (three short circuited stubs) and 0.1 dB ripple, as y1 = y3 = 0.40, y1,2 = y2,3 = 1.05 and y2 = 0.48, where yi, yi,j and yj,i are the element values of optimum distributed high pass filter, where i = j = 1,2,3. The corresponding impedances are calculated as Z1 = Z3 = 124.68 Ω, Z1,2 = Z2,3 = 47.45 Ω and Z2 = 103.53 Ω [11]. All the vias dimensions are 0.5 mm in diameter. The overall electrical length of the conventional filter is 4θC, where the unit elements have electrical length = 2θC.

The lengths of the input and output transmission lines are selected depending on the length of the short circuited stub. Since the proposed configuration employs the shorted stubs embedded in the transmission lines, the length of the input and output transmission lines are selected as λg/8.

Table 1: Dimensions of the filter

Filter elements	Impedance (Ω)	Length (mm)	Width (mm)
Microstrip line side stubs, $Z_1 = Z_3$	124.68	15.82	0.82
Microstrip line centre stub, Z_2	103.53	15.70	1.30
Unit element (UE), $Z_{12} = Z_{23}$	47.45	30.28	5.22

The filter is designed on a RT/duroid 5880 substrate with a dielectric constant of 2.2, thickness h = 1.57 mm and loss tangent 0.0009. The Method of Moments based IE3D simulation software tool from Zealand, USA, is used for the purpose of simulation. The conventional BPF is shown in Fig. 2 and the dimensions are specified as shown in Table 1. The characteristics of the filters are obtained in terms of S-parameters, as shown in Fig. 3.

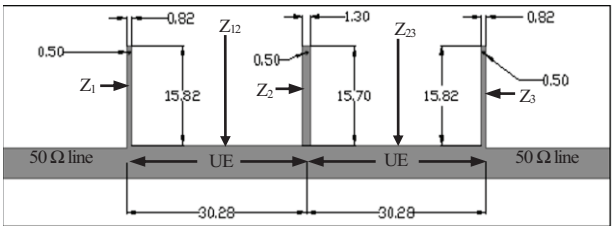

Fig. 2. Conventional BPF with Z12 = Z23 = 47.45 Ω.

The impedance of the unit elements Z12 = Z23 = 47.45 Ω of conventional BPF is replaced with the impedance of 50 Ω, to maintain uniformity. This does not alter the characteristics of the filter significantly as shown in Fig. 3. It is observed that the out-of-band characteristic needs improvement. Next, the conventional BPF is analyzed with DGS configuration, with an intention to improve the out-of-band characteristic and also to reduce the total length of the filter

A parametric study is carried out to determine the

proper dimension of the lattice (DGS) [32- 33] for generating the attenuation pole at the desired location over the out-of-band. Following the procedure as in [32-33] for the location of attenuation pole at 8.9 GHz, the lattice dimension is obtained as x = 4 mm, y = 2 mm and g = 0.5 mm. The incorporation of DGS helps in two ways. First, it generates an attenuation pole at the desired location, thus offering an improved out-of-band characteristic. Secondly, it also miniaturizes the length of the filter, as the length of the unit elements are now half of the original length. Hence, a unit element of electrical length 2θC of conventional BPF is now replaced by the unit element of electrical length θC after incorporating a DGS, as shown in Fig. 4.

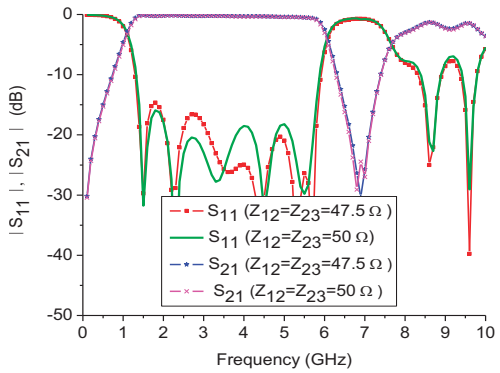

Fig. 3. Simulated result for S-parameters.

The filter configuration is further modified by folding the central shorted stub in L-shape configuration and embedding the two shorted side stubs in 50 ohm transmission lines, thus offering a compact configuration, as shown in Fig. 5 (a); where W1 = 1.42 mm, W2 = 0.58 mm and W3 = 0.56 mm.

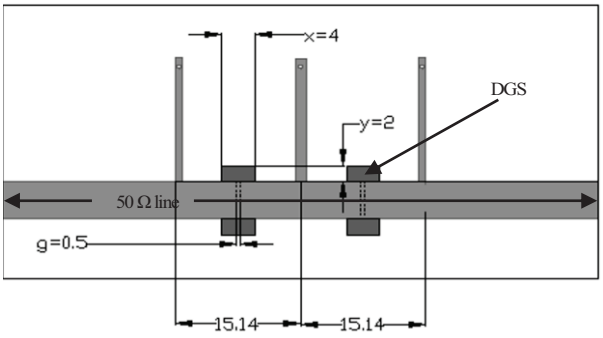

Fig. 4. Wide BPF with DGS.

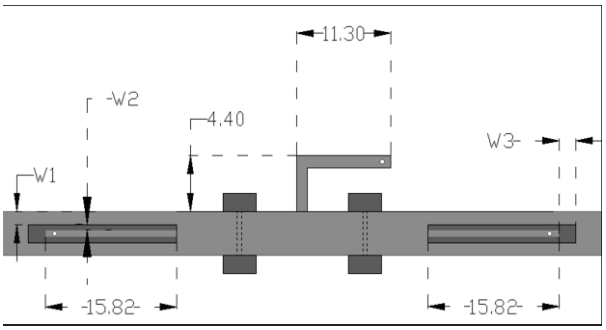

(a)

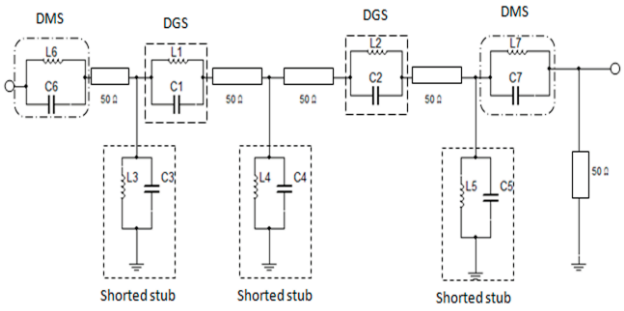

(b)

Fig. 5. (a) Proposed compact embedded filter and (b) equivalent circuit of proposed compact embedded filter.

The equivalent circuit representation of the proposed compact embedded filter is shown in Fig. 5 (b), where the DGS and DMS configurations are represented as a parallel combination of L and C, connected in series with 50 ohm microstrip line and the shorted stub is represented as parallel L and C, connected in shunt.

A. Effect of slot/gap parameters (W_1, W_2)

Four set of values of slot W1 and gap W2 are selected as follows: (I) W2 = 0.38 mm and W1 = 1.62 mm; (II) W2 = 0.58 mm and W1 = 1.42 mm; (III) W2 = 0.78 mm and W1 = 1.22 mm; (IV) W2 = 0.98 mm and W1 = 1.02 mm.

The simulated results of the variation of the slot W1 and gap W2 are shown in Fig. 6.

For the (I) data set, improved performance in the passband is observed. However, due to the limitations in our PCB fabrication facility, the (II) data set is considered as the existing fabrication facility does not support the strip/slot dimensions less than 0.5 mm.

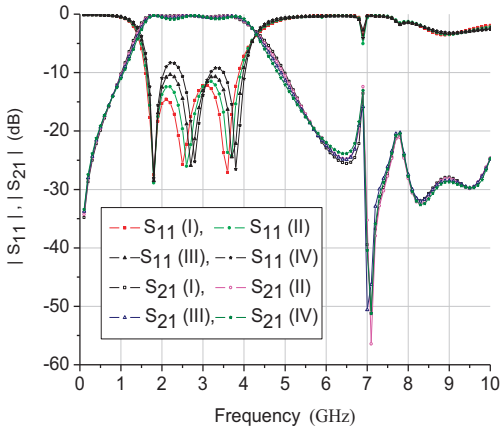

Fig. 6. Simulated result of S-parameters for different W1 and W2.

B. Effect of gap parameters (W3)

For constant W2 = 0.58 mm, three set of values of gap W3 are taken; as (I) W3 = 0.36 mm, (II) W3 = 0.56 mm and (III) W3 = 0.76 mm. It is seen that the results do not show any significant change with respect to W3, as shown in Fig. 7. Therefore, W3 is chosen as 0.56 mm. The characteristics of the two configurations, Figs. 4 and 5 (a) are compared in Fig. 8.

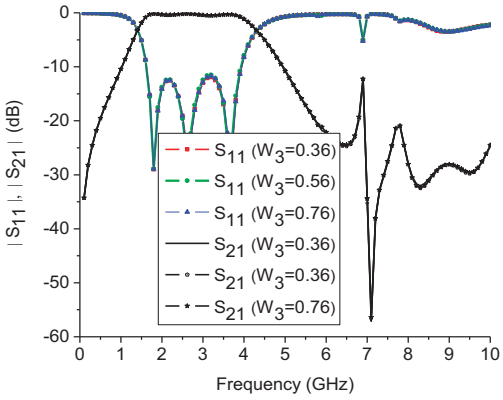

Fig. 7. Simulated result of S-parameters for gap W3.

It is evident from Fig. 8, that employing the DGS improves the out-of-band characteristics. However, a reduction in the bandwidth of the filter in the passband is observed when the stubs are outside. This may be attributed to the larger electrical length offered in case of DGS, which in turn limits the passband [26-27]. However, this problem of bandwidth reduction is overcome when the stubs are embedded in I/P and O/P transmission lines (Fig. 5 (a)), as depicted in Fig. 8. The reason behind this improvement is reduction in effective electrical length in case of embedded stubs. A passband of more than 2.5 GHz and a very wide rejection bandwidth is obtained in the out-of-band region. Size reduction of approximately 49.16% is achieved in the proposed compact filter. Figure 9 shows the filter response in terms of group delay, which shows almost a constant group delay in the passband as desired.

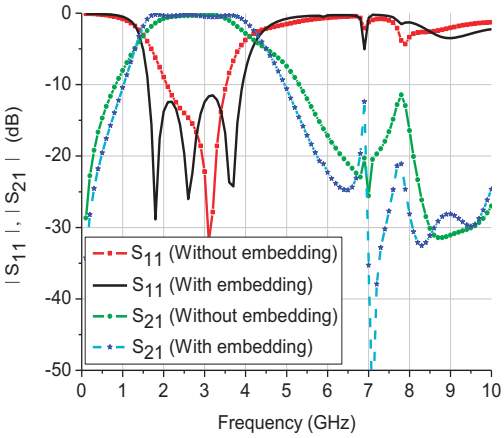

Fig. 8. Simulated result of the filter with DGS; with and without embedded stub.

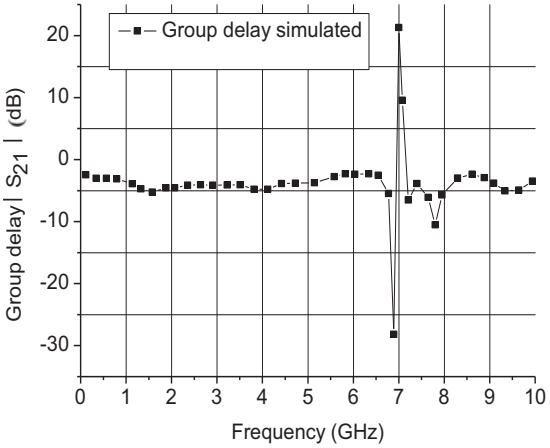

Fig. 9. Simulated result of the proposed compact embedded BPF.

Table 2: Performance of filters

Configuration	10 dB passband (GHz)	10 dB rejection bandwidth in out-of-band (GHz)	Area occupied (length×width) in mm2
Conventional BPF (length of 50 Ω line = λg/8)	1.3 to 5.8 = 4.5	6.2 to 7.6 = 1.4	102.54×20.85 = 2137.96
Conventional BPF (length of 50 Ω line = λg/16)	1.3 to 5.8 = 4.5	6.2 to 7.6 = 1.4	83.03×20.85 = 1731.17
Proposed BPF (without embedding)	2.28 to 3.75 = 1.47	5.2 to 10 = 4.8	102.54×20.85 = 2137.96
Proposed compact embedded BPF	1.6 to 4.1 = 2.5	4.88 to 10 = 5.12	102.54×10.54 = 1086.77

III. EXPERIMENTAL RESULTS

The prototype filter is fabricated and the photograph of the top and bottom view of the filter is shown in Figs. 10 (a) and 10 (b).

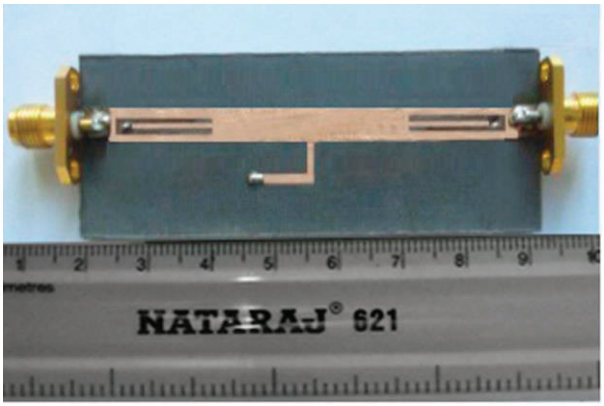

(a) Top view

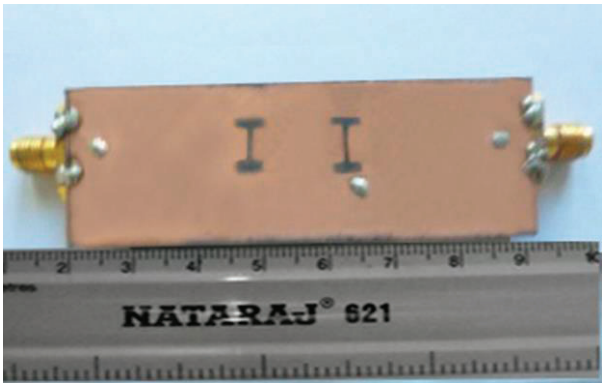

(b) Bottom view

Fig. 10. Prototype of the proposed compact embedded structure.

Finally, the response of the fabricated filter is measured using PNA series Vector Network Analyzer and the response is compared with the simulated result, as shown in Fig. 11.

A comparison of the simulated response with the measured response, shows a good agreement. The performance of the filter in passband and out-of-band for three configurations under investigation, is tabulated in Table 2.

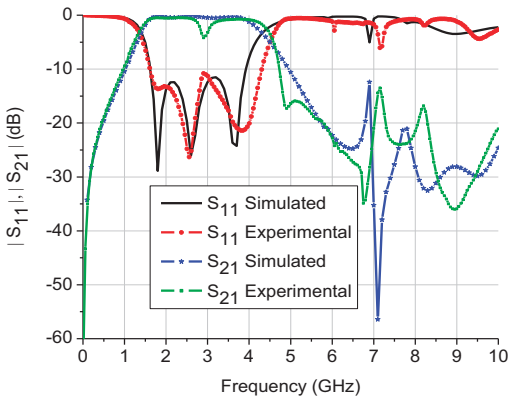

Fig. 11. Experimental and simulated result of the proposed compact embedded filter.

IV. CONCLUSION

A compact wideband filter is implemented based on the concept of embedded stub and DGS. The proposed structure is realized in two steps. First, the conventional wideband filter is miniaturized in terms of the length of unit element by the application of DGS, then further reduction is obtained by embedding the shorting side stubs in the microstrip line and folding the central shorted stub in L-shape. The proposed compact embedded bandpass filter structure shows a size reduction of 49.16 % along with a good passband and improved out-of-band rejection bandwidth.

REFERENCES

[1] J. T. Kuo and E. Shih, "Wideband bandpass filter design with three-line microstrip structures," *IEE Proc-Microwave Antennas Propagat.*, vol. 149, pp. 243-247, 2002.

[2] L. H. Hsieh and K. Chang, "Compact, low insertion-loss, sharp-rejection and wide-band microstrip bandpass filters," *IEEE Transactions on Microwave Theory and Techniques*, vol. 51, pp. 1241-1246, 2003.

[3] N. W. Chen and K. Fang, "An ultra-broadband coplanar-waveguide bandpass filter with sharp skirt selectivity," *IEEE Microwave and Wireless Components Letters*, vol. 17, pp. 124-126, 2007.

[4] L. Zhu and W. Menzel, "Compact microstrip bandpass filter with two transmission zeros using stub-tapped half-wavelength line resonator," *IEEE Microwave and Wireless Components Letters*, vol. 13, pp. 16-18, 2003.

[5] K. Srisathit, A. Worapishet and W. Surakampontorn, "Design of triple-mode ring resonator for wideband microstrip bandpass filters," *IEEE Transactions on Microwave Theory and Techniques*, vol. 58, pp. 2867-2877, 2010.

[6] M. H. Ren, D. Chen and C. H. Cheng, "A novel wideband bandpass filter using a cross-shaped multiple-mode resonator," *IEEE Microwave and Wireless Components Letters*, vol. 18, pp. 13-15, 2008.

[7] L. Zhu, S. Sun and W. Menzel, "Ultra-wideband (UWB) bandpass filters using multiple-mode resonator," *IEEE Microwave and Wireless Components Letters*, vol. 15, pp. 796-798, 2005.

[8] K. M. Shum, W. T. Luk, C. H. Chan and Q. Xue, "A UWB bandpass filter with two transmission zeros using a single stub with CMRC," *IEEE Microwave and Wireless Components Letters*, vol. 17, pp. 43-45, 2007.

[9] S. W. Wong and L. Zhu, "EBG-embedded multiple-mode resonator for UWB bandpass filter with improved upper-stopband performance," *IEEE Microwave and Wireless Components Letters*, vol. 17, pp. 421-423, 2007.

[10] S. W. Wong and L. Zhu, "Ultra-wide bandpass filters with sharpened roll-off skirts, extended upper-stopband and controllable notch-band," *Microwave and Optical Technology Letters*, vol. 50, pp. 2958-2961, 2008.

[11] J. S. Hong and M. J. Lancaster, *Microstrip Filters for RF/Microwave Applications*, Wiley, New York, 2001.

[12] J. Church, D. West, P. Danger and S. K. Sharma, "A novel wideband microstrip fractal bandpass filter with a notch band at 5-6 GHz," *Microwave and Optical Technology Letters*, vol. 52, pp. 1413-1416, 2010.

[13] S. Chaimool and P. Akkaraekthalin, "A compact wideband bandpass filter using modified NB-SRR's with wide upper bandstop," *Microwave and Optical Technology Letters*, vol. 52, pp. 551-553, January 2010.

[14] A. S. Liu, T. Y. Huang and R. B. Wu, "A dual wideband filter design using frequency mapping and stepped impedance resonators," *IEEE Transactions on Microwave Theory and Techniques*, vol. 56, pp. 2921-2929, 2008.

[15] B. Wu, X. Lai, T. Su and C. H. Liang, "Wideband cross-coupled filter using defected stepped impedance resonator," *Microwave and Optical Technology Letters*, vol. 52, pp. 558-561, 2010.

[16] H. Adam, A. Ismail, M. A. Mahdi, M. S. Razalli, A. Alhawari and B. Esfeh, "X-band miniaturized wideband bandpass filter utilizing multilayered microstrip hairpin resonator," *Progress In Electromagnetics Research (PIER)*, vol. 93, pp. 177-188, 2009.

[17] M. A. S. Soriano, G. T. Penalva and E. Bronchalo, "Compact wideband bandstop filter with four transmission zeros," *IEEE Microwave and Wireless Components Letters*, vol. 20, pp. 313-315, 2010.

[18] A. M. Abbosh, "Planar bandpass filters for ultra wideband applications," *IEEE Transactions on Microwave Theory and Techniques*, vol. 55, pp. 2262-2269, 2007.

[19] J. G. Garcia, J. Bonache and F. Martin, "Application of electromagnetic bandgaps to the design of ultra-wide bandpass filters with good out-of-band performance," *IEEE Transactions on Microwave Theory and Techniques*, vol. 54, pp. 4136-4140, 2006.

[20] R. Lei and L. Zhu, "Compact UWB bandpass filter using stub loaded multiple-mode resonator," *IEEE Microwave and Wireless Components Letters*, vol. 17, pp. 40-42, 2007.

[21] L. Han, K. Wu and X. P. Chen, "Compact ultra wideband bandpass filter using stub-loaded resonator," *Electronics Letters*, vol. 45, pp. 504-506, 2009.

[22] Z. Zang, "Numerical analysis of optical bistability based on fiber bragg grating cavity containing a high nonlinearity doped-fiber," *Optics Communications,* vol. 285, pp. 521-526, 2012.

[23] Z. G. Zang and Y. J. Zhang, "Analysis of optical switching in a Yb3+-doped fiber bragg grating by using self-phase modulation and cross-phase modulation," *Applied Optics*, vol. 51, pp. 3424-3430, 2012.

[24] Z. G. Zang and Y. J. Zhang, "Low-switching power (<45mW) optical bistability based on optical nonlinearity of ytterbium-doped fiber with a fiber bragg grating," *Journal of modern Optics*, vol. 59, pp. 161-165, 2012.

[25] Z. G. Zang and W. X. Yang, "Theoretical and experimental investigation of all-optical switching based on cascaded LPFGs separated by an erbium based fiber," *Journal of Applied Physics*, vol. 109, pp. 103-106, 2011.

[26] F. Karshenas, A. R. Mallahzadeh and J. Rashed-Mohassel, "Size reduction and harmonic suppression of parallel coupled-line bandpass filters using defected ground structure," *Applied Computational Electromagnetics Society (ACES) Journal*, vol. 25, no. 2, pp. 149-155, February 2010.

[27] N. M. Garmjani and N. Komjani, "Improved microstrip folded tri-section stepped impedance resonator bandpass filter using defected ground structure," *Applied Computational Electromagnetics Society (ACES) Journal*, vol. 25, no. 11, pp. 975-983, November 2010.

[28] S. U. Rehman, A. A. Sheta and M. A. S. Alkanhal, "Compact bandpass filters with bandwidth control using defected ground structure (DGS)," *Applied Computational Electromagnetics Society (ACES) Journal*, vol. 26, no. 7, pp. 624-630, July 2011.

[29] G. E. Al-Omair, S. F. Mahmoud and A. S. Al-Zayed, "Lowpass and bandpass filter designs based on DGS with complementary split ring resonators," *Applied Computational Electromagnetics Society (ACES) Journal*, vol. 26, no. 11, pp. 907-914, November 2011.

[30] S. Gao, S. Xiao and J. L. Li, "Compact ultra-wideband (UWB) bandpass filter with dual notched bands," *Applied Computational Electromagnetics Society (ACES) Journal*, vol. 27, no.10, pp. 795-800, October 2012.

[31] C. W. Hsue, R. Mittra, Y. H. Tsai and C. C. Hsu, "Microwave notch filters using embedded stubs," *Microwave and Optical Technology Letters*, vol. 51, no. 12, pp. 2839-2842, December 2009.

[32] H. Ishida and K. Araki, "Design and analysis of UWB bandpass filter with ring filter," *IEEE MTT-S International Microwave Symposium Digest*, vol. 3, pp. 1307-1310, 2004.

[33] A. K. Tiwary and N. Gupta, "Design of compact coupled microstrip line bandpass filter with improved stopband characteristics," *Progress in Electromagnetics Research C (PIER C)*, vol. 24, pp. 97-109, 2011.

Anjini Kumar Tiwary was born in 1972. He received his M.E. degree and Ph.D. degree from Birla Institute of Technology, Ranchi, India in 2009 and 2013, respectively. Currently he is an Assistant Professor for the Electronics and Communication Engineering Department, Birla Institute of Technology, Ranchi, India. His research interest is the design of microwave and millimeter-wave planar circuits.

Nisha Gupta received her Bachelor's and Master's degrees in Electronics and Telecommunication and Electrical and Electronics Engineering, both from Birla Institute of Technology, Mesra, Ranchi, India. She received her Ph.D. degree from the Indian Institute of Technology, Kharagpur, India. She was a Maintenance Engineer at Shreeram Bearings Ltd., Ranchi during 1982-83 and was a Programmer at Ranchi University, Ranchi from 1983-86. She was a Junior Scientific Officer in a DRDO sponsored project at Department of Electronics and Electrical Communication Engineering, Indian Institute of Technology, Kharagpur, from 1986-89 and a Institute Research Scholar and Research Associate (CSIR) in the same department from 1990-96. She was a post-doctoral fellow at the University of Manitoba, Canada from 1997-98 before joining the Department of Electronics and Communication Engineering, Birla Institute of Technology in 1999 as a Reader. Currently she is a Professor in the same department. She has authored and coauthored more than 51 technical journal articles. Her research interests are Computational Electromagnetics, RF circuits and Antennas for Wireless Communication and AI techniques in Wireless and Mobile Communication.

UWB Microstrip-Fed Slot Antenna with Band-Rejection Performance Using an SRR Conductor-Backed Plane

Nasser Ojaroudi [1], Noradin Ghadimi [1], and Yasser Ojaroudi [2]

[1] Young Researchers and Elite Club
Ardabil Branch, Islamic Azad University, Ardabil, Iran
noradin.ghadimi@gmail.com

[2] Young Researchers and Elite Club
Germi Branch, Islamic Azad University, Germi, Iran

Abstract ─ In this article, a novel and compact ultra-wideband (UWB) slot antenna with band-notched function is presented. This antenna consist of a square radiating stub, a 50Ω microstrip feed-line, a ground plane with a pair of rotated T-shaped strips protruded inside square slots and a Split Ring Resonator (SRR) conductor-backed plane. In this design, by cutting a pair of modified square slots with rotated T-shaped strips protruded inside slots, additional resonance is excited and hence much wider impedance bandwidth can be produced. In order to achieve a band-notched function, an SRR parasitic structure was inserted in the ground plane. The measured results show that the proposed antenna can achieve the Voltage Standing Wave Ratio (VSWR) requirement of less than 2.0 in frequency range from 3.1 GHz to 13.15 GHz, with band-rejection performance of 5.08 GHz to 6 GHz, to avoid interference from WLAN communications. The presented microstrip-fed slot antenna exhibits good radiation behavior. The antenna has a small size.

Index Terms ─ Band-notched function, protruded T-shaped strips, SRR conductor-backed plane and UWB microstrip-fed antenna.

I. INTRODUCTION

One of key issues in UWB communication systems is the design of a compact antenna, while providing wideband characteristic over the whole operating band. Consequently, a number of microstrip antennas with different geometries have been experimentally characterized [1-2]. Moreover, other strategies to improve the impedance bandwidth have been investigated [3-4].

The frequency range for UWB systems between 3.1-10.6 GHz will cause interference to the existing wireless communication systems. For example, the Wireless Local Area Network (WLAN) for IEEE 802.11a operating in 5.2/5.8 GHz; therefore, the UWB antenna with a band-notched function is required. In this paper, a compact microstrip-fed slot antenna with band-notched characteristic for UWB applications has been presented. In the proposed antenna, by using a pair of rotated T-shaped strips protruded inside square slots in the ground plane, an additional resonance was excited. By obtaining this resonance, the usable upper frequency of the antenna is extended from 9.3 GHz to 13.15 GHz. To generate a frequency notch band function, we used an SSR conductor-backed plane. The designed antenna has a small size and the impedance bandwidth of the designed antenna is higher than the UWB antennas reported recently [5-8].

II. ANTENNA DESIGN

The presented slot antenna fed by a microstrip line is shown in Fig. 1, which is printed on a FR4 substrate of thickness of 0.8 mm, permittivity of 4.4 and loss tangent of 0.018. The width W_f of the microstrip feed line is fixed at 1.5 mm. The basic antenna structure consists of a square radiating stub, a feed line and a ground plane. The

Submitted On: January 21, 2013
Accepted On: April 5, 2014

proposed antenna is connected to a 50Ω SMA connector for signal transmission.

In this work, we start by choosing the aperture length, L_S. We have a lot of flexibility in choosing this parameter. The length of the aperture mostly affects the antenna bandwidth. As L_S decreases, so does the antenna *BW* and vice versa. In the next step, we have to determine the aperture width, W_S. The aperture width is approximate, whereas the slot wavelength depends on a number of parameters; such as the slot width as well as the thickness and dielectric constant of the substrate on which the slot is fabricated. The last and final step in the design is to choose the width of the radiating patch, W_R. This parameter is approximate, whereas the guided wavelength is the microstrip line [2].

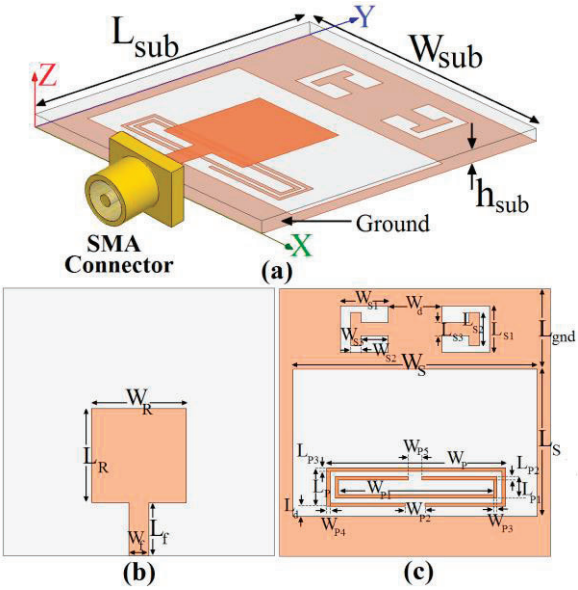

Fig. 1. Geometry of the proposed microstrip slot antenna: (a) side view, (b) top layer and (c) bottom layer.

In this design, the pair of protruded T-shaped strips inside the square slots in the ground plane are playing important roles in the broadband characteristics of the proposed antenna. Regarding Defected Ground Structures (DGS) theory, the created slots in the ground plane provide additional current paths. Moreover, these structures change the inductance and capacitance of the input impedance, which in turn leads to changing the bandwidth. Therefore, by cutting a pair of square slots in the ground plane, much enhanced impedance bandwidth may be achieved

In order to generate a band-notched property, an SRR conductor-backed plane was used. At the notched frequency, the current flows are more dominant around the SRR structure and they are directed oppositely between the parasitic element and the radiating stub. As a result, the desired high attenuation near the notch frequency can be produced [6].

The optimized values of the proposed antenna design are specified in Table 1.

Table 1: The values of the proposed antenna design parameters

$W_{sub} = 20mm$	$L_{sub} = 20mm$	$h_{sub} = 0.8mm$
$W_f = 1.5mm$	$L_f = 4mm$	$W_R = 7mm$
$L_R = 7mm$	$W_S = 18mm$	$L_S = 11mm$
$W_{S1} = 3.5mm$	$L_{S1} = 3.5mm$	$W_{S2} = 2mm$
$L_{S2} = 2.5mm$	$W_{S3} = 0.75mm$	$L_{S3} = 1mm$
$W_d = 4mm$	$L_d = 0.75mm$	$W_P = 14mm$
$L_P = 2.5mm$	$W_{P1} = 12.5mm$	$L_{P1} = 1.5mm$
$W_{P2} = 1.5mm$	$L_{P2} = 0.25mm$	$W_{P3} = 0.25mm$
$L_{P3} = 0.25mm$	$W_{P4} = 0.25mm$	$W_{P5} = 1mm$
$L_{gnd} = 6mm$		

III. RESULTS AND DISCUSSIONS

In this Section, the microstrip slot antenna with various design parameters was constructed and the numerical and experimental results of the input impedance and radiation characteristics are presented and discussed. Ansoft simulation software High-Frequency Structure Simulator (HFSS) [9] is used to optimize the design and agreement between the simulation and measurement is obtained.

The configuration of the various antenna structures were shown in Fig. 2. VSWR characteristics for the ordinary slot antenna (Fig. 2 (a)), ordinary antenna with a pair of rotated T-shaped strips protruded inside square slots in the ground plane (Fig. 2 (b)) and the proposed slot antenna (Fig. 2 (c)) are compared in Fig. 3. As shown in Fig. 3, it is observed that the upper frequency bandwidth is affected by using the pair of rotated T-shaped strips protruded inside square

slots. To generate a band notch function, we use an SRR parasitic structure in the ground plane.

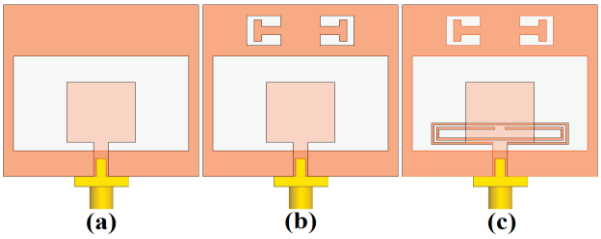

Fig. 2. (a) Ordinary slot antenna, (b) ordinary antenna with a pair of rotated T-shaped strips protruded inside square slots in the ground plane and (c) the proposed slot antenna.

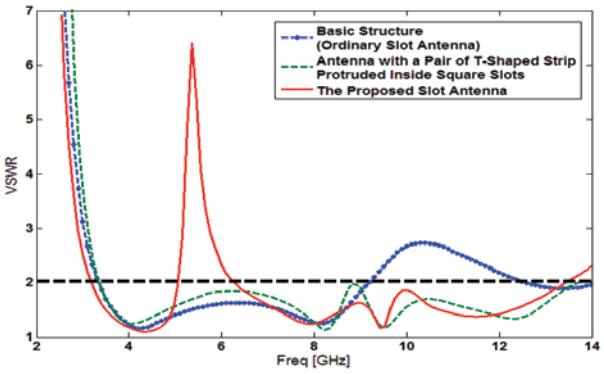

Fig. 3. Simulated VSWR characteristics for the various antennas shown in Fig. 2.

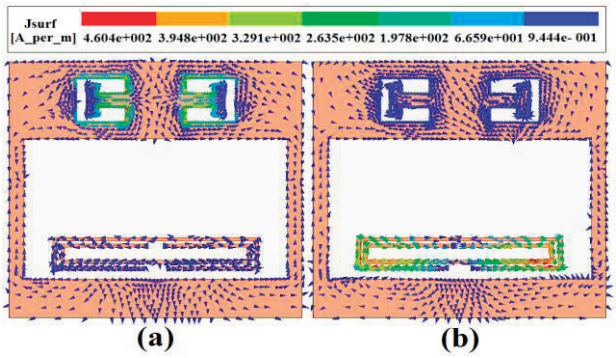

Fig. 4. Simulated surface current distributions on the ground plane: (a) at the extra resonance frequency in 9.5 GHz and (b) at the notched frequency in 5.5 GHz.

In order to know the phenomenon behind this multi-resonance and band-stop performance, simulated current distributions for the proposed antenna in the ground plane at 9.5 GHz and 5.5 GHz are shown in Fig. 4. It can be observed in Fig. 4 (a), that the current concentrated on the edges of the interior and exterior of the rotated T-shaped strips. Therefore, the antenna impedance changes at these frequencies due to the resonant properties of these structures [2]. Another important design parameter of this structure is the SRR conductor-backed plane. Figure 4 (b) presents the simulated current distributions at the notched frequency (5.5 GHz). As shown in Fig. 4 (b), in the notched frequency the current flows are more dominant around of the SRR conductor-backed plane [10].

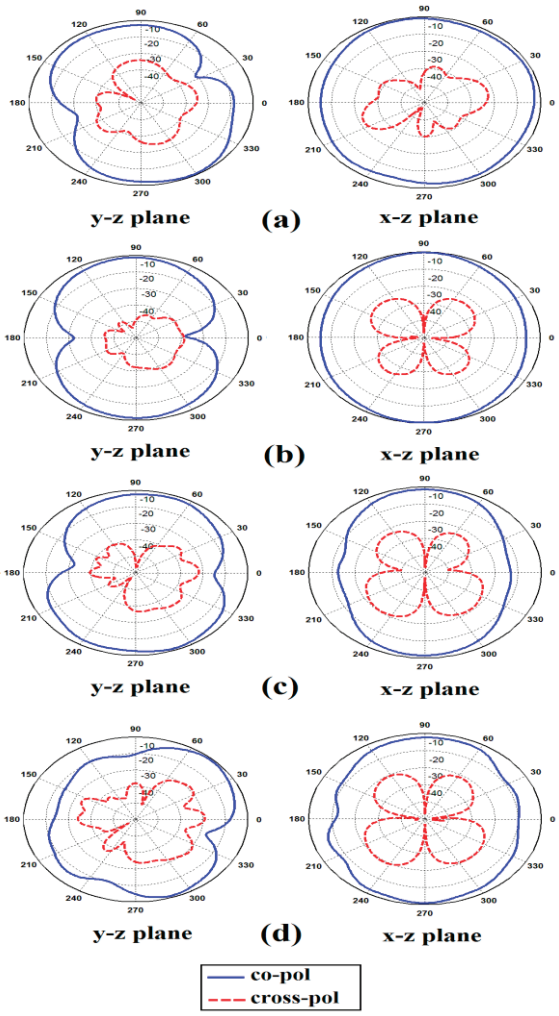

Fig. 5. Measured radiation patterns of the proposed antenna: (a) 4 GHz, (b) 6.5 GHz, (c) 9 GHz and (d) 12 GHz.

Figure 5 depicts the measured and simulated radiation patterns of the proposed antenna,

including the co-polarization and cross-polarization in the H-plane (x-z plane) and E-plane (y-z plane). It can be seen that the quasi-omnidirectional radiation pattern can be observed on x-z plane over the whole UWB frequency range, especially at the low frequencies. The radiation patterns on the y-z plane display a typical figure-of-eight, similar to that of a conventional dipole antenna. It should be noticed that the radiation patterns in E-plane become imbalanced as frequency increases, due to the increasing effects of the cross polarization. The patterns indicate at higher frequencies; more ripples can be observed in both E and H-planes, owing to the generation of higher-order modes. The cross-polarization component also increases at higher frequencies, due to the increased horizontal surface currents [11-14].

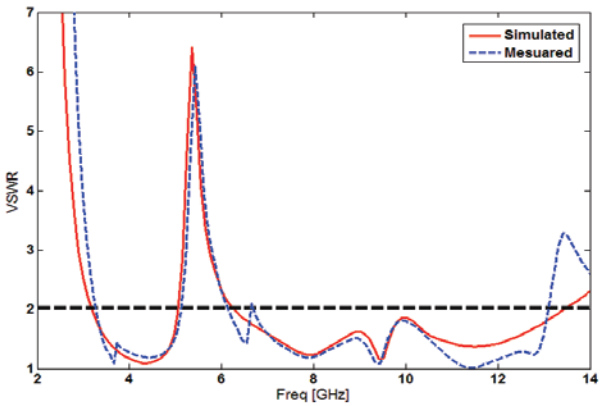

Fig. 6. Measured and simulated VSWR characteristics for the proposed antenna.

Simulated and Measured VSWR for the proposed antenna were shown in Fig. 6. The fabricated antenna has the frequency band of 3.1 GHz to 13.15 GHz, with band-notched function around 5.1-6 GHz.

However, as shown in Fig. 6, there exists a discrepancy between measured data and the simulated results. This discrepancy is mostly due to a number of parameters; such as the fabricated antenna dimensions as well as the thickness and dielectric constant of the substrate on which the antenna is fabricated and the wide range of simulation frequencies. In a physical network analyzer measurement, the feeding mechanism of the proposed antenna is composed of a SMA connector and a microstrip line (the microstrip feed-line is excited by a SMA connector); whereas, the simulated results are obtained using the Ansoft simulation software (HFSS). That in HFSS by default, the antenna is excited by a wave port that it is renormalized to a 50-Ohm full port impedance at all frequencies. In order to confirm the accurate VSWR characteristics for the designed antenna, it is recommended that the manufacturing and measurement processes need to be performed carefully. Moreover, SMA soldering accuracy and FR4 substrate quality need to be taken into consideration.

IV. CONCLUSION

In this paper, we propose a novel design of ultra-wide band slot antenna with band-notched function. The presented antenna can operate from 3.1 GHz to 13.15 GHz, with rejected band in 5-6 GHz. By applying a pair of rotated T-shaped strips protruded inside square slots plane, additional resonances are excited and hence much wider impedance bandwidth can be produced. In order to generate a frequency band-stop performance, we inserted an SRR conductor-backed plane. The designed antenna has a small size. Simulated and experimental results show that the proposed antenna could be a good candidate for UWB applications.

ACKNOWLEDGMENT

The authors are thankful to Microwave Technology (MWT) Company staff, for their beneficial and professional help (www.microwave-technology.com).

REFERENCES

[1] J. Y. Sze and K. L. Wong, "Bandwidth enhancement of a microstrip line-fed printed wide-slot antenna," *IEEE Trans. Antennas Propag.*, vol. 49, pp. 1020-1024, 2001.

[2] Y. W. Jang, "Experimental study of large bandwidth three-offset microstrip line-fed slot antenna," *IEEE Microw. Wireless Comp. Lett.*, vol. 11, pp. 425-426, 2001.

[3] M. K. Kim, Y. H. Suh and I. Park, "A t-shaped microstrip line-fed wide-slot antenna," *Proc. IEEE AP-S Int. Symp.*, pp. 1500-1503, 2000.

[4] M. Ojaroudi, and A. Faramarzi, "Multiresonance small square slot antenna for ultra-wideband applications," *Microwave and Optical Tech. Letters*, vol. 53, no. 9, pp. 2145-2149, September 2011.

[5] M. Ojaroudi, S. Yzdanifard, N. Ojaroudi and R. A. Sadeghzadeh, "Band-notched small square-ring antenna with a pair of t-shaped strips protruded inside the square ring for UWB applications," *IEEE Antennas Wireless Propag Lett*., vol. 10, pp. 227-230, 2011.

[6] N. Ojaroudi and M. Ojaroudi, "Small square slot antenna with dual band-notch function by using inverted t-shaped ring conductor-backed plane," *Microwave and Optical Tech. Letters*, vol. 54, no. 10, pp. 2267-2270, October 2012.

[7] W. J. Lui, C. H. Cheng, Y. Cheng, et al., "Frequency notched ultra-wideband microstrip slot antenna with a fractal tuning stub," *Electron Lett*., no. 41, pp. 294-296, 2005.

[8] S. W. Su, K. L. Wong and F. S. Chang, "Compact printed ultra-wideband slot antenna with a band-notched operation," *Microwave Opt Technol Lett.*, vol. 45, pp. 128-130, 2005.

[9] "Ansoft high frequency structure simulation (HFSS)," ver. 13, *Ansoft Corporation*, 2010.

[10] N. Ojaroudi, H. Ojaroudi and N. Ghadimi, "Quad-band planar inverted-f antenna (PIFA) for wireless communication systems," *Progress In Electromagnetics Research Letters*, vol. 45, pp. 51-56, 2014.

[11] N. Ojaroudi, "Compact UWB monopole antenna with enhanced bandwidth using rotated l-shaped slots and parasitic structures," *Microw. Opt. Technol. Lett.*, vol. 56, pp. 175-178, 2014.

[12] N. Ojaroudi, S. Amiri and F. Geran, "A novel design of reconfigurable monopole antenna for UWB applications," *Applied Computational Electromagnetics Society (ACES) Journal*, vol. 28, no. 6, pp. 633-639, July 2013.

[13] N. Ojaroudi, "Application of protruded strip resonators to design an UWB slot antenna with WLAN band-notched characteristic," *Progress in Electromagnetics Research C*, vol. 47, pp. 111-117, 2014.

[14] N. Ojaroudi, "Microstrip monopole antenna with dual band-stop function for UWB applications," *Microw. Opt. Technol. Lett*., vol. 56, pp. 818-822, 2014.

A Novel UWB Antenna with Triple Band-Notched Characteristics

Xiao-Lin Yang, Yan Wang, and Gang Chen

School of Physical Electronics
University of Electronic Science and Technology of China, Cheng Du 610054, China
842743945@qq.com, yxlin@uestc.edu.cn, 369780081@163.com

Abstract ─ A novel planar monopole antenna with 3.9/5.5/8 GHz triple band-notched characteristics is proposed. The monopole antenna is composed of microstrip line and radiating patch where the large circle following connects with a small half circle, whereas the ground plane is printed on the other side. By adding a simple T-shaped resonator on the bottom side, two band-notched characteristics in the C-band (3.7-4.2 GHz) and X-band (7.6-8.6 GHz) are obtained at the same time. The band-notched characteristic in the WLAN (5-6 GHz) is obtained by etching spline curved strip in the radiating patch. The measured results are roughly consistent with the simulated. The proposed antenna is printed on a 22 mm × 32 mm, polytetrafluoroethylene (PTFE) substrate with relative permittivity of 2.65 and substrate thickness of 0.5 mm.

Index Terms - Band-notched, monopole antenna, T-shaped.

I. INTRODUCTION

Ultra-wideband (UWB) communication systems have attracted great attention in the wireless world due to the many advantages, such as high speed data rate, low probability of intercept and low cost. However, over the released UWB operation bandwidth (3.1~10.6 GHz), there are some bands occupied by the existing wireless systems. For example, C-band, WLAN networks and some satellite service systems operating in 3.7-4.2 GHz, 5-6 GHz and 7.6-8.6 GHz, respectively [1-2], which will be caused interference with UWB systems. In order to get rid of the interferences of these bands, many methods have been reported, such as using different shape slot on the radiating patch or the ground plane [3-7]. Another main approach is introducing parasitic elements using split ring resonator, or the combination of these methods. Generally, only one or two notched bands can be achieved by the antennas mentioned above. Recently some antennas with triple-band have been studied [8-11], but its band-notches are controlled, respectively and their dimensions are relatively large. A recent trend in band notched UWB antenna design is to impose the multi-band notched characteristics. This article offers a new design strategy on the ways of band control and triple band-notched Characteristics addressing three merits as follows:

i. The proposed antenna has simple and miniaturized structure. The structure has relatively small dimension (22 mm×32 mm) comparing with the antenna dimension (46 mm×48 mm) [12].
ii. In this letter, the measured peak value of the antenna's VSWR in the stop bands are 6.8, 7 and 14; all higher than 6.5, which is even better than the ones achieved by the structures proposed in [13-15] (lower than 5, 4.2 and 5.6 in, respectively). Higher and sharper band rejection achieved for each of the notches makes the avoidance of interference more effective.
iii.

By adding a simple T-shaped resonator on the bottom side, as well as adding a spline curved strip parasitic element in the radiating patch aimed for the triple desired band rejections function at C-band (3.4- 4.2 GHz), X-band (7.6-8.6 GH-z) and WLAN (5-6 GHz). T-shaped structure has a simpler optimization due to the lower number of degrees of freedom and can control two stop bands. Moreover, the segmenting structure that brings on band notched characteristic could

Submitted On: January 21, 2013
Accepted On: March 30, 2014

probably be applied to other monopole patches with various patch shapes.

II. ANTENNA DESIGN AND PARAMETER STUDY

A. Antenna configuration

The geometry of the proposed antenna is described in Fig. 1 (a). The antenna is printed on substrate of PTFE with thickness of 0.5 mm, relative permittivity of 2.65. The radiating patch and a 50 Ω microstrip line are printed on the top layer and the ground plane is printed on the bottom layer. A photograph of the fabricated antenna is presented in Fig. 1 (b).

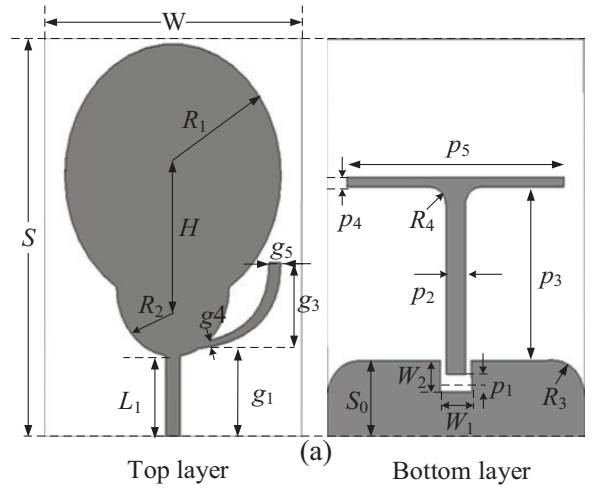

(a)

(b)

Fig. 1. (a) Geometry of the proposed antenna, (b) photograph of the fabricated proposed antenna; units (mm).

B. Parametric optimization

The width of the microstrip line is 1.4 mm to achieve characteristic impedance of 50 Ω from 2.8-10.6 GHz. The optimizing values of each parameter are as follows: w=22, s=32, L1=6.5, R1=10.5, R2=5.5, R3=3, H=9, w1=2.5, w2=3 and S0=6.2, all units with mm. The impedance band is from 2.8-10.6 GHz. In this study, by cutting a rectangular slot in the ground plane the characteristics at the higher frequency can be enhanced. The rectangular slot acts as an impedance matching element to control the impedance bandwidth of the proposed antenna because it creates additional surface current paths in the antenna. Therefore, additional resonance is excited and hence much wider impedance bandwidth can be produced [16], especially at the higher band. The gap between the radiating patch and ground plane (S_0) affects the band dispensation because it acts as a matching network [17]. The optimum UWB impedance bandwidth from 2.8-10.6 GHz is obtained with S_0=6.2 mm. The simulated VSWR of monopole antenna with and without a rectangular slot is shown in Fig. 2. Obviously, the property of frequency band from 8-10 GHz has been improved.

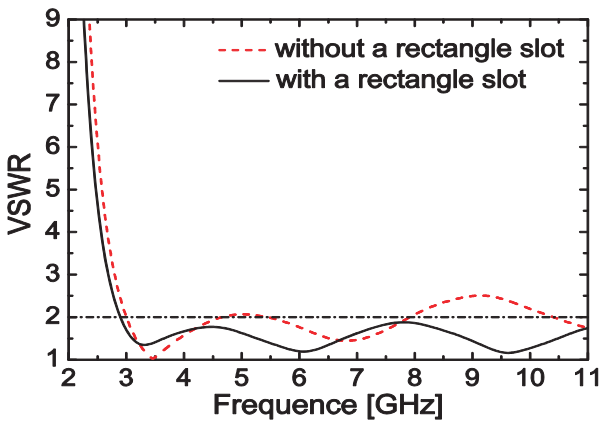

Fig. 2. Simulated results of the antenna; with and without a rectangle slot.

C. Antenna with spline curved strip parasitic element

By adding a spline curved strip parasitic element in the radiating patch of the antenna, a frequency band notched for WLAN is achieved. The band-notch frequency mainly depends on the length of the strip. By comparing Figs. 3 (a) and (c), we can see that at the radiating frequency 3 GHz the surface current concentrated on the edges of the radiating patch, as well as the ground plane as shown in Fig. 4 (a); while at the notch frequency, the surface current concentrated on the

edge of the interior and exterior of the spline curved strip parasitic element as shown in Fig. 3 (c). The reason is the spline curved strip perturbs the resonant response at the band-notch frequency. The frequency given by the dimensions of the WLAN band-notch feature can be formulated as [10]:

$$f_{WLAN\_notch} = \frac{c}{4(g_3 + g_4)\sqrt{\varepsilon_{eff}}}. \qquad (1)$$

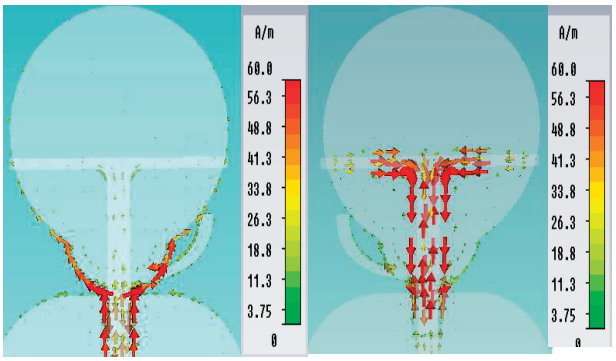

(a) 3 GHz (b) 3.95 GHz

(c) 5.5 GHz (d) 8 GHz

Fig. 3. Simulated results of the surface current distributions at frequency: (a) 3 GHz, (b) 3.95 GHz, (c) 5.5 GHz and (d) 8 GHz.

The various band-notch characteristics can be achieved by carefully choosing the parameters for the spline curved strip element. Figure 4 exhibits simulated band rejection characteristics against various g_1, g_2 and g_3 of the parasitic element with fix g_4= 0.7 mm and g_5=1.2 mm. It can be seen that as g_2 and g_3 increase, the WLAN notched-band shifts toward low frequency, while g_1 is as inverse. The reason is that g_1 increase lead to the length of the strip decrease. These results correspond with the caculated formula (1). Ultimately, the optimal parameters of the spline curved strip are as follows: g_1=7.16 mm, g_2=10.5 mm, g_3=7 mm, g_4=0.7 mm and g_5=1.2 mm.

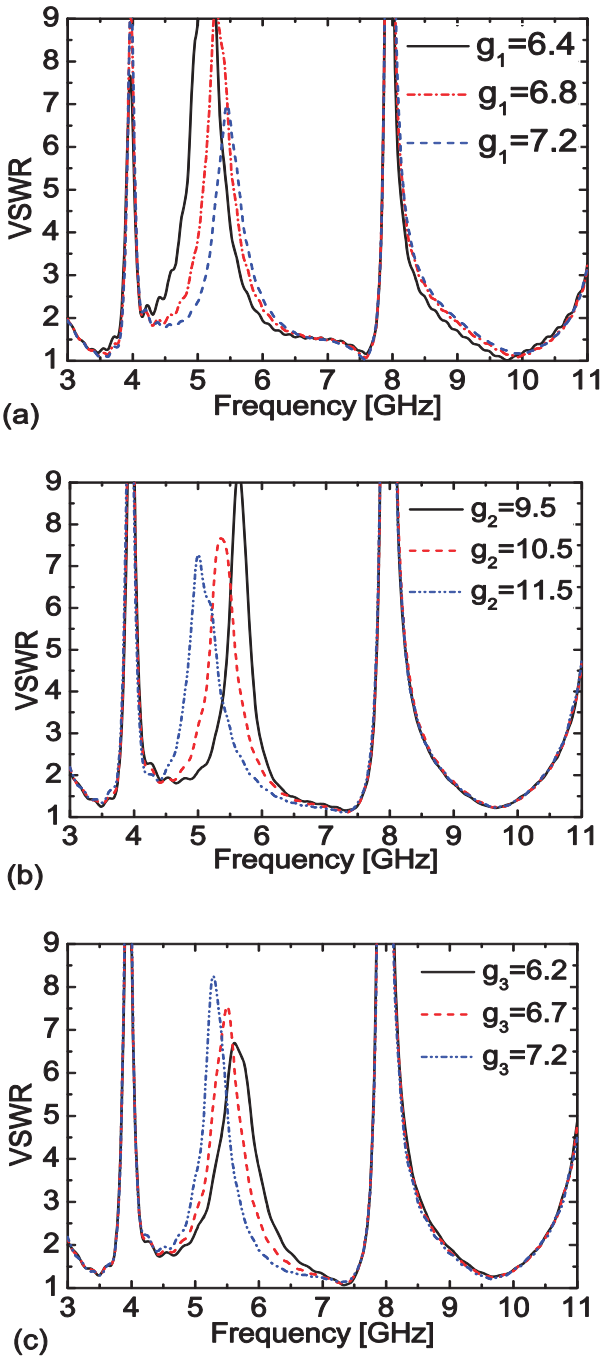

Fig. 4. Simulated band-rejection characteristics of the proposed antenna with notched band for: (a) g_1, (b) g_2 and (c) g_3; units (mm).

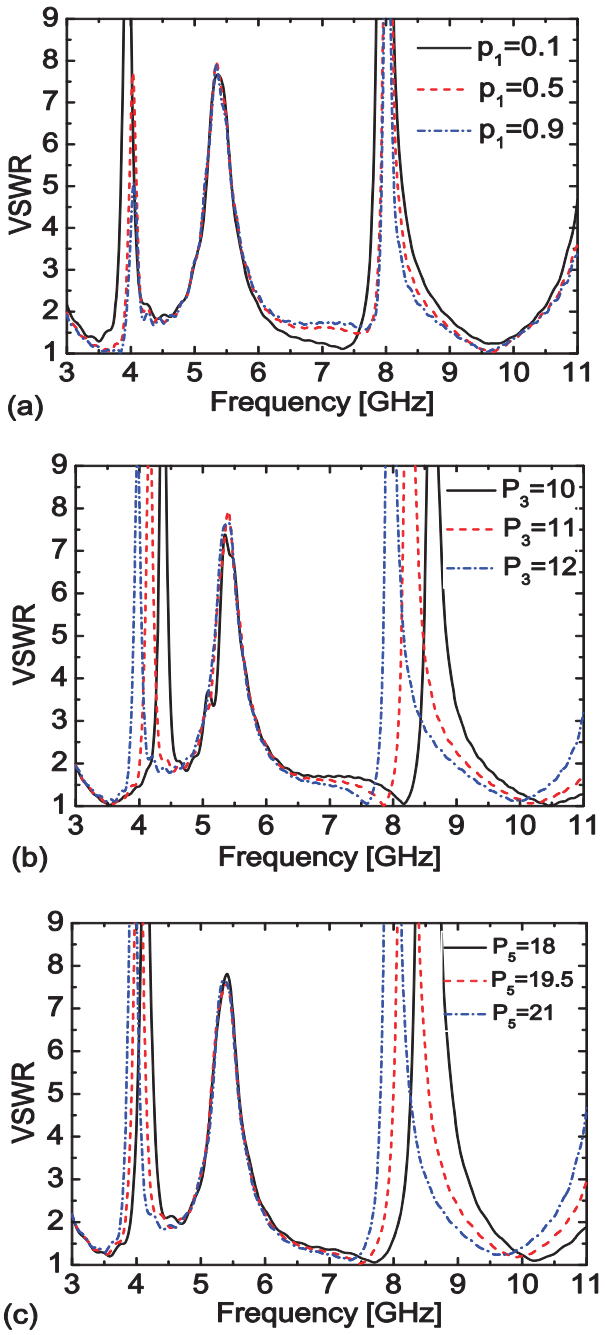

Fig. 5. Simulated band-rejection characteristics of the proposed antenna with varying parameters: (a) p_1, (b) p_2, (c) p_3 and (d) p_5; units (mm).

D. T-shaped parasitic element

To achieve the other two band-notched characteristics for C-band and X-band, a T-shaped stub is printed on the bottom layer. This structure changes the reactance of the input impedance. The T-shaped strip coupled to the ground plane with the rectangular slot, which act as the stop filter at a certain frequency. In order to explain the band-notched function of the proposed structure, the surface current distribution was analyzed. Figures 3 (b) and 3 (d) illustrate the simulated surface current distribution of notched-band frequencies 3.9 GHz and 8 GHz, respectively. It can be seen that at band-notched frequency the current distribution is clustered along the edges of the T-shaped strip. The resultant radiation fields cancel out and sharp attenuation near the notch frequency is produced. Hence, the antenna does not radiate efficiently and the stop band is achieved. The notched center frequency and the bandwidth can be controlled by adjusting the dimensions of the T-shaped parasitic strip. The parameters of the proposed antenna are studied by changing one parameter at a time and fixing the others. The sensitive parameters for various p_1, p_3 and p_5 of the T-shaped strip with p_2=1.9 mm, p_4=0.8 mm and R_4=1.5 mm, are given in Fig. 5. It is observed that the p_1 determines the notched bandwidth. As p_1 increases, the notched bandwidth increases. While the p_3 and p_5 mainly determine the location of notched band. As p_3 and p_5 increase, the center frequency of the notched band shifts toward the low frequency. Therefore, it can be concluded that the rejected band can be easily obtained by tuning these parameters. Lastly, the optimized parameters are listed as follow: p_1=0.1 mm, p_2=1.9 mm, p_3=15 mm, p_4=0.8 mm, p_5=21 mm and R_4=1.5 mm.

III. RESULTS AND DISCUSSIONS

A prototype of the proposed antenna was fabricated and the VSWR was measured with an Agilent E8363B vector network analyzer. Figure 6 (a) shows the performance of the measured and simulated VSWR of UWB antenna with triple band-notched characteristics. The measured results showed that the proposed antenna exhibits a wide impendence bandwidth from 2.8 GHz to 11 GHz; while it achieved triple stop band of 3.7-4.2 GHz, 5-6.2 GHz and 8.1-9 GHz, respectively. Comparing to simulated results, the measured center frequency of the band-notched shifts toward higher and the gain also has the frequency shift, as shown in Fig. 6 (b). The reasons maybe led by the deviation substrate relative permittivity between simulated and fabricated. The losses of the coaxial line and coaxial connectors are possible reason of the disagreement between the simulated and the measured peak gain.

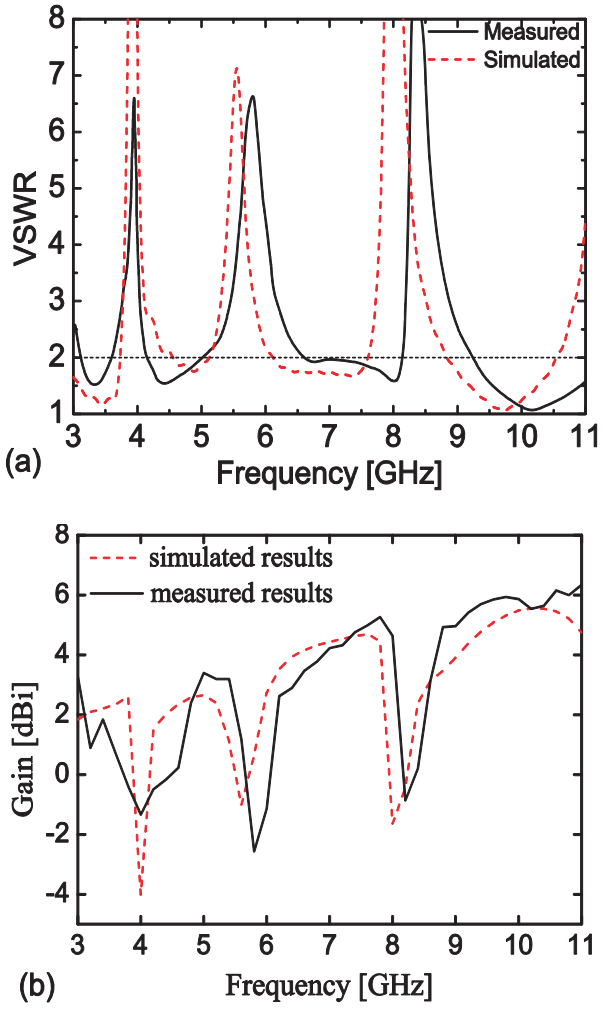

Fig. 6. (a) Measured and simulated VSWR of the proposed UWB antenna with triple band-notched function, (b) measured and simulated the peak gain of the proposed UWB antenna with triple band-notched function.

Figure 7 illustrates the measured radiation pattern in the E-plane and H-plane at the frequencies of 4.5, 6.4 and 8 GHz. It can be seen that the radiation patterns in the H-plane for the three frequencies are nearly omnidirectional.

IV. TRANSFER FUCTION STUDY

On UWB antenna designing, it is crucial to evaluate the system transfer function. In order to suppress the signal distortions, it should make the group delay as sharp as possible in notch-band and a constant outside of the notch-band.

The simulated group delay of the proposed antenna is presented in Fig. 8 (a). It can be seen that in operating band the variation of the group delay is within 1, while in notched band the group delay is sharp change.

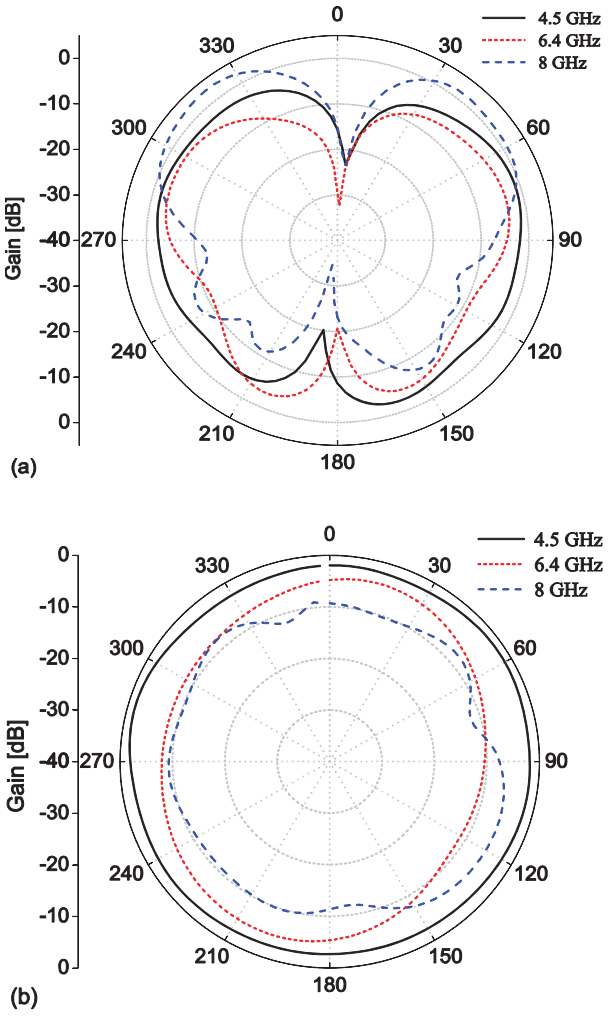

Fig. 7. Measured radiation patterns at: (a) E-plane and (b) H-plane.

Meanwhile, in order to study the level of distortion in the radiated pulses, the fidelity of the signals was computed. The fidelity of the pulses of an antenna can be calculated to assess the quality of the received pulse and select a proper detection template [18]. The definition of the fidelity can be written as:

$$F = \max_{\tau}\left[\frac{\int_{-\infty}^{+\infty} E_r(t)Ut(t+\tau)}{\sqrt{\int_{-\infty}^{+\infty}\left|E_r(t)^2\right|dt}\times\sqrt{\int_{-\infty}^{+\infty}\left|U_t(t)^2\right|dt}}\right], \quad (2)$$

where E_r refers to the normalized waveform of the received pulse and U_t is the template pulse; which was taken to be the normalized source pulse in this case. The calculated fidelity for the antenna is around 0.75, as shown in Fig. 8 (b). This provides a good time domain performance of the presented antenna and guarantees little distortion of the transmitted and received signals.

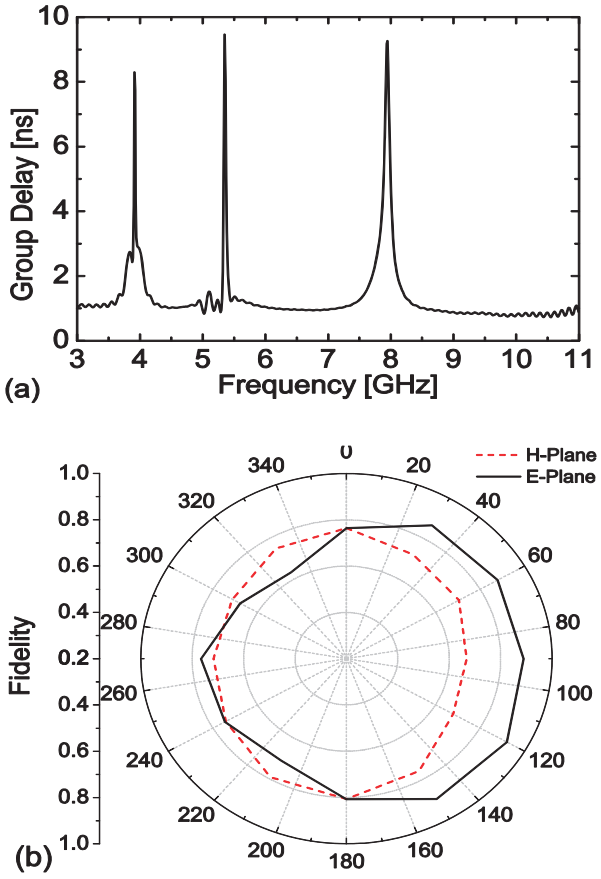

Fig. 8. Simulated results of: (a) group delay and (b) fidelity.

V. CONCLUTION

A novel compact UWB monopole antenna with triple band-notched characteristics is presented and investigated. The proposed antenna covers the frequency band of 2.8 GHz to 10.6 GHz with three rejection bands around 3.7-4.2 GHz, 5-6 GHz and 7.6-8.6 GHz. The radiation patterns in the H-plane are nearly omnidirectional and a typical monopole-like pattern in the E-plane over the entire UWB band. The gain is stable in operating bands, while with a sharp decrease in notched bands. The group delay and fidelity studying indicated that this antenna has good time domain characteristics over the operating bands and notable band-notched properties in required frequencies. Overall, the proposed antenna may be a good candidate for portable UWB systems.

ACKNOWLEDGMENT

This work was supported by the Fundamental Research Funds for the Central Universities ZYGX2011J049.

REFERENCES

[1] K. Zhang, Y. Li and Y. Long, “Band-notched UWB printed monopole antenna with a novel segmented circular patch,” *IEEE Antennas and Wireless Propagation Letters*, vol. 9, pp. 1209-1212, 2010.

[2] Y. S. Li, W. Li and W. Yu, "A multi-band/UWB MIMO/diversity antenna with an enhanced isolation using radial stub loaded resonator," *Applied Computational Electromagnetics Society (ACES) Journal*, vol. 28, no. 1, pp. 8-20, January 2013.

[3] D. S. Cai, Z. Y. Lei, Y. Ding and D. Zhao, “A compact coplanar waveguide fed monopole antenna with dual band-notched application,” *Microwave and Optical Technology Letters*, vol. 54, no. 3, pp. 677-681, March 2012.

[4] Z. L. Zhou, L. Li and J. S. Hong, "A novel compact monopole antenna with triple high quality rejected bands for UWB applications," *Applied Computational Electromagnetics Society (ACES) Journal*, vol. 27, no. 8, pp. 654-659, August 2012.

[5] O. M. H. Ahmed, A. M. Elboushi and A. R. Sebak, “Design of half elliptical ring monopole antennas with elliptical slot in ground plane for future UWB applications,” *Microwave and Optical Technology Letters*, vol. 54, no. 1, pp.181-187, January 2012.

[6] M. M. Abdollahi, H. R. Dalili Oskouei, M. Akbari and M. Mighani, "A novel compact UWB antenna with triple band-notches for WiMAX/WLAN/ITU bands," *Applied Computational Electromagnetics Society (ACES) Journal*, vol. 27, no. 12, pp. 1014-1021, December 2012.

[7] D. Z. Kim, W. I. Son, W. G. Lim, H. L. Lee and Y. Jong-Won, “Integrated planar monopole antenna with microstrip resonators having band-notched characteristics,” *IEEE Trans*., vol. 58, no. 9, pp. 1837-2842, September 2010.

[8] W. T. Li, X. W. Shi and Y. O. Hei, “Novel planar UWB monopole antenna with triple band-notched characteristics,” *IEEE Antenna and Wireless Propagation Letters*, vol. 8, pp. 1094-1098, 2009.

[9] D. O. Kim and C. Y. Kim, "CPW-fed ultra-wideband antenna with triple band-notch function," *Electronics Letters*, vol. 46, no. 18, pp. 246-1248, September 2010.

[10] S. Natarajamani, S. K. Behera and S. K. Patra, "A triple band-notched planar monopole antenna for ultrawide band applications," *Microwave and Optical Technology Letters*, vol. 54, no. 2, pp. 539-543, February 2012.

[11] Y. Zhang, W. Hong, C. Yu, Z. Q. Kuai, Y. D. Don and J. Y. Zhou, "Planar ultra-wideband antennas with multiple notched bands based on etched slots on the patch and/or split ring resonators on the feed line," *IEEE Trans*., vol. 56, no. 9, pp. 3063-3068, September 2008.

[12] Y. S. Hu, M. Li, G. P. Gao, J. S. Zhang and M. K. Yang, "A double-frinted trapezoidal patch dipole antenna for UWB application with band-notched characteristic," *Progress In Electromagnetics Research* (*PIER)*, 103, pp. 259-269, 2010.

[13] Y. Zhang, W. Hong, C. Yu, Z. Q. Kuai, Y. D. Don and J. Y. Zhou, "Planar ultra-wideband antennas with multiple notched bands nased on etched slots on the patch and/or split ring resonators on the feed line," *IEEE Trans*., vol. 56, no. 9, pp. 3063-3068, September 2008.

[14] K. H. Kim and S. O. Park, "Analysis of the small band-rejected antenna with the parasitic strip for UWB," *IEEE Trans. Antennas Propag*., vol. 54, no. 6, pp. 1688-1692, June 2006.

[15] K. H. Kim, Y. J. Cho, S. H. Hwang and S. O. Park, "Band-notched UWB planar monopole antenna with two parasitic patches," *Electron. Lett*., vol. 41, no. 14, pp. 783-785, July 2005.

[16] S. K. Mishra, R. K. Gupta, A. Vaidya and J. Mukherjee, "Low-cost, compact printed circular monopole UWB antenna with 3.5/5.5 GHz band-notched characteristics," *Microwave and Optical Technology Letters*, vol. 54, no. 1, pp. 242-246, January 2012.

[17] N. Ojaroudi, M. Ojaroudi and H. Ebarhimian, "Band-notched UWB microstrip slot antenna with enhanced bandwidth by using a pair of c-shaped slots," *Microwave and Optical Technology Letters*, vol. 54, no. 2, February 2012.

[18] T. S. P. See and Z. N. Chen, "Experimental characterization of UWB antennas for on-body communications," *IEEE Trans. Antennas Propag*., vol. 57, pp. 866-874, April 2009.

Xiaolin Yang received his Ph.D. degree in Applied Physics from Lanzhou University, in 2005. He is currently an Associate Professor at the School of Physical Electronics, University of Electronic Science and Technology of China. His current research interests are microwave circuits and systems and Ultra-wideband antenna.

Yang Wang was born in Anhui Province, China. She received her Bachelor degree in Physics from Anqin Teachers College, Anqin, in 2010 and is currently working towards her M.S. degree in Electronic and Communication Engineering at UESTC. Her research interests are in UWB antenna.

Gang Cheng was born in Jiangsu Province, China. He received his Bachelor degree in Optical Information Sciences and Technology from Southwest University of Science and Technology, Mianyang, in 2010 and is currently working towards his M.S. degree in Electronic and Communication Engineering at UESTC. His research interests are in reconfigurable antenna.

Design of Compact CPW-Fed Planar Antenna with Dual Notched Bands Using Slotted Conductor-Backed Plane for UWB Application

M. Moosazadeh, and Z. Esmati

Department of Electrical Engineering
Islamic Azad University, Urmia Branch, Urmia, Iran
m.moosazadeh14@gmail.com, zahra.esmati@yahoo.com

Abstract ─ A compact design of a Coplanar Waveguide Fed (CPW-Fed) monopole antenna with Ultra Wideband (UWB) performance and dual band-notched characteristics is proposed. Dual band-notched characteristics are achieved by U-shaped slot inside the slotted conductor-backed plane and a pair of mirror rectangular-shaped slots at the two sides of the truncated conductor-backed plane. Also, wider impedance bandwidth can be achieved with this structure. The proposed antenna has a small size of 18×18 mm^2 and measured to cover the bandwidth for UWB (2.7-14.5 GHz) for VSWR < 2, except the bandwidths of 3.1-3.6 for WiMAX and 5-6 GHz for WLAN. The antenna has an omnidirectional radiation across the whole ultra wideband as validated by the measured radiation pattern and gain.

Index Terms – Coplanar Waveguide (CPW) antennas, frequency band-notched function, Ultra Wideband (UWB) antenna.

I. INTRODUCTION

Quick development of wireless communication in the field of UWB technology and its applications has increased demand in commerce and industry. There has been great progress in the design of ultra wideband antennas and devices in recent years [1]. On the other hand, the printed monopole antenna exhibits very main parameters in designing UWB antennas, such as easy to manufacture structure, compact size, low cost and omnidirectional radiation pattern across the band from 3.1 GHz to 10.6 GHz [2]. However, there are several narrow bands that might become potential interferences within the UWB frequency spectrum, such as IEEE802.16.

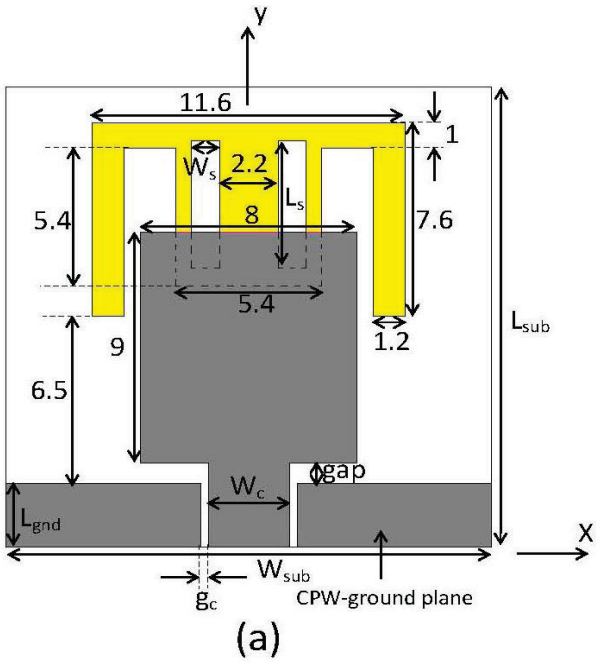

Fig. 1. Geometry of the propose antenna: (a) dimensions (units: mm) and (b) photograph of fabricated antenna.

The UWB antenna with band stop performance is

Submitted On: January 26, 2013
Accepted On: March 30, 2014

concerning the UWB antenna where band-notched characteristics have been reported; WiMAX (3.3-3.6 GHz) and the Wireless Local Area Network (WLAN) for IEEE802.11a (5.15-5.825 GHz).

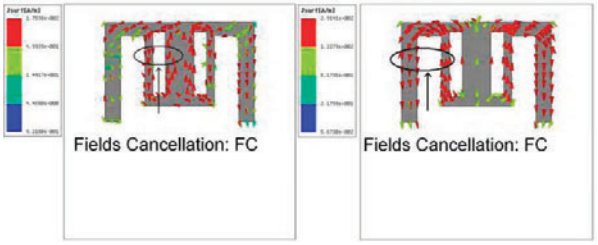

Fig. 2. Simulated current distribution of the dual band-notched monopole antenna at: (a) 3.3 GHz and (b) 5.5 GHz.

These designs use different types of slots, slits and parasitic elements in the radiator, the ground plane or even in the feeder to achieve the required band-notching characteristics with limited impact on the required pass band [3-12].

In this paper, a novel compact CPW-Fed UWB antenna with dual band-notch characteristics and increased bandwidth is presented. In this designed antenna, the target is to present a compact structure with a step-by-step design procedure. By having a pair of mirror rectangular-shaped slots etched and a U-shaped slot embedded on the conductor-backed plane, a dual band-notched characteristic is created. Wider impedance bandwidth is achieved by use of the final structure of conductor-backed plane, which provides a wide usable fractional bandwidth of more than 137% (2.7-14.5 GHz). Measured results of the realized antenna with the different structures of conductor-backed plane are presented.

II. ANTENNA DESIGN

Figure 1 shows the geometry and configuration of the proposed antenna with $W_{sub} \times L_{sub}$ dimensions. The proposed antenna with compact dimensions of 18×18 mm^2, is constructed on a 0.8 mm thickness FR4 substrate with relative dielectric constant ε_r = 4.4 and loss tangent of 0.02. The antenna is fed by a 50Ω Coplanar Waveguide (CPW). A rectangular patch with the dimensions of 8×9 mm^2 is connected to the CPW ground plane. In the first step of the design, the dimensions of the substrate, radiator and CPW ground plane are optimized using the software HFSS for an UWB frequency coverage.

For the impedance matching, the distance between the patch and the ground plane is indicated with a gap, which provides suitable control between the lower edge patch and the ground plane. The optimum gap between the radiator and the ground plane is 0.3 mm. To modify the performance of the antenna by creating two sub-bands at the WiMAX (3.3-3.6 GHz) and WLAN (5.15-5.825 GHz), the conductor-backed is slotted in the manner shown in Fig. 1. A pair of mirror rectangular-shaped slots has created the first notched band centered at 3.3 GHz, whereas the U-shaped slot inside the conductor-backed is responsible for making the second notched band centered at 5.5 GHz. The photograph of the fabricated band-notched UWB antenna with the final optimal design is shown in Fig. 1 (b).

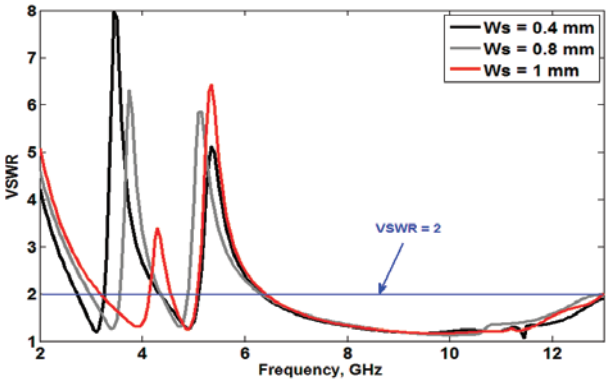

Fig. 3. Simulated band-rejection of the proposed antenna for various values W_s.

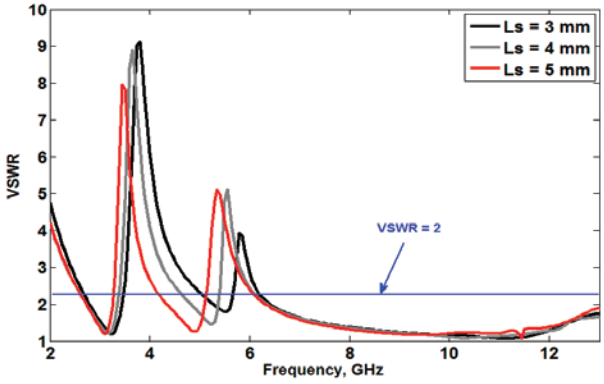

Fig. 4. Simulated band-rejection of the proposed antenna for various values L_s.

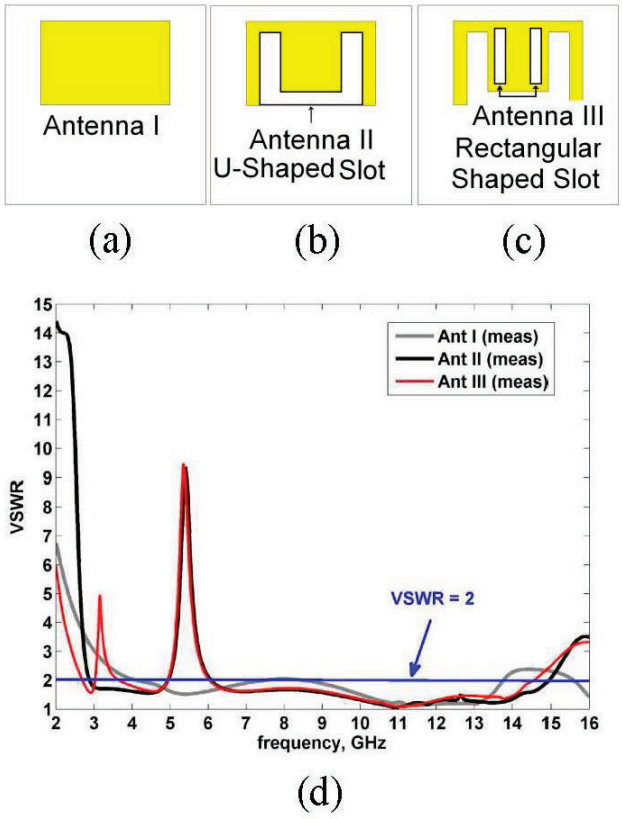

Fig. 5. Geometry of conductor-backed plane: (a) ordinary conductor-backed plane, (b) with U-shaped slot, (c) with a pair of mirror rectangular-shaped slots and (d) measured VSWR characteristics for a, b and c.

The modified conductor-backed is designed to achieve better impedance matching over the entire UWB frequency band.

III. RESULT AND DISCUSSIONS

The simulated results are obtained using the electromagnetic software Ansoft HFSS. Figure 2 shows the current distribution at the first and second notch frequency. It is clear from Fig. 2 (a) that the current flows inside conductor-backed in opposite directions at the two edges of the rectangular slots at 3.3 GHz. Thus, the total effective radiation is very low and a notched band is achieved. In Fig. 2 (b), the surface current at 5.5 GHz at the indoor U-shaped slot is in reverse direction to the current in the outer edges of the slot. Thus, the overall radiation at this band is very limited and a second notched band is achieved.

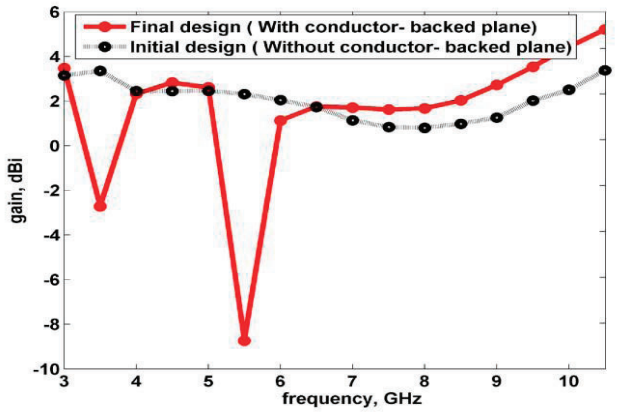

Fig. 6. The measured gain of the proposed antenna, with and without conductor-backed plane.

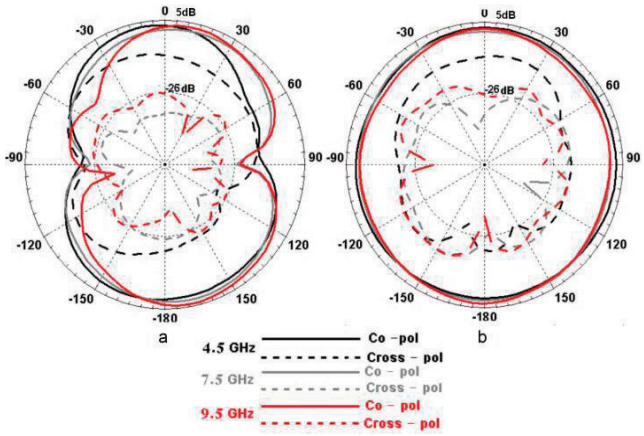

Fig. 7. Measured radiation pattern of the proposed antenna: (a) on E-plane and (b) on H-plane.

Through parametric study, the optimum value for each parameter is investigated. The width of the rectangular-shaped slots inside the conductor-backed plane is the main parameter in determining the first band-notched function. The effect of varying the size of the W_s is indicated in Fig. 3. As shown, it is clear that when W_s increases from 0.4 to 1mm, the first band-notched frequency shifts down from around 4.1 to 3.28 GHz. To generate the second band-notched characteristic for WLAN, the length of rectangular slot is investigated. The simulated VSWR curve with various values of the L_s is plotted in Fig. 4. The results indicate that the second band-notched of the proposed antenna can be effectively controlled by adjusting L_s.

The developed antenna that has the dimensions W_{sub} = 18 mm and L_{sub} = 18 mm was tested using an Agilent 8722ES Vector Analyzer (VNA). The two bands centered at 3.3 GHz and 5.5 GHz are notched with VSWR that is larger than 5 for the first band and 10 for the second band. However, it is clear from Fig. 5 (a) that the antenna has a poor performance by use of the rectangular-shaped structure, which should be part of the UWB spectrum. To improve the performance at that band and to obtain dual band-notched, a slotted conductor-backed structure is indicated at the bottom layer in Fig. 5 (c). By use of the design, it is worth mentioning that using the slotted conductor-backed plane in the manner shows in Fig. 5 (c); it not only enables the rejection of the undesired sub-bands, but it also improves the performance at the upper frequency band. Figure 5 (d) clearly shows that the impedance bandwidth of proposed antenna very well covers the intended VSWR < 2 from 2.7 GHz to 14.5 (137%) GHz and has dual band-notched characteristics (VSWR > 2) in 3.1-3.6 GHz and 5-6 GHz. Also, it can be observed that by using the filter structures inside conductor-backed, the lowest frequency is significantly decreased from 4 GHz to 2.7 GHz. Figure 6 shows the measured maximum antenna gain from 3 GHz to 11 GHz for the developed antenna. The simulated gain of a rectangular patch structure also confirms the effect of the utilized approach in the rejection of two sub-bands. Figure 6 indicates that the realized dual band-notched antenna has good gain flatness, except at the two notched bands. As shown in Fig. 6, gain decreases the measure drastically at the frequency bands. Figure 7 shows radiation patterns for three different frequencies, 4.5, 7.5 and 9.5 GHz of the UWB band in H-plane (xoz-plane) and E-plane (yoz-plane); for the antenna with double band notches. Figure 7 approximately exhibits an omnidirectional radiation pattern in H-plane and a dipole-like radiation pattern in the E-plane.

IV. CONCLUSION

A compact CPW-Fed printed monopole antenna with ultra wideband performance and dual band-notched characteristics has been presented. The first notched band aimed at preventing any interference with existing WiMAX systems and is achieved by using a pair of mirror rectangular-shaped slots in the conductor-backed plane. The second notched band aimed at preventing the interference with the 5 GHz WLAN systems and is achieved by use of the U-shaped slot embedded inside the slotted conductor-backed plane. Experimental results show that the fabricated antenna with proper dimensions and aforementioned characteristics such as small size, light weight and good omnidirectional radiation patterns, is a very good candidate for UWB applications.

REFERENCES

[1] "First report and order in the matter of revision of part 15 of the commission's rules regarding ultra-wideband transmission systems," ET docket 98-153, *Federal Communications Commission, FCC 02-48*, April 22, 2002.

[2] M. Moosazadeh, C. Ghobadi and M. Dousti, "Small monopole antenna with checkered-shaped patch for UWB application," *IEEE Antennas Wireless Propa. Lett*., vol. 9, pp. 1014-1017, 2010.

[3] M. Mighani, M. Akbari and N. Felegari, "A CPW dual band notched UWB antenna," *Applied Computational Electromagnetics Society (ACES) Journal*, vol. 27, no. 4, pp. 352-359, April 2012.

[4] M. Moosazadeh, A. M. Abbosh and Z. Esmati, "Design of compact planar ultra-wideband antenna with dual-notched bands using slotted square patch and pi-shaped conductor-backed plane," *IET Microw. Antennas Propag*., vol. 6, pp. 290-294, 2012.

[5] Z. L. Zhou, L. Li and J. S. Hong, "A novel compact monopole antenna with triple high quality rejected bands for UWB applications," *Applied Computational Electromagnetics Society (ACES) Journal*, vol. 27, no. 8, pp. 654-659, August 2012.

[6] M. Moosazadeh and Z. Esmati, "Small monopole antenna design with band-notched characteristics using inverted t-shaped form on the patch," *Microwave Opt Technol. Lett*., vol. 54, pp. 100-103, 2012.

[7] X. L. Ma, W. Shao and G. Q. He, "A novel dual narrow band-notched CPW-fed UWB slot antenna with parasitic strip," *Applied Computational Electromagnetics Society (ACES) Journal*, vol. 27, no. 7, pp. 581-586, July 2012.

[8] H. K. Yoon, Y. J. Yoon, H. Kim and C. H. Lee, "Flexible ultra-wideband polarization diversity antenna with band-notch functions," *IET Microw. Antennas Propag*., vol. 5, pp. 1463-1470, 2011.

[9] J. Wiliam and R. Nakkeeran, "A new UWB slot antenna with rejection of WiMAX and WLAN bands," *Applied Computational Electromagnetics Society (ACES) Journal*, vol. 25, no. 9, pp. 787-793, September 2010.

X. J. Liao, H. C. Yang, N. Han and Y. Li, "UWB antenna with dual narrow band-notches for lower and upper WLAN bands," *Electron Lett*., vol. 46, pp. 1593-1594, 2010.

[10] M. M. Abdollahi, H. R. Dalili Oskouei, M. Akbari and M. Mighani, "A novel compact UWB antenna with triple band-notches for WiMAX/WLAN/ITU bands," *Applied Computational Electromagnetics Society (ACES) Journal*, vol. 27, no. 12, pp. 1014-1021, December 2012.

[11] M. Moosazadeh and Z. Esmati, "A small CPW-fed ultra-wideband antenna with dual band-notched characteristics," *Microwave Opt Technol. Lett*., vol. 54, pp.1528-1532, 2012.

Mahdi Moosazadeh was born in 1980 in Oroumieh, Iran. He received his B.Sc degree in Electrical Engineering from Azad University, Urmia Branch and M.Sc. degree in Electrical Engineering from Science and Research Department, Tehran Branch. From 2010 until 2012, he was a Teaching Assistant with the Department of Electrical Engineering, Islamic Azad University, Urmia Branch, Iran. His research interests include analysis and design of microstrip antennas, monopole antennas, microwave structures and electromagnetic theory. Since 2013, he is working towards his Ph.D degree at the University of Western Sydney.

Zahra Esmati was born in 1987 in Oroumieh, Iran. She received her B.Sc degree in Electrical Engineering from Azad University, Urmia Branch. Her research interests include analysis and design of microstrip antennas, monopole antennas, ultra-wideband (UWB) and small antennas for wireless communications and microwave/millimeter systems.

Planar Ultra-Wideband (UWB) Antenna with C-Band Rejection Using Self-Complementary Structures

Nasser Ojaroudi [1], Noradin Ghadimi [1], and Yasser Ojaroudi [2]

[1] Young Researchers and Elite Club
Islamic Azad University, Ardabil Branch, Ardabil, Iran
noradin.ghadimi@gmail.com

[2] Young Researchers and Elite Club
Islamic Azad University, Germi Branch, Germi, Iran

Abstract ─ In this paper, we describe an application of the Self-Complementary Structures (SCS) to design a low-profile UWB monopole antenna with band-notched function. The proposed antenna consists of a square radiating patch with a rotated Z-shaped slot, a ground plane with a rectangular slot and rotated Z-shaped parasitic structure inside slot; which provides a wide usable fractional bandwidth of more than 125% (2.81-12.63 GHz), with band-notched function around 3.7-4.2 GHz, to avoid interference from C-band communications. In the presented antenna, by using a rotated Z-shaped parasitic structure inside the rectangular slot in the ground plane, additional resonances are excited and hence much wider impedance bandwidth can be produced; especially at the higher band. To generate a band-stop characteristic, we use the self-complementary structure of the configuration that was inserted in the ground plane, which is a rotated Z-shaped slot at square radiating patch; with this design we can give a C-band rejection performance. The designed antenna has a small dimension of $12\times18\times0.8$ mm^3.

Index Terms ─ Microstrip-fed antenna, rotated Z-shaped structure, Self-Complementary Structure (SCS), ultra-wideband system.

I. INTRODUCTION

In UWB communication systems, one of key issues is the design of a compact antenna while providing wideband characteristic over the whole operating band. Consequently, a number of microstrip antennas with different geometries have been experimentally characterized [1-2]. Moreover, other strategies to improve the impedance bandwidth have been investigated [3-4]. The frequency range for UWB systems between 3.1-10.6 GHz will cause interference to the existing wireless communication systems. For example, the Wireless Local Area Network (WLAN) for IEEE 802.11a operating in 5.2/5.8 GHz or 3.7-4.2 GHz for C-band; therefore, the UWB antenna with a band-notched function is required.

In this paper, a different method for designing a novel and compact microstrip-fed monopole antenna with band-notched characteristic for UWB applications has been presented. In this structure, by using a rotated Z-shaped parasitic structure inside rectangular slot in the ground plane, an additional resonance in higher frequencies was excited. By obtaining this resonance, the usable upper frequency of the antenna is extended from 10.3 GHz to 12.63 GHz. To generate a frequency notch band function, we use a rotated Z-shaped slot with variable dimensions. The designed antenna has a small size and the impedance bandwidth of the designed monopole antenna is higher than the UWB antennas reported recently [5-8].

II. ANTENNA DESIGN

The proposed antenna fed by a 50-Ohm microstrip line is shown in Fig. 1, which is printed on a FR4 substrate with thickness of 0.8 mm and permittivity of 4.4. The width of the microstrip

Submitted On: February 1, 2013
Accepted On: April 22, 2014

feed line is fixed at 1.5 mm. The basic antenna structure consists of a square radiating patch, a feed line and a ground plane. The square radiating patch with rotated Z-shaped slot is connected to a feed line, as shown in Fig. 1. On the other side of the substrate, a conducting ground plane has a self-complementary structure of the radiating stub configuration that is a rotated Z-shaped parasitic structure inside a rectangular slot. The proposed antenna is connected to a 50Ω SMA connector for signal transmission.

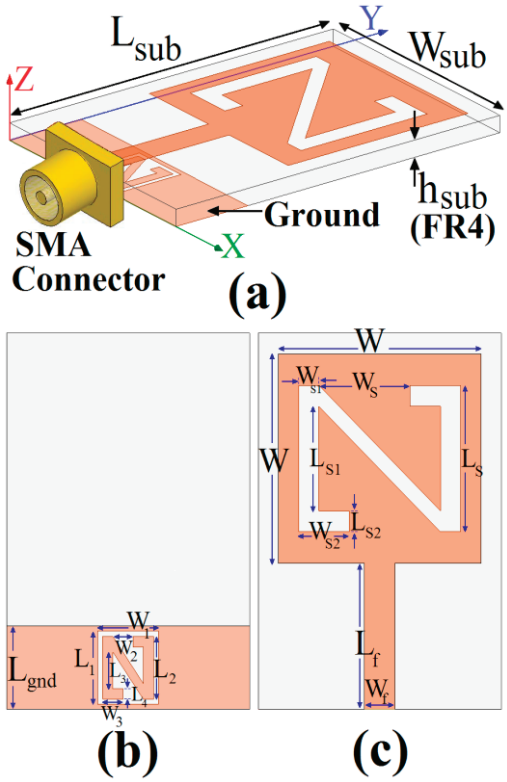

Fig. 1. Geometry of the proposed microstrip-fed monopole antenna: (a) side view, (b) bottom layer and (c) top layer.

In this proposed antenna, the rotated Z-shaped parasitic structure inside rectangular slot is playing an important role in the broadband characteristics of this antenna, because the creating slot in the ground plane provides an additional current path and improves its impedance bandwidth without any cost of size or expense [6]. In addition, using the square radiating patch with rotated Z-shaped slot with variable size generates the frequency band-notch function [7]. At the notch frequency, the current concentrated on the edges of the interior and exterior of the rotated Z-shaped slot. As a result, the desired high attenuation near the notch frequency can be produced. The variable band-notch characteristics can be achieved by carefully choosing the parameters of W_{S2} for the rotated Z-shaped slot.

The optimal dimensions of the designed antenna are specified in Table 1.

Table 1: The dimensions of the designed antenna

Param.	mm	Param.	mm	Param.	mm
W_{Sub}	12	L_{Sub}	18	h_{Sub}	0.8
W_S	4.5	L_S	7	W	10
W_f	1.5	L_f	7	L_{gnd}	4
W_{S1}	1	L_{S1}	5	W_{S2}	2.5
L_3	1	W_1	3	L_1	3.5
W_2	1	L_3	3	W_3	1
L_3	1.7				

III. RESULTS AND DISCUSSIONS

The proposed microstrip-fed monopole antenna with various design parameters were constructed and the numerical and experimental results of the input impedance and radiation characteristics are presented and discussed. The Ansoft simulation software High-Frequency Structure Simulator (HFSS) [9] is used to optimize the design.

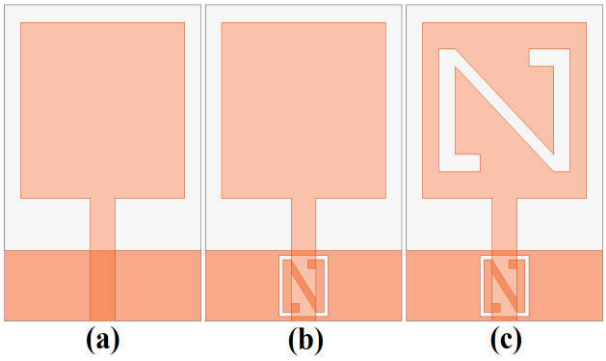

Fig. 2. (a) Ordinary square antenna, (b) square antenna with a rotated Z-shaped parasitic structure inside rectangular slot in the ground plane and (c) the proposed monopole antenna.

The configuration of the presented monopole antenna was shown in Fig. 1. Geometry for the

ordinary square monopole antenna (Fig. 2 (a)), with a rectangular slot with rotated Z-shaped parasitic structure inside slot in the ground plane (Fig. 2 (b)) and the proposed monopole antenna (Fig. 2 (c)), structures are shown in Fig. 2. VSWR characteristics for the structures that were shown in Fig. 2 are compared in Fig. 3. As shown in Fig. 3, it is observed that the upper frequency bandwidth is affected by using the rotated Z-shaped parasitic structure inside slot in the ground plane and the notch frequency bandwidth is sensitive to the rotated Z-shaped slot at square radiating patch. The input impedance of the proposed monopole antenna on a Smith chart is shown in Fig. 4.

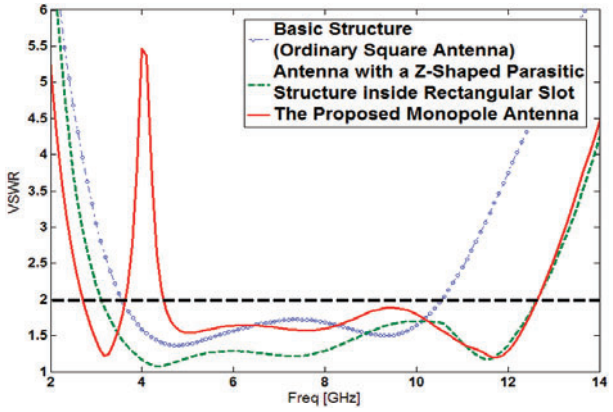

Fig. 3. Simulated VSWR characteristics for the various monopole antennas shown in Fig. 2.

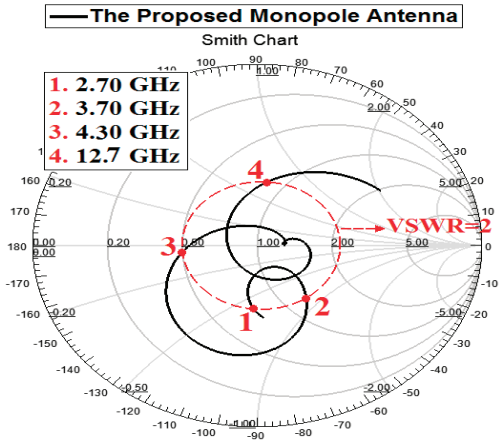

Fig. 4. Smith chart demonstration of the simulated input impedance for the proposed antenna.

To understand the phenomenon behind this additional resonance performance, the simulated current distributions at 11.5 GHz on the ground plane and radiating patch for the proposed antenna are presented in Figs. 5 (a) and 5 (b). It is found that by using the rotated Z-shaped parasitic structure inside rectangular slot, third resonance can be achieved. This behavior is mainly due to the change of surface current path by the dimensions of Z-shaped strip, as shown in Fig. 5 (a). Another important design parameter of this structure is the rotated Z-shaped slot at square radiating patch. Figures 5 (c) and 5 (d) present the simulated current distributions on the ground plane and radiating patch at the notched frequency (4.2 GHz). As shown in Fig. 5 (d), at the notched frequency the current flows are more dominant around of the rotated Z-shaped slot.

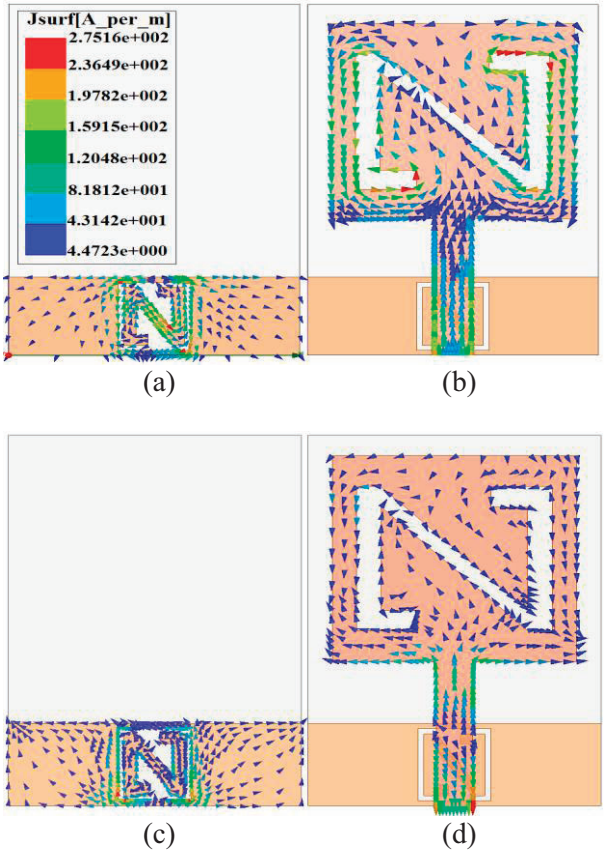

Fig. 5. Simulated surface current distributions for the proposed antenna: (a) in the ground plane at 11.5 GHz, (b) on the radiating stub at 5.5 GHz, (c) in the ground plane at 5.5 GHz and (d) at the radiating patch at 11.5 GHz.

Figure 6 shows the simulated VSWR curves with different values of W_{S2}. As shown in Fig. 6,

when the width of the rotated Z-shaped slot increases from 1.5 mm to 5.5 mm, the center of notched frequency is decreased from 4.2 GHz to 3.4 GHz; also, filter bandwidth is varied from 1.3 GHz to 0.7 GHz. From these results, we can conclude that the notch frequency is controllable by changing the width of the rotated Z-shaped slot.

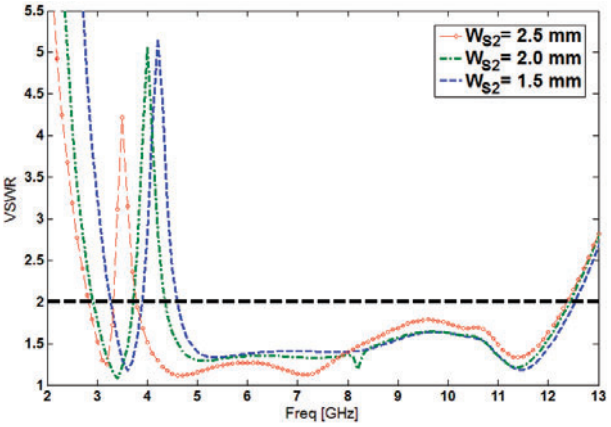

Fig. 6. Simulated VSWR characteristics for the proposed antenna with different values of W_{S2}.

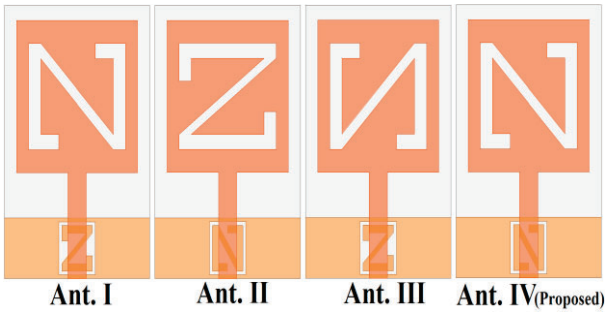

Fig. 7. Various configurations of the proposed design.

Configurations of the proposed design with different rotation of Z-shaped structures are presented in Fig. 7. VSWR characteristics for the various structures that were shown in Fig. 7 are compared in Fig. 8. As seen, it is observed that the upper frequency bandwidth is affected by using the correct direction of Z-shaped parasitic structure inside slot in the ground plane and the notch frequency bandwidth is sensitive to the rotated Z-shaped slot at square radiating patch. The proposed design (Ant. IV) has a good impedance matching with desired band-stop function, in comparison to the other structure shown in Fig. 7.

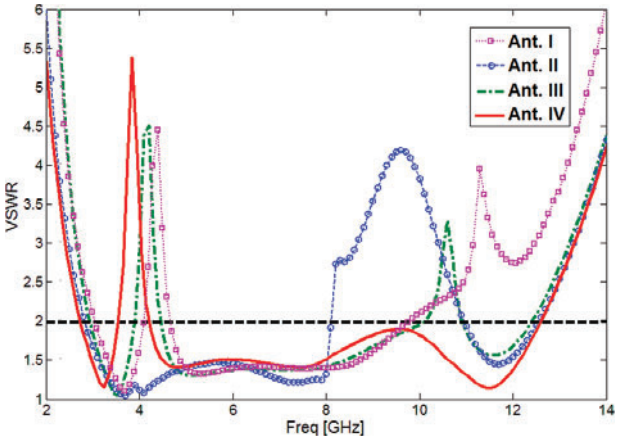

Fig. 8. Simulated VSWR characteristics for the various antennas shown in Fig. 7.

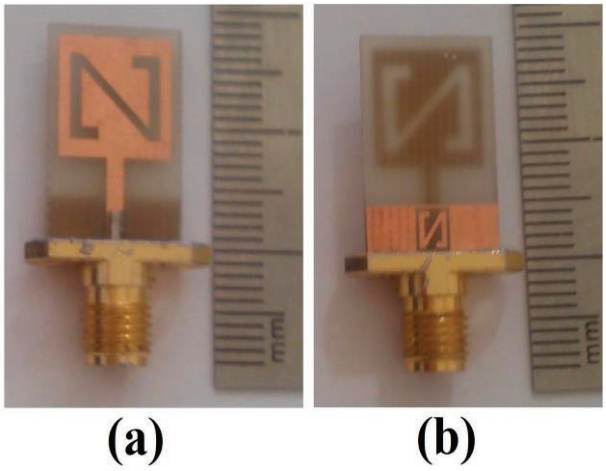

Fig. 9. Realized antenna: (a) top view and (b) bottom view.

The proposed antenna with final design as shown in Fig. 9, was built and tested. The VSWR characteristic of the antenna was measured using a network analyzer in an anechoic chamber. The radiation patterns have been measured inside an anechoic chamber using a double-ridged horn antenna as a reference antenna, placed at a distance of 2 m. Also, the two-antenna technique using a spectrum analyzer and a double-ridged horn antenna as a reference antenna, placed at a distance of 2 m is used to measure the radiation gain in the z axis direction (x-z plane).

Measurement set-up of the proposed antenna for the VSWR and antenna gain and radiation pattern characteristics are shown in Fig. 10.

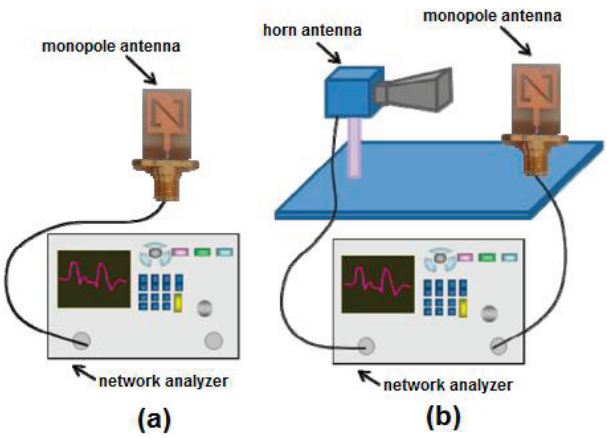

Fig. 10. Measurement set-up of the proposed antenna: (a) VSWR and (b) antenna gain and radiation patterns.

The measured and simulated VSWR characteristic of the proposed antenna was shown in Fig. 11. The fabricated antenna has the frequency band of 2.81-12.63 GHz, with band-notched function around 3.7-4.2 GHz, to avoid interference between UWB and C-band communications.

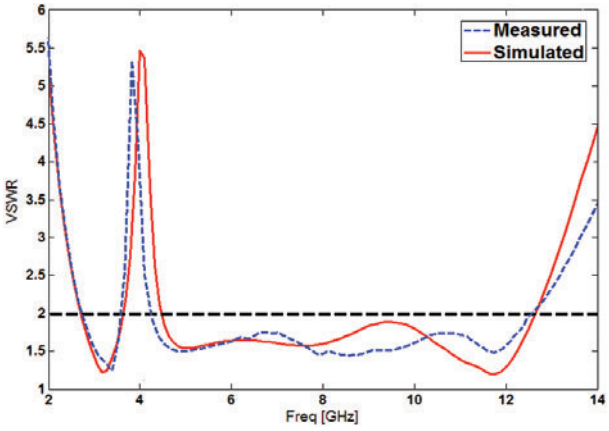

Fig. 11. Measured and simulated VSWR characteristics for the proposed antenna.

Figure 12 shows the measured radiation patterns, including the co-polarization in the H-plane (x-z plane) and E-plane (y-z plane). The radiation patterns on the y-z plane display a typical figure-of-eight, similar to that of a conventional dipole antenna. It should be noticed that the radiation patterns in E-plane become imbalanced as frequency increases, due to the increasing effects of the cross-polarization. It can be seen that the quasi-omnidirectional radiation pattern can be observed on x-z plane over the whole UWB frequency range; especially at the low frequencies. The patterns indicate at higher frequencies and more ripples can be observed in both E and H-planes, owing to the generation of higher-order modes [17-20].

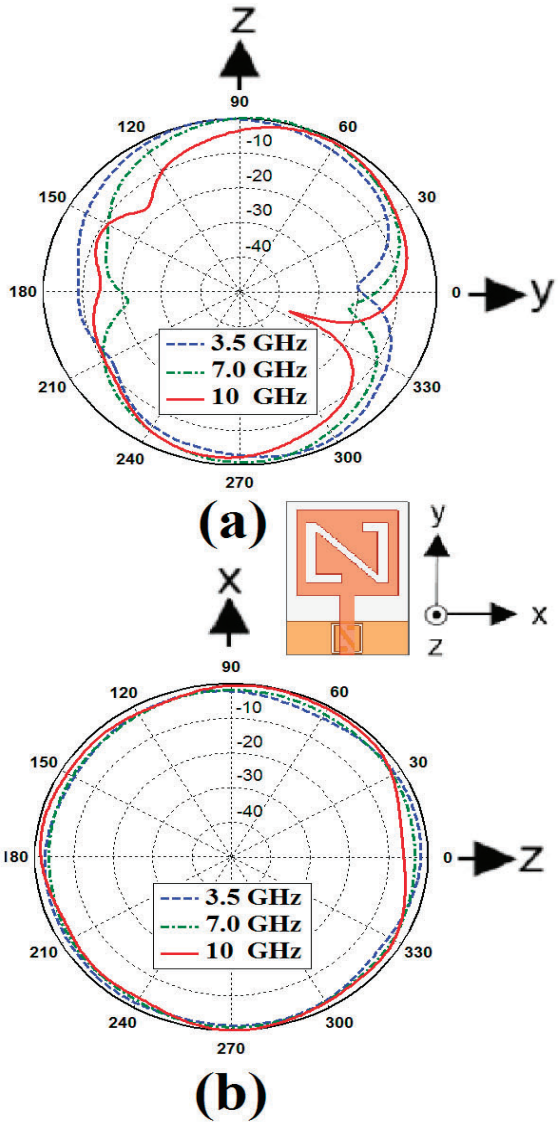

Fig. 12. Measured radiation patterns of the proposed antenna: (a) E-plane and (b) H-plane.

The simulated 3D radiation patterns of the proposed antenna at 3.5, 7 and 10 GHz are shown

in Fig. 13. As illustrated, the radiation pattern looks like a doughnut, similar to that of a dipole pattern at 3.5 GHz. At 7 GHz and 10 GHz, the radiation pattern is somewhat like a pinched doughnut (i.e. omnidirectional). As the frequency moves toward the upper end of the bandwidth, the radiation pattern is somewhat slightly distorted as it reaches higher frequencies (i.e. 10 GHz and above).

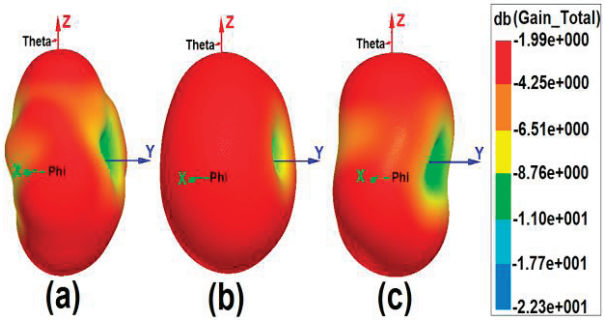

Fig. 13. Simulated 3-D radiation patterns of the proposed antenna: (a) 3.5 GHz, (b) 7 GHz and (c) 10 GHz.

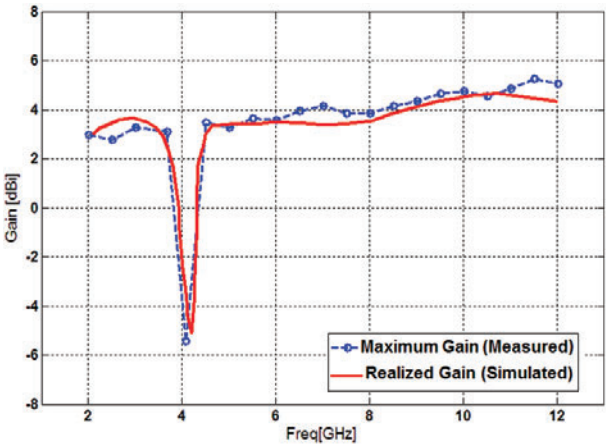

Fig. 14. Measured maximum gain for the proposed antenna.

Figure 14 illustrates the measured and simulated maximum and realized gains of the proposed antenna. The antenna gain has a flat property, which increases by the frequency. As illustrated, a sharp decrease of maximum gain in the notched frequency band was shown in Fig. 9. Also, the proposed microstrip-fed monopole antenna has sufficient and acceptable antenna gain levels in the operation bands.

Table 2 summarizes the previous designs and the proposed antenna. As seen, the proposed antenna has a very compact size with very wide bandwidth, compared to the pervious works. In addition, compared with previous band-notched antennas, the proposed antenna displays a good omnidirectional radiation pattern even at lower and higher frequencies. Also, the proposed microstrip-fed monopole antenna has sufficient and acceptable antenna gain levels in the operation bands.

Table 2: Comparison of previous designs with the proposed antenna

Ref.	Size (mm)	FBW (%)	Gain (dBi)
[15]	30×30×1.6	130% (2-12.4)	2.8~5.3
[16]	20×20×0.8	47% (3.7-6.1)	3-3.7
[17]	20×20×0.8	110% (3-10.8)	2~4.5
[18]	20×20×0.8	112% (3-11.2)	3.2-5
[19]	12×18×1.6	28% (3.3-4.4)	1.8~2.8
[20]	12×18×1.6	117% (3-11.5)	2.5-3.5
This Work	12×18×0.8	125% (2.8-12.6)	3~.5.1

The radiating mechanism of the proposed antenna is more novel than was explained in previous works. Main novelty of the proposed design is the application of self-complementary structures, to create an extra frequency resonance and enhance the bandwidth. The proposed structure is the combination of the monopole antenna with the dipole and slot antenna. In this study, the modified ground-plane structure is the combination of the monopole antenna and the slot antenna. The embedding parasitic structure on the other side of the substrate of the monopole antenna acts as a dipole. As seen, the proposed antenna has a compact size with very wide bandwidth, compared to the pervious works for UWB applications. Additionally, the antenna has a good antenna gain level in the operation bands [21-23].

IV. CONCLUSION

In this paper, a novel design of ultra-wideband monopole antenna with variable band-notched function is proposed. The presented antenna can operate from 2.81 GHz to over 12.63 GHz, with VSWR < 2 and with a rejection band around 3.7 GHz to 4.2 GHz. By using a rotated Z-shaped

parasitic structure inside rectangular slot in the ground plane, additional resonance at higher frequency range is excited and much wider impedance bandwidth can be produced. In order to generate a frequency band-stop performance, we use the self-complementary structure of the inserted structure in the ground plane; which is the rotated Z-shaped slot at radiating patch. The designed antenna has a small size. The measured results show good agreement with the simulated and measured results. Experimental results show that the presented antenna could be a good candidate for UWB applications.

ACKNOWLEDGMENT

The authors are thankful to Microwave Technology (MWT) Company staff, for their beneficial and professional help (www.microwave-technology.com).

REFERENCES

[1] N. Ojaroudi, "Compact UWB monopole antenna with enhanced bandwidth using rotated l-shaped slots and parasitic structures," *Microw. Opt. Technol. Lett*., vol. 56, pp. 175-178, 2014.

[2] N. Ojaroudi, S. Amiri and F. Geran, "A novel design of reconfigurable monopole antenna for UWB applications," *Applied Computational Electromagnetics Society (ACES) Journal*, vol. 28, no. 6, pp. 633-639, July 2013.

[3] J. Jung, W. Choi and J. Choi, "A small wideband microstrip-fed monopole antenna," *IEEE Microwave Letters*, vol. 15, no. 10, pp. 703-705, October 2005.

[4] J. Jung, W. Choi and J. Choi, "A compact broadband antenna with an l-shaped notch," *IEICE Trans. Commun*., vol. E89-B, no. 6, 1968-1971, June 2006.

[5] N. Ojaroudi, "Application of protruded strip resonators to design an UWB slot antenna with WLAN band-notched characteristic," *Progress in Electromagnetics Research C*, vol. 47, pp. 111-117, 2014.

[6] N. Ojaroudi, "Microstrip monopole antenna with dual band-stop function for UWB applications," *Microw. Opt. Technol. Lett*., vol. 56, pp. 818-822, 2014.

[7] N. Ojaroudi, S. Amiri and F. Geran, "Reconfigurable monopole antenna with controllable band-notched performance for UWB communications," *20th Telecommunications Forum, TELFOR 2012*, November 20-22, 2012, Belgrade, Serbia, pp. 1176-1178, 2013.

[8] T. G. Ma and S. J. Wu, "Ultra-wideband band-notched folded strip monopole antenna," *IEEE Trans. Antennas Propag.*, vol. 55, no. 9, pp. 2473-2479, 2007.

[9] "Ansoft high frequency structure simulatior (HFSS)," ver. 13, *Ansoft Corporation*, 2010.

[10] A. Valizade, C. Ghobadi, J. Nourinia, N. Ojaroudi and M. Ojaroudi, "Band-notch slot antenna with enhanced bandwidth by using Ω-shaped strips protruded inside rectangular slots for UWB applications," *Applied Computational Electromagnetics Society (ACES) Journal*, vol. 27, no. 10, pp. 816-822, October 2012.

[11] G. Zhang, J. S. Hong, B. Z. Wang and G. Song, "Switched band-notched UWB/WLAN monopole antenna," *Applied Computational Electromagnetics Society (ACES) Journal*, vol. 27, no. 3, pp. 256-260, March 2012.

[12] H. Siahkal-Mahalle, M. Ojaroudi and N. Ojaroudi, "Enhanced bandwidth small square monopole antenna with band-notched functions for UWB wireless communications," *Applied Computational Electromagnetics Society (ACES) Journal*, vol. 27, no. 9, pp. 759-765, September 2012.

[13] M. T. Partovi, N. Ojaroudi and M. Ojaroudi, "Small slot antenna with enhanced bandwidth and band-notched performance for UWB applications," *Applied Computational Electromagnetics Society (ACES) Journal*, vol. 27, no. 9, pp. 772-778, September 2012.

[14] N. Ojaroudi, S. Amiri, F. Geran and M. Ojaroudi, "Band-notched small monopole antenna using triple e-shaped structures for UWB systems," *Applied Computational Electromagnetics Society (ACES) Journal*, vol. 27, no. 12, pp. 1022-1028, December 2012.

[15] A. Kamalvand, C. Ghobadi, J. Nourina, M. Ojaroudi and N. Ojaroudi, "Omni-directional/multi-resonance CPW-fed small slot antenna for UWB applications," *Applied Computational Electromagnetics Society (ACES) Journal*, vol. 28, no. 9, pp. 829-835, September 2013.

[16] M. Ojaroudi, N. Ojaroudi and N. Ghadimi, "Enhanced bandwidth small square slot antenna with circular polarization characteristics for WLAN/WiMAX and c-band applications," *Applied Computational Electromagnetics Society (ACES) Journal*, vol. 28, no. 2, pp. 156-161, February 2013.

[17] M. Ojaroudi and N. Ojaroudi, "Ultra-wideband small rectangular slot antenna with variable band-stop function," *IEEE Trans. Antennas Propag*., vol. 62, pp. 490-494, 2014.

[18] M. Ojaroudi and N .Ojaroudi, "Ultra-wideband slot

antenna with frequency band-stop operation," *Microw. Opt. Technol. Lett*., vol. 55, pp. 2020-2023, 2013.

[19] J. Mazloum, A. Jalili, M. Ojaroudi and N. Ojaroudi, "Compact oscillator feedback active integrated antenna by using interdigital coupling strip for WiMAX applications," *Applied Computational Electromagnetics Society (ACES) Journal*, vol. 28, no. 9, pp. 844-850, September 2013.

[20] N. Ojaroudi and M. Ojaroudi, "Small square monopole antenna having variable frequency band-notch operation for UWB wireless communications," *Microw. Opt. Technol. Lett.*, vol. 54, pp. 1994-1998, 2012.

[21] N. Ojaroudi, H. Ojaroudi and N. Ghadimi, "Quad-band planar inverted-f antenna (PIFA) for wireless communication systems," *Progress In Electromagnetics Research Letters*, vol. 45, pp. 51-56, 2014.

[22] N. Ojaroudi and N. Ghadimi, "Design of CPW-fed slot antenna for MIMO system applications," *Microw. Opt. Technol. Lett*., vol. 56, pp. 1278-1281, 2014.

[23] N. Ojaroudi and N. Ghadimi, "Dual-band CPW-fed slot antenna for LTE and WiBro applications," *Microw. Opt. Technol. Lett*., vol. 56, pp. 1013-1015, 2014.